FLOW REGIMES OF SUBMERGED GAS JETS

by

Enrique Oscar Hoefele
Chem.Eng., Universidad de Chile, Santiago, 1972

A THESIS SUBMITTED IN PARTIAL FULFILLMENT
OF THE REQUIREMENTS FOR THE DEGREE OF
MASTER OF APPLIED SCIENCE

in

THE FACULTY OF GRADUATE STUDIES
Department of Metallurgy

We accept this thesis as conforming
to the required standard

THE UNIVERSITY OF BRITISH COLUMBIA
August 1978

© Enrique Oscar Hoefele

In presenting this thesis in partial fulfilment of the requirements for an advanced degree at the University of British Columbia, I agree that the Library shall make it freely available for reference and study. I further agree that permission for extensive copying of this thesis for scholarly purposes may be granted by the Head of my Department or by his representatives. It is understood that copying or publication of this thesis for financial gain shall not be allowed without my written permission.

Department of Metallurgy

The University of British Columbia
2075 Wesbrook Place
Vancouver, Canada
V6T 1W5

Date 5th of October, 1978

ABSTRACT

The behaviour of a gas jet injected into a liquid has been studied as a function of gas and liquid densities, gas flow rate, tuyere diameter and tuyere design. A novel technique has been developed to study the interaction of a submerged gas jet into injected opaque liquids. The jet is blown through a "half-tuyere" fastened to the plexiglas side wall of the liquid-containing vessel. In this way the jet can be viewed and photographed with a high speed camera. Also pressure measurements have been made at various points along the tuyere using a fast-response pressure transducer. This method was employed to study air, helium and argon injected into mercury, zinc chloride solution and water, as a function of gas rate. The results of pressure and cinematography show that two limiting types of behaviour can be identified: jet pulsations at low gas flow rates and steady jetting at high gas rates. For a high-density liquid the transition occurs at the point where, with increasing back pressure, the jet becomes underexpanded. Industrial experiments performed in a nickel converter confirmed that these two types of regimes are also found when blowing into a high-temperature melt. From the results obtained, a modified operating practice for matte converting has been suggested, in order to improve substantially tuyere and refractory life.

TABLE OF CONTENTS

LIST OF TABLES

LIST OF FIGURES

ACKNOWLEDGEMENTS

I would like to thank sincerely my research supervisor, Dr. Keith Brimacombe, for his friendly assistance and guidance throughout the course of this research project.

Thanks are extended to the Professors and fellow graduate students of the Department of Metallurgy, in particular to Mr. Peter Gorog for his valuable help in the writing of the text. Thanks are also due to Messrs. Jim Walker and Ed Klassen who built the pieces of equipment necessary to perform this work.

I would also like to thank Dr. Ron Orr of the INCO Smelter in Thompson, Manitoba for his interest that made possible the performance of the industrial tests.

I am grateful to the University of British Columbia, and through it to the people of Canada, for their hospitality and financial assistance in the form of a graduate scholarship.

CHAPTER 1

INTRODUCTION

1.1 Metallurgical Uses of Submerged Gas Injection

The injection of submerged gas jets into liquid metals is a technique that has been successfully applied to several metallurgical processes. Several examples may be mentioned. Copper and nickel matte converting are well established processes that have been in operation for more than half a century. New continuous copper smelting processes, such as the Noranda process, employ basically the same blowing techniques that are used in traditional matte converting. The fire-refining of blister copper employs submerged injection of oxidizing and reducing gases. In steelmaking, new bottom-blown processes, like Q-BOP and LWS, employ a submerged concentric tuyere to inject oxygen shielded with another gas such as a hydrocarbon, steam or fuel oil, whereas the SIP process injects the gas through a tuyere into an open hearth furnace. New processes for stainless steel production, such as AOD and CLU, are also based on submerged injection of gas, as well as argon-ladle degassing and ladle desulphurization. Other non-ferrous processes that use submerged gas injections that are in operation or under study include the smelting of sulphide concentrates of copper, nickel,

cobalt and lead, as well as the treatment of tin slags.

The frequent use of submerged gas injection can be understood since the increased area of contact between the gas and the melt, together with the high degree of turbulence obtained in the bath when blowing a high speed jet, give rise to high rates of heat and mass transfer. These increased rates make gas injection a very attractive method to obtain a large output using a relatively small reactor.

In spite of its widespread use in metallurgical processes, submerged gas injection is not a technique that is free of operational difficulties. Among the problems encountered are entrainment of metal in the exit gases and tuyere plugging due to solidification of the bath in contact with the nozzle tip (in copper and nickel matte converting, the tuyeres need to be punched manually or mechanically). But the main problem is tuyere and refractory erosion. The exothermic chemical reactions between the gas and the molten metal, the high temperatures of operation, and the flow patterns that exist in the bath provide harsh conditions for the tuyeres and the adjacent refractory bricks. Maintenance repairs have to be scheduled regularly at high cost, thereby necessitating the installation of additional reactors in order to maintain a constant output for a

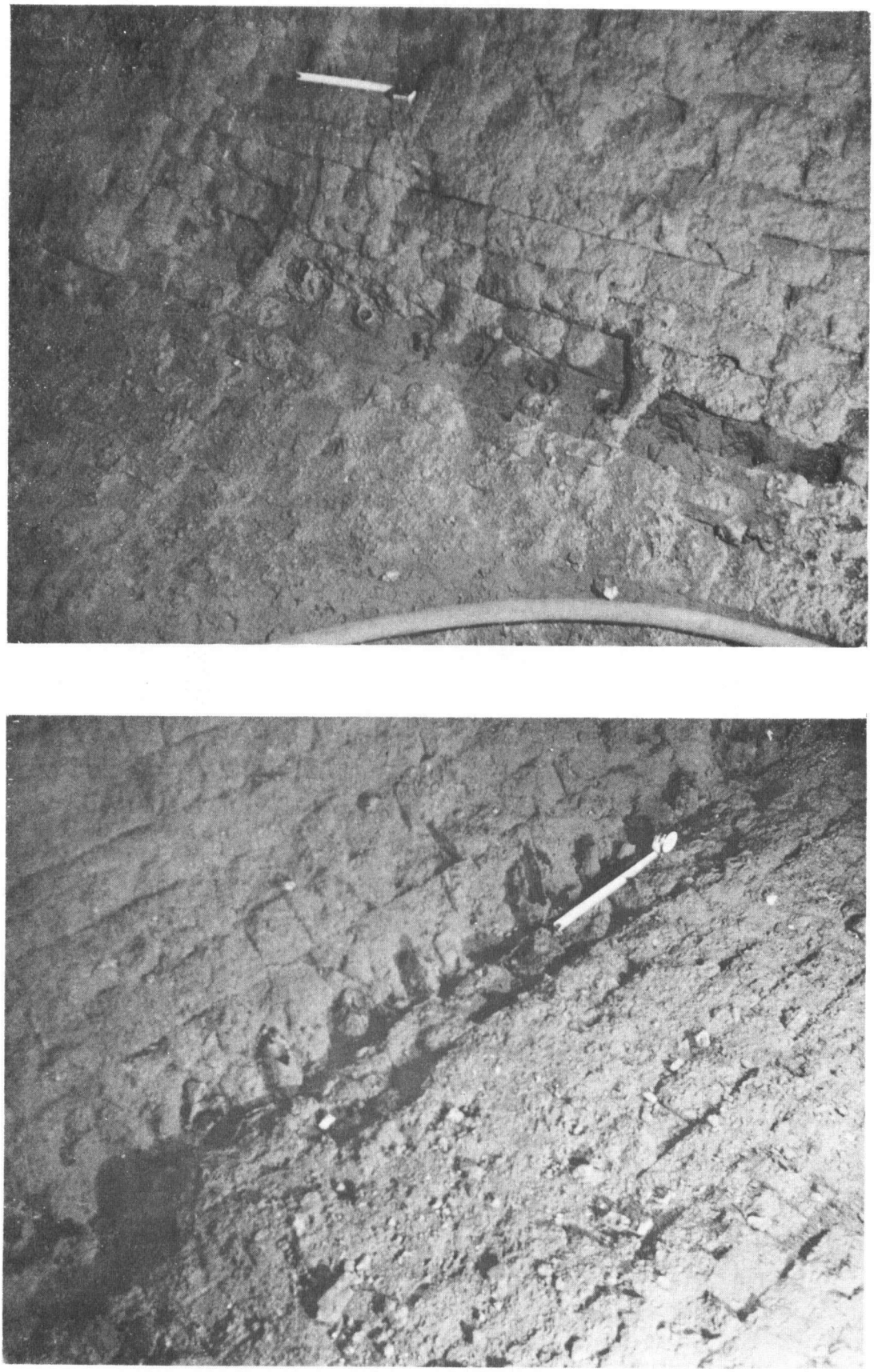

Fig. 1 Photograph of Tuyere Line in the Inside of a Matte Converter.

smelter. Figure 1 is a photograph of the refractory lining of a copper converter, after it has been shut down for maintenance and repair. Marked erosion of the refractories around the tuyere line is clearly visible. Thus, refractory that is usually 60 cm. thick at the start of a campaign can be reduced to a thickness of 25 cm. in the tuyere zone, after 3 months of operation. The time necessary for repairs is approximately one third of the operational time of a copper converter. Refractory erosion depends also on the metallurgical system involved (composition of slags, operating temperature). But obviously an important factor is the lack of knowledge of the flow conditions that exist in the reactor, and particularly, of the behaviour of the gas jet in the molten bath.

1.2 Previous Studies on Submerged Gas Injection

A review of the technical literature on bubble formation in liquids has been included in the work by Oryall[1]. It is generally accepted that three distinct regimes of bubble formation can be identified as a function of gas flow rate.

i) Static Regime

At very low flow rates and Reynolds number (Re < 500) the frequency of bubble formation is proportional to the gas flow rate (usually below 100 bubbles per minute), while the bubble size is almost constant and depends

only on the orifice diameter.

ii) Dynamic Regime

For 500 < Re < 2100, the bubble volume increases with gas flow rate while the frequency remains almost constant (usually higher than 500 bubbles per minute).

iii) Non-homogeneous Jets

At higher flow rates (Re > 2100) a bubble stream is produced where larger bubbles of irregular shape issuing from the orifice explode into smaller bubbles very close to the tip of the nozzle.

Most of the previous work on submerged gas injection into liquids has been performed at low gas flow rates, under conditions of laminar flow. However these conditions do not correspond to those found in industrial practice, where the gas jets are blown at high flow rates and turbulent conditions to maximize productivity and good mixing of the reactants.

Only a few investigations have been performed on high velocity, submerged gas jets. Themelis et al[2] derived a model for the trajectory of a gas jet injected horizontally into a liquid based on momentum transfer between the gas and the liquid,and on the effect

of buoyancy on the gas jet. They showed that the theoretical results agree with experimental data for the air-water system. On the basis of this comparison they predicted the trajectory of an air jet into copper matte in a Peirce-Smith copper converter with the assumption that the cone angle of the jet was the same as for the air-water system. However, Oryall and Brimacombe[3] showed that the model of Themelis et al, when used with a cone angle of 20°, greatly overestimates the horizontal penetration of an air jet into mercury. When an experimentally determined cone angle of 155° is used instead, the model more accurately predicts the measured trajectories, although it underestimates the horizontal penetration. Therefore it appears that the physical properties of the liquid along with those of the jet fluid have a strong influence on the jet expansion angle and trajectory.

Engh and Bertheusen[4] derived a model for the jet trajectory by modifying one of the basic assumptions of the model of Themelis et al (i.e. the diameter of the cone being proportional to the distance along the jet axis rather than to the horizontal distance from the orifice). This model also predicts satisfactorily the trajectory of air jets into water. However, it has been proven that these models have severe

limitations. After a thorough analysis of both models, McKelliget et al[5] showed that Engh and Bertheusen's model fails to reflect the conical shape of the jet away from the nozzle orifice. Although the model of Themelis et al appears to match the experimental data using mercury, this is fortuitous, since the model breaks down at large expansion angles. Moreover both models break down when the jet radius is equal to the radius of curvature of the jet axis. Therefore it appears that in order to realistically model the behaviour of a submerged gas jet injected into a metallurgical melt, a more fundamental approach is required which involves the measurement of the effect of the physical properties of both the gas and the liquid on the jet characteristics.

Only a few studies have been made related to high-velocity jets discharging into molten metals. Spesivtsev et al[6] derived an expression that describes the horizontal penetration of the jet as a function of the Froude number (N'_{Fr}) and compared the calculated values with their experimental data as shown in Figure 2. It was found that their relationship is in reasonable agreement with the data obtained for gas jets in water, $ZnCl_2$ solution and "Thoulet's solution" but shows poor agreement with the results for the air-mercury system. The same work stresses the large effect of the specific gravity

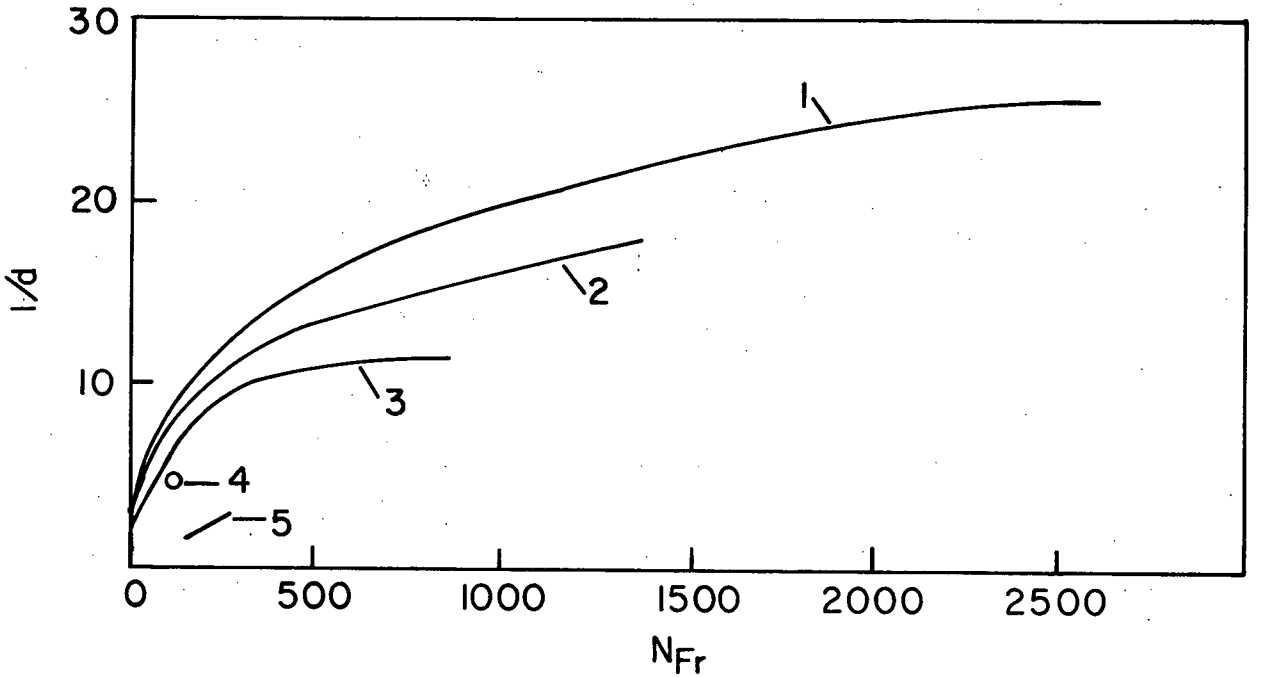

Variation of dimensionless length of the horizontal jet section with the Froude number; 1-Water; 2- $ZnCl_2$ solution; 3-Tula solution; 4-Liquid Ni_3S_2; 5-Mercury;

$$N_{Fr} = \frac{\rho_g \, v_0^2}{[\rho_l - \rho_g] g \, d_0}$$

Fig. 2 Jet Penetration as a Function of the Froude Number.

of the liquid on the character of the jet. It is also pointed out that an increase in the density of the melt has the same effect on jet behaviour as an increase in the bath temperature. Therefore they conclude that in an actual melt, the behaviour of the gas jet is similar to that in a mercury bath.

Oryall and Brimacombe[3] studied the behaviour of air jets injected horizontally into a mercury bath. Employing an electro-resistivity probe, they measured the gas volume fraction and the bubble frequency at all points within the jet. They found that the expansion angle for the air-mercury system is approximately 155° and that in the range of gas flows studied, the jet penetrates only a short distance into the bath and rises in a column-like manner.

A few other works related to gas injection into liquid metals have been reported and a complete survey of these previous works can be found in the work by Oryall[1]. However most of those studies provide little information about the behaviour of gas jets in metallurgical melts.

1.3 Objectives of the Present Study

The thrust of this work is to obtain basic information

about the fundamentals of a gas jet injected horizontally into a liquid. Due to the difficulties in performing the experiments, isothermal, non-reactive, gas-liquid systems have been chosen.

The main objectives are the following:

i) To study the behaviour of gases injected horizontally into liquids on an instantaneous basis. To achieve this a novel technique has been developed to view the jet and permit high speed films of the jet to be taken. In addition, those events in the jet that can be observed directly through the cine film have been related to measurements of gas pressure made along the tuyere.

ii) On the basis of the results from the cinematography and pressure measurements, to study the effect of parameters such as tuyere diameter and tuyere design for a wide range of gas flows.

iii) To study the effect of the physical properties of the system on the jet characteristics. Mercury, zinc chloride solution and water were used as liquid media. The effect of gas density was studied by injecting air, argon and helium.

iv) To compare the results from the laboratory experiments to data obtained from tests performed in an industrial matte converter under real operating conditions. In this way it is possible to determine the validity of the conclusions derived from the laboratory tests.

v) Finally, on the basis of the experimental data collected from laboratory and industrial tests, to make suggestions that might lead to improvements in the present gas injection practice and to increase tuyere and refractory life.

CHAPTER 2

LABORATORY EXPERIMENTAL WORK

2.1 Jets in Mercury

Gas jets were injected into mercury through horizontal nozzles. High-speed films of the jets were taken and pressure measurements in different positions along the tuyere were made. In this way, pressure and Mach number profiles were obtained, while pressure oscillations recorded at the tip of the nozzle were related to the events observed through the high-speed films of the jets. The films also permitted measurement of jet contour along with the forward and backward penetration of gas in the bath.

2.1.1 Experimental Apparatus

The apparatus employed in the experiments is illustrated schematically in Figure 3. It consisted of a converter-shaped vessel containing the mercury, a gas-delivery system to supply gas to the tuyeres, a high-speed camera to film the jets, and a fast-response, pressure transducer coupled to a storage oscilloscope to measure and record the pressure along the tuyere.

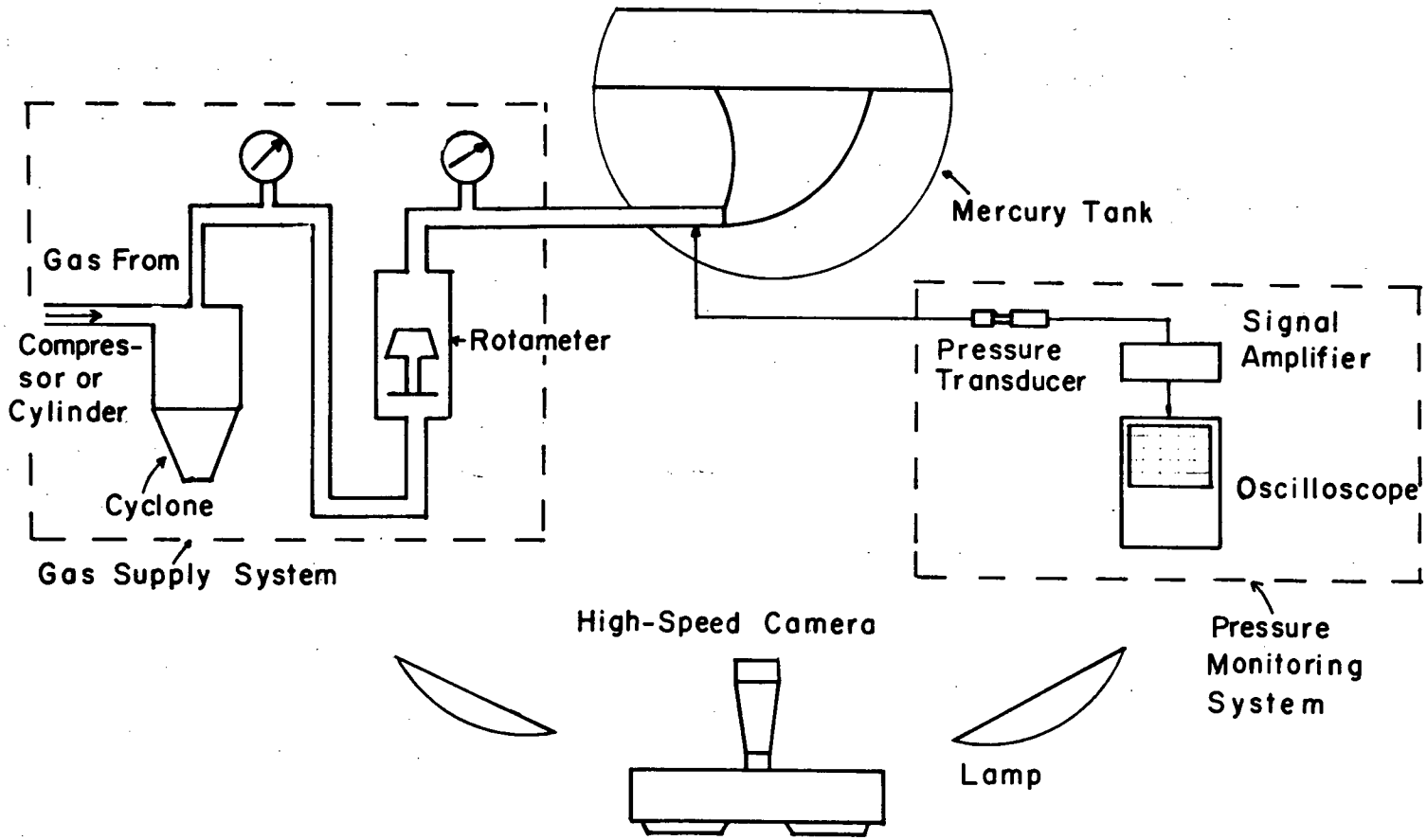

Fig. 3 Schematic of the Apparatus.

2.1.1.1 Mercury Tank

The mercury-containing vessel was made from a 40.6 cm. I.D. carbon steel pipe, cut 15 cm. long and truncated 8.9 cm. above its axis, as shown in Figure 4. The endwalls of the tank were made from 1.9 cm. thick transparent plexiglas plate. Horizontal baffles were fixed to the plexiglas to minimize slopping of the bath. The top of the tank was sealed to avoid spillage of mercury, and the exit gases were directed through a granulated-sulphur filter to remove mercury vapours before being discharged to a fume hood. The tank was filled with mercury to a height of 9.1 cm. above the tuyere centreline.

2.1.1.2 Tuyeres

To allow visual observation of the jet, "half-tuyeres" were employed. The tuyeres were made from 4.95 cm. diameter, black iron rod, with a cone-shaped end. A hole was drilled along the axis of the rod which was then split in half. The half-tuyeres were fastened to the plexiglas sidewalls of the tank. Straight-bore and convergent-divergent tuyeres were used, as shown in Figure 5. For comparative purposes, tests using a "full-tuyere" were also performed. For these

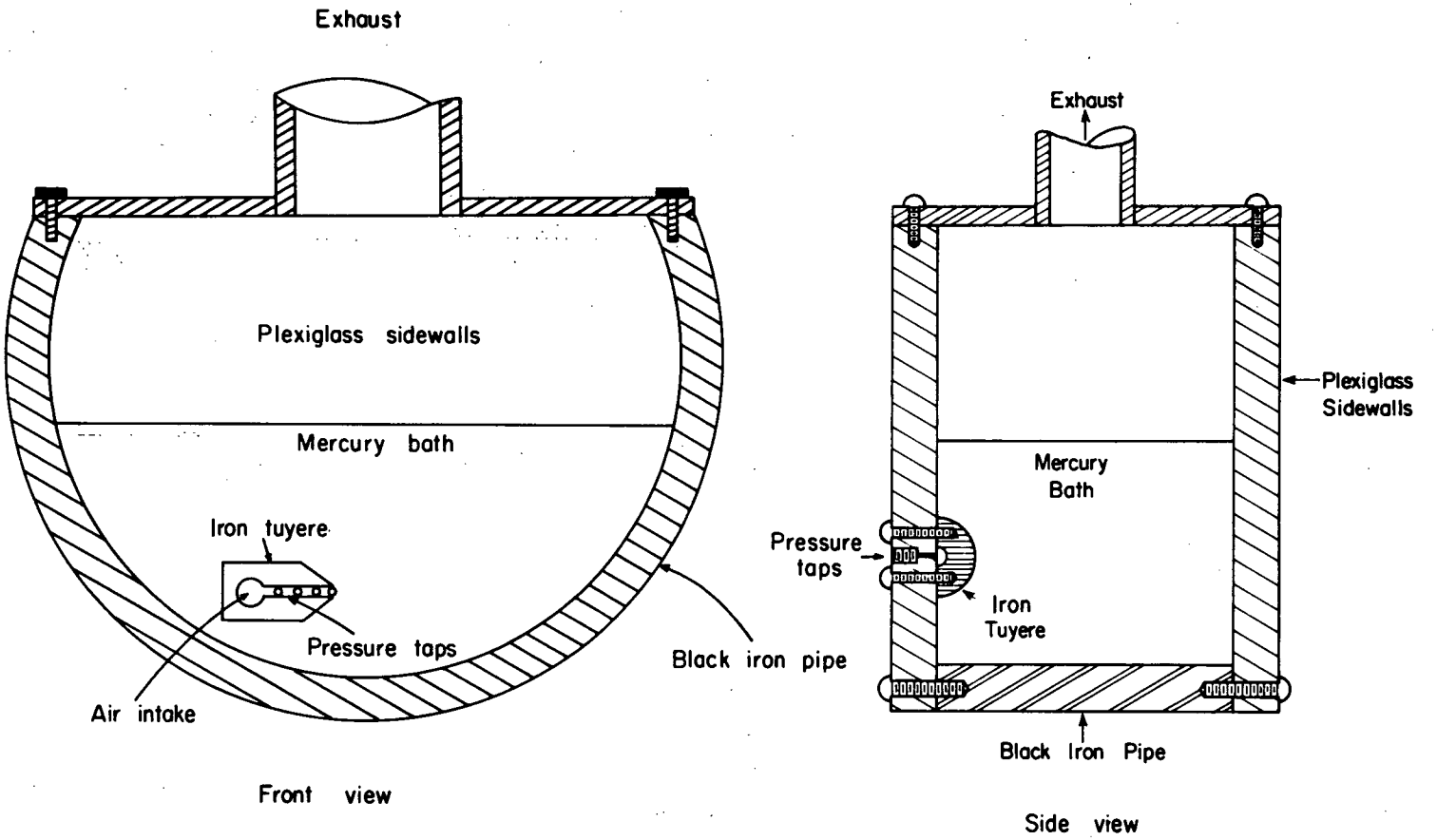

Fig. 4 The Mercury Tank.

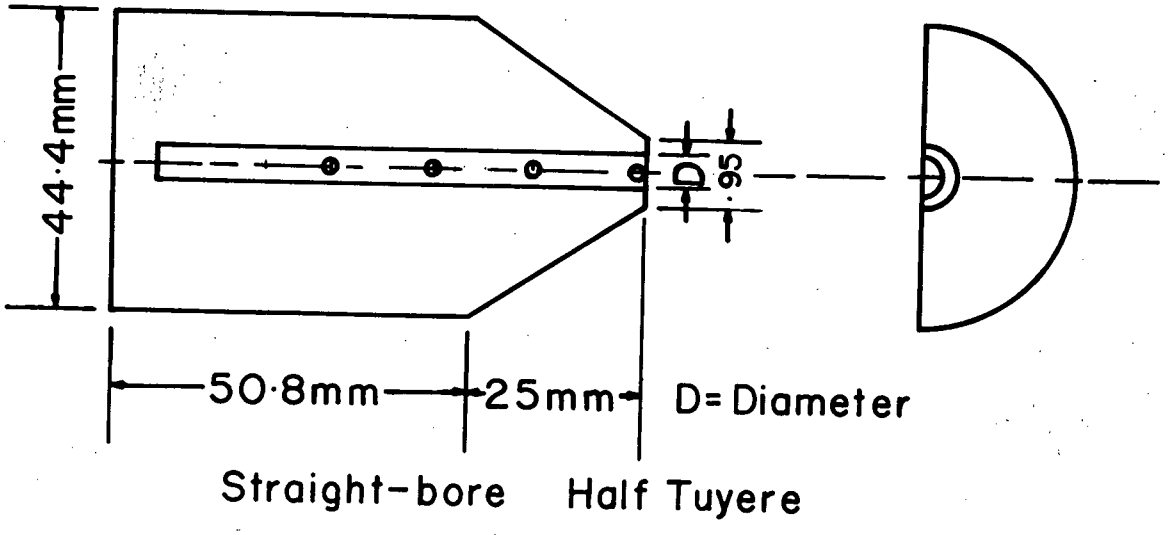

Straight-bore Half Tuyere

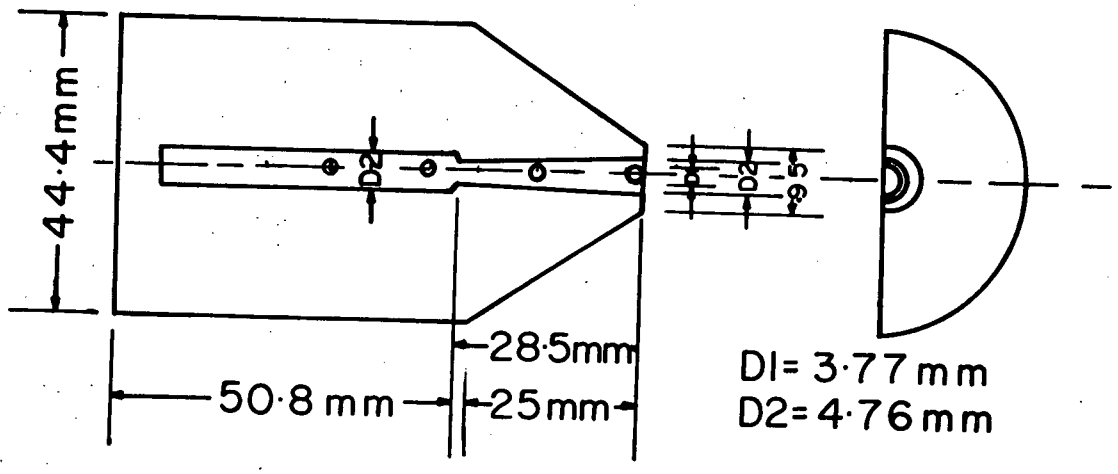

Convergent–Divergent Half Tuyere

Fig. 5 Types of Tuyeres.

experiments, a full-tuyere was inserted horizontally through the mercury vessel at a position midway between the plexiglas sidewalls. The depth of the tuyere submergence was the same for both full and half-tuyeres.

The different diameters used for both the straight-bore half-tuyere and full-tuyere are shown in Table I. In the case of the convergent-divergent tuyere, the design specifications were as follows:

Minimum diameter at the constriction = 0.377 cm.

Maximum diameter before the constriction = 0.476 cm (equal to the maximum diameter at the exit)

Ratio between areas at the constriction and at the exit = 1.594

The ratio between the specific heats at constant pressure, C_p, and at constant volume, C_v, is equal to 1.4 (value for air). Thus, if before the constriction the Mach number is 0.40, at the exit it will be 1.93. This design was based on tables of Appendix D (Compressible Flow Tables) of the book by Hansen[7].

2.1.1.3 Gas-Delivery System

Two sources of air were used in the current work. For low-pressure tests, air was supplied by a compressor at a gauge pressure of 0.7 MPa (100 psig). A Harris regulator and a needle valve were used to reduce the pressure near the apparatus and to control the flow. The air was directed through a centrifugal separator, and strainer to remove oil and condensed water. For the high-pressure air tests, and for the helium and argon tests, bottled gas was utilized. In this way back pressures higher than 100 psi were obtained. The gas flow was measured using a rotameter. Bourdon-type pressure gages placed at both the entrance and exit of the rotameter allowed mass flow rates to be accurately calculated. Corrections were also made when using gases of different densities. To calculate the gas flow at the tuyere exit, both the atmospheric pressure and the static head of mercury were considered.

2.1.1.4 High-Speed Cinematography

High-speed films of the jet were taken using a Hycam camera (model K2054E). Most films were obtained at a speed of 800 frames per second, but speeds of 400 and 1000 frames per second were also used. Black and white, 4-X Kodak film (400 ASA) was used

throughout the work. Illumination was provided by a Pallite VIII lamp with a total power of 2400 watts or by two 500-watt lateral lamps. The light was reflected by the mercury bath at the sidewall, whereas bubbles in the jet, being curved surfaces, did not reflect. Thus, on the negative film, the bubbles appear quite distinctly as light spots in contrast to the bath which is dark.

2.1.1.5 Pressure Measurements

In order to measure the pressure in the tuyere, the plexiglas sidewall was tapped in four positions along the axis of the half-tuyeres as shown in Figure 5. The first pressure tap was located just upstream of the nozzle exit, internally tangent to the exit plane. In the case of the full-tuyere, the pressure taps were inserted through the walls of the tuyere pipe. The pressure was measured with a fast-response, Bell and Howell-CEC pressure transducer (type 4-313-0001). The output signal from the transducer was then recorded on a Tektronix storage oscilloscope (Type 564). The pressure traces observed on the oscilloscope screen were photographied with a Polaroid camera. Thus, detailed information was obtained regarding average pressures along the tuyere as well as pressure oscillations at the tip of the nozzle.

2.1.2 General Procedure

First a set of flow conditions was chosen as follows: type of tuyere, type of gas, pressure and gas flow. Next the gas was turned on, the sidewall of the tank was illuminated, and a high speed film was taken (about 5 seconds were required to take a 100-foot film at a speed of 800 frames per second). Then maintaining the same flow conditions, the pressure was measured in the four positions along the tuyere to obtain the average pressure profile. The pressure oscillations at the tuyere tip were recorded subsequently with the storage oscilloscope, and Polaroid photographs of the resulting traces were taken for each set of flow conditions. In the case of full-tuyeres only pressure measurements were made, because the jet was not visible.

2.1.3 Conditions for the Tests

The following parameters were studied in the mercury tests:

i) Gas density - air, helium and argon

ii) Tuyere diameter

iii) Tuyere design - straight-bore (half and full-tuyere) and convergent-divergent (half-tuyere).

Table I

RANGE OF VARIABLES

System	Tuyere Type	Nozzle Diameter (cm)	Mass Flux Range [g cm^{-2} s^{-1}]	Mach Number Range (inside the tuyere)
Air-Mercury	Straight-bore, half-tuyere	0.2 0.325 0.476	4 to 150	0.09 to 0.90
Air-Mercury	Straight-bore, full-tuyere	0.325	5 to 75	0.20 to 0.90
Air-Mercury	Convergent-Divergent half-tuyere	D_{min} = 0.372 D_{max} = 0.476	5 to 85	0.12 to 1.30
Helium-Mercury	Straight-bore half-tuyere	0.2	10 to 55	0.47 to 0.75
Argon-Mercury	Straight-bore half-tuyere	0.2	30 to 180	0.43 to 0.75

The range of variables is summarized in Table I.

2.1.4 Validity of the Method

Because the tank wall may significantly affect the jet behaviour, an important aspect of the work was to evaluate the validity of employing half-tuyeres to study the behaviour of submerged gas jets in liquids. To investigate the influence of wall proximity, results obtained with a half-tuyere were compared to corresponding data measured for a full-tuyere under similar flow conditions. Three types of checks were made:

i) Jet profiles for several flows in half-tuyeres were compared to the average values obtained by Oryall and Brimacombe, who used full-tuyeres. Figure 6 shows the contour of the jet under similar flow conditions (N_{Fr} = 19.6; tuyere dia. = 0.476 cm) for both studies. It can be seen that in the two cases the profiles are in good agreement, especially at short distances from the tip. Both methods show the wide angle of expansion, the rearward penetration of the gas, and the almost vertical trajectory of the jet. The agreement is not as good at greater distances from the tip of the nozzle. This can be partly explained by the retarding action of the wall and also

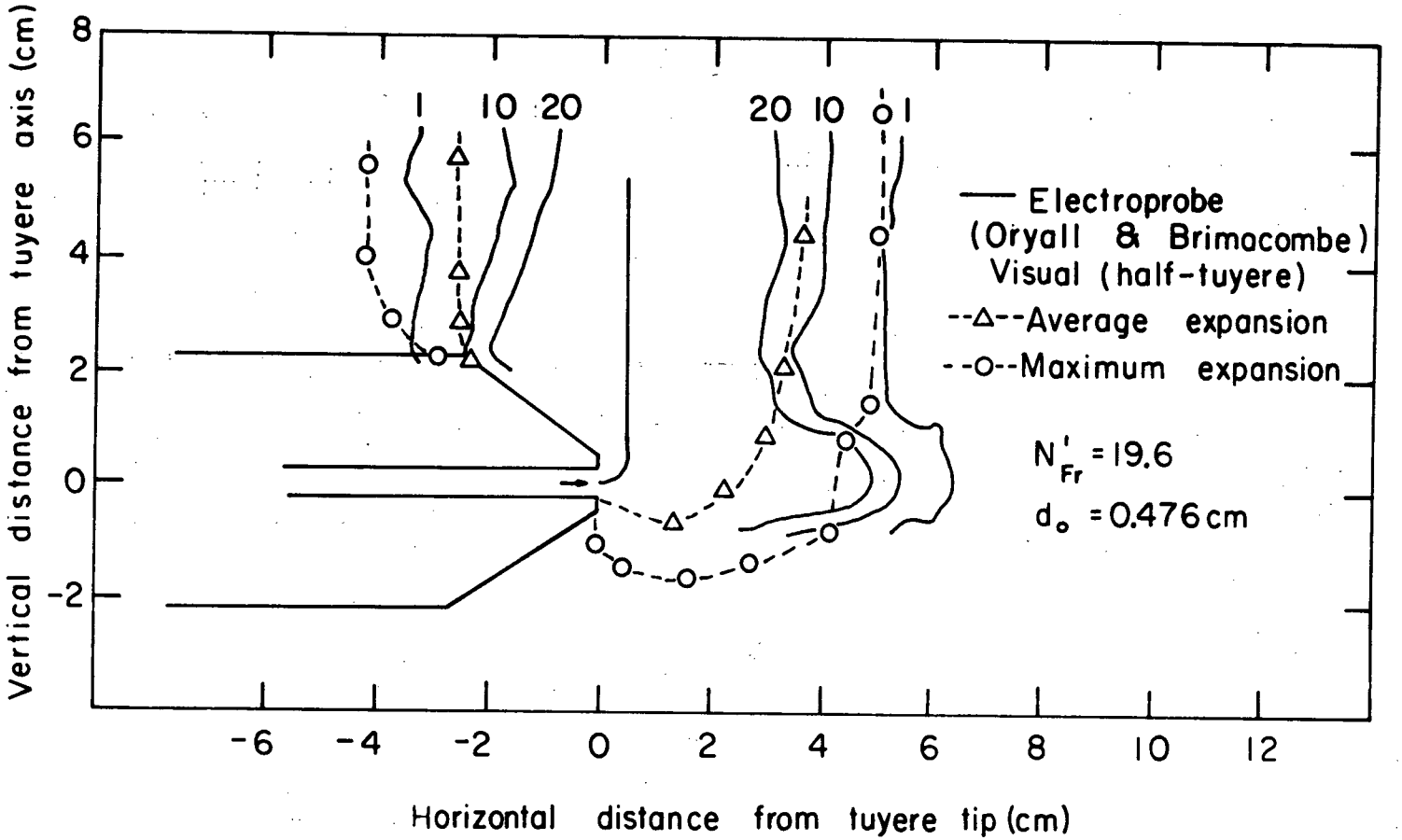

Fig. 6 Jet Contours for Half- and Full-Tuyeres.

by the fact that some bubbles move away from the wall and cannot be seen in the film.

ii) A second comparison, was made by analysing the pressure oscillations at the tip of full and half-tuyeres. Figure 7 shows pressure pulses for full and half-tuyeres, under similar flow conditions. It can be observed that the pressure traces are similar in shape and frequency for a wide range of gas flows.

iii) A third comparison, was achieved by examining pressure and Mach number profiles in the two types of tuyeres. Good quantitative agreement was again found as can be observed comparing Figures 46 and 47, or 51 and 52, of Appendix III.

Thus, it can be concluded that a half-tuyere, attached to a transparent wall, gives representative results inside the tuyere and also at short distances (10 to 15 diameters) beyond the tip of the nozzle. The events at the tip itself can be observed very accurately. At greater distances from the tip the results have qualitative value. The results of these tests show that the technique employed in this work is a useful method of studying gas injection into opaque liquids.

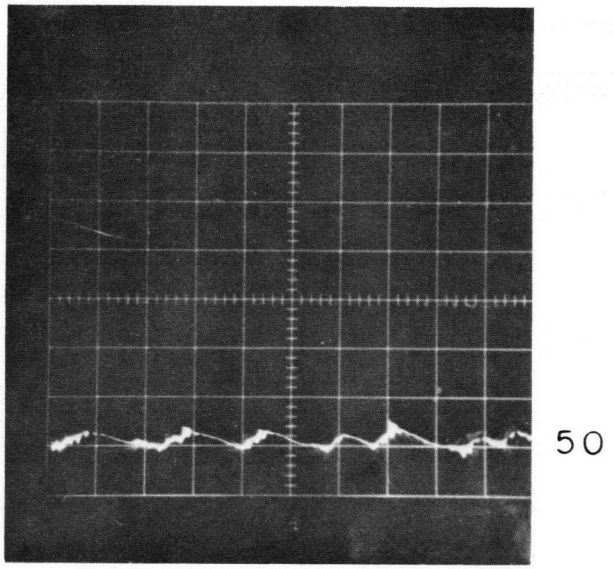

1.- Half-tuyere, 0.325 cm. dia.,
2.29 psi/div, Mach=0.464

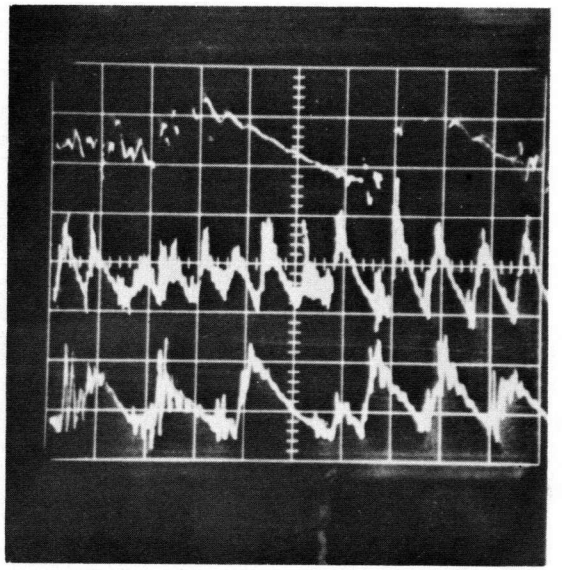

2.- Full-tuyere, 0,325 cm. dia.,
0.963 psi/div, Mach=0.459

Pressure Oscillations, Air-Hg

Fig. 7 Pressure Pulses for Half and Full-Tuyeres.

2.2 Jets in Water and in Aqueous Solutions of $ZnCl_2$

Gas jets were also injected horizontally into both water and an aqueous solution of zinc chloride. Although the solutions are transparent, half-tuyeres were used in order to obtain results that could be more easily compared to the mercury tests. Another reason for using half-tuyeres is that the illumination techniques are simpler than those for a jet produced by a full-tuyere in the centre of a bath.

The $ZnCl_2$ solution used was nearly saturated, having a density of 1.9 g cm^{-3}. The physical properties of the liquids and gases employed in the experiments are shown in Table II.

2.2.1 Experimental Apparatus and Procedure

The apparatus was very similar to that employed in the mercury tests. The main difference was the use of another tank with dimensions of 55.9 cm in length, 26.7 cm in width and 34.3 cm in height. In order to avoid the corrosive properties of the solutions employed,the vessel was made entirely of 1.905 cm thick plexiglas plates. Horizontal baffles were attached to the plexiglas sidewalls to avoid

Table II

COMPARATIVE PHYSICAL PROPERTIES OF GASES AND LIQUIDS AT 20°C

	Air	Helium	Argon	Water	$ZnCl_2$ aq. Solution	Mercury
Density [g cm^{-3}]	1.29×10^{-3}	0.18×10^{-3}	1.78×10^{-3}	1.0	1.9	13.6
Surface Tension [dynes cm^{-1}]	-	-	-	73.5	71.6	465
Viscosity [C_p]	1.8×10^{-2}	1.9×10^{-2}	2.2×10^{-2}	1.0	12 to 13	1.6
Kinematic Viscosity	0.140	0.106	0.124	0.010	0.066	0.001

slopping of the bath. The tank was sealed with a plexiglas cover and the exit gases were directed to a fume hood. The tank was filled with solution to a height of 17 cm above the tuyere centre-line. A horizontal half-tuyere made of plexiglas was fastened to the sidewall of the tank, and again, pressure taps were drilled through the plexiglas sidewall along the tuyere axis. The remainder of the apparatus was similar to that used in the mercury tests. A pressure transducer and storage oscilloscope were again used to measure and record the pressure along the tuyere while the high-speed camera was employed to obtain films of the jets. The general procedure followed was the same as for the mercury tests.

CHAPTER 3

LABORATORY RESULTS

3.1 Jets in Mercury

The air-mercury system was the most thoroughly studied for a wide range of gas flows, different nozzle diameters and tuyere designs.

Frame-by-frame analysis of the high-speed films was conducted using a film analyzer and digitizer. In this way it was possible to obtain the contour of the jet along with the forward and backward penetrations. Also, individual photographs from the films were isolated easily to illustrate the different flow regimes that were obtained in the jets.

The pressure and Mach number profiles were plotted with respect to the distance from the tuyere tip. Forward and backward penetrations, as well as the jet trajectory, were represented by the dimensionless number ℓ/d (ℓ = penetration of the jet; d = nozzle diameter). The frequency and amplitude of pressure pulses in the tuyere were measured from photographs of the oscilloscope traces.

The results for helium and argon injected into mercury were presented in the same manner.

3.1.1 Effect of Gas Flow

3.1.1.1 Observations from High-Speed Films

Analysis of the high-speed films quickly showed that, depending on gas flow rate, two flow jetting regimes could be distinguished: a "pulsing" regime at low flows, and a "steady jetting" regime at high flows. In the pulsing regime, the jet is not continuous but consists of large bubbles or gas pulses which form at the tuyere and then rise almost vertically. This behaviour can be observed in Figure 8, which shows a sequence of six photographs taken from a high-speed film of air injected into mercury at a Mach number of 0.3. Photos 1 to 3 show one such bubble being formed at the tip of the nozzle. It grows essentially upward with little forward penetration. In Photo 4 the bubble is fully formed and commences to rise. Photos 5 and 6 show the bubble rising vertically while mercury has flowed into the space vacated by the bubble in front of the nozzle. Another important feature of the pulsing regime is that during much of its ascent the bubble does not break up. This observation indicates that when a low gas flow is used a relatively

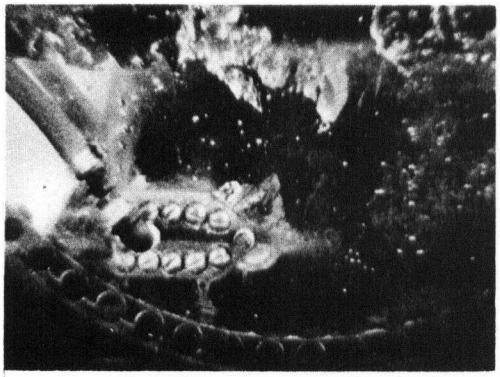

1.- t = 0 s

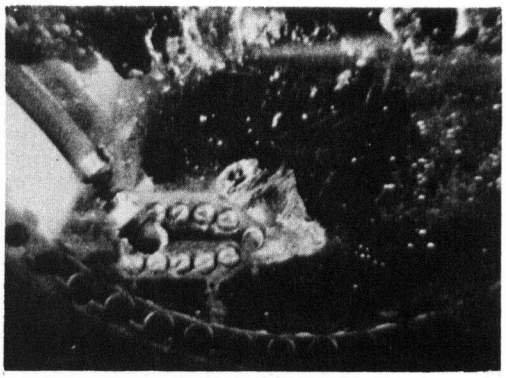

2.- t= 0.018s

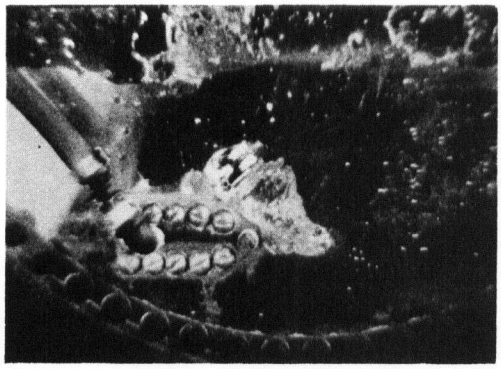

3.- t= 0.036 s

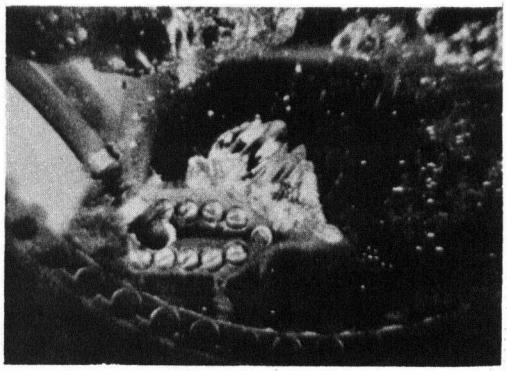

4.- t= 0.054 s

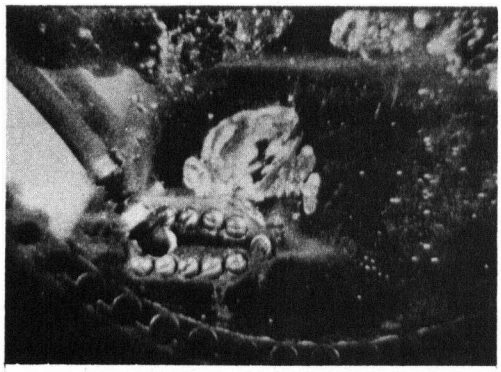

5.- t= 0.074 s

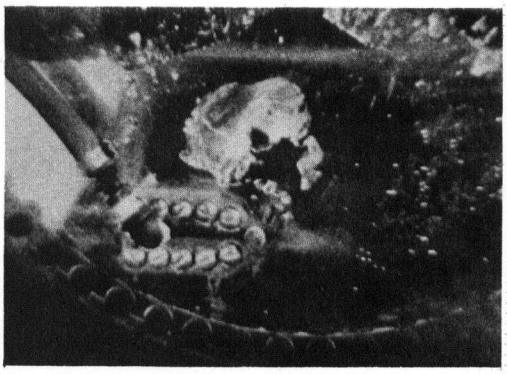

6.- t= 0.094s

Air in mercury d_o=0.476cm Ma_o=0.30 $\dot{M}$ =15.6g/cm^{2}s

Fig. 8 Sequence of Photographs from High-Speed Films, for Low Flow of Air into Mercury.

small surface area of contact is generated.

The steady-jetting regime was found at higher gas flows. Figure 9 shows a sequence of six photographs taken from a high-speed film of air discharging into mercury, for a "nominal" Mach number of 1.2 at the tip*. Photos 1 and 2 show the gas penetration in the bath to be greater than that in the pulsing regime. As shown in Photos 3 and 4, a neck is seen to form a short distance downstream of the nozzle tip. Photos 5 and 6 indicate that the bubble rises following a path that penetrates deep into the bath. It can also be observed that after the bubble is formed and rises, part of the jet remains at the tip preventing the mercury bath from fully enveloping the nozzle. This regime, characterized by the continuous presence of a short stable jet at the nozzle tip, was formed for nominal Mach numbers greater than 1. From these photos it should be noticed that the

---

* Note: Mach numbers upstream of the tip correspond to the speed of the gas in a straight-bore pipe, and are always less than one regardless of the back pressure. When the gas reaches the tip of the nozzle, it undergoes a multidirectional expansion. The Mach numbers calculated at this point do not give a direct measurement of the linear speed of the gas. Instead, they give a measure of the degree of underexpansion or supercriticality of the jet at that position. Therefore, in relation to the tip of the nozzle, they are called "nominal" Mach numbers.

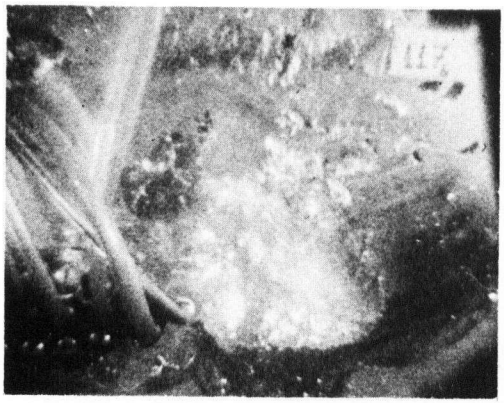

1.- t = 0 s

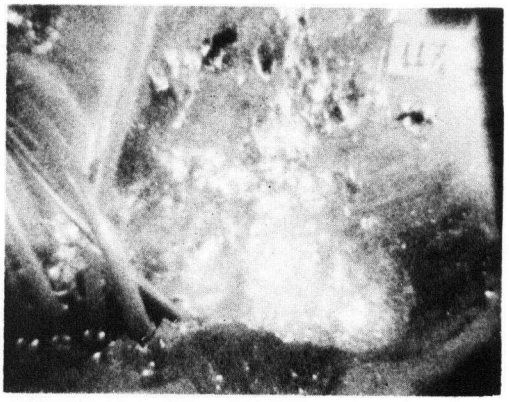

2.- t = 0.016 s

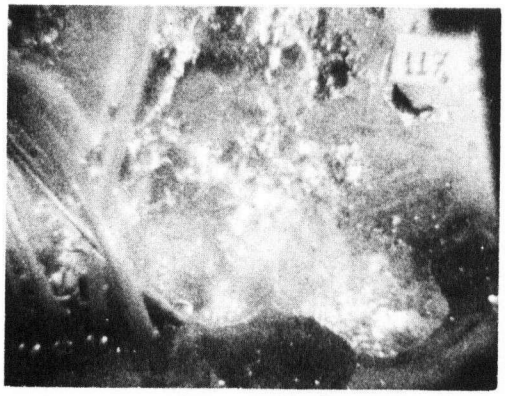

3.- t = 0.034 s

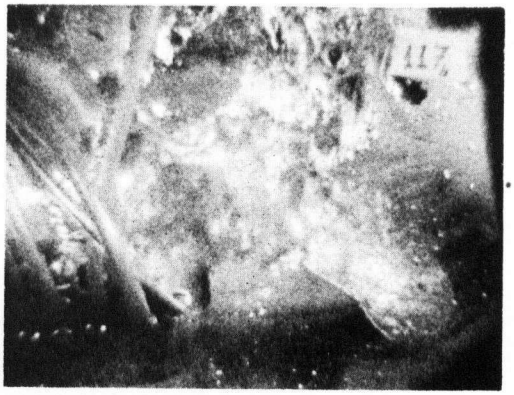

4.- t = 0.050 s

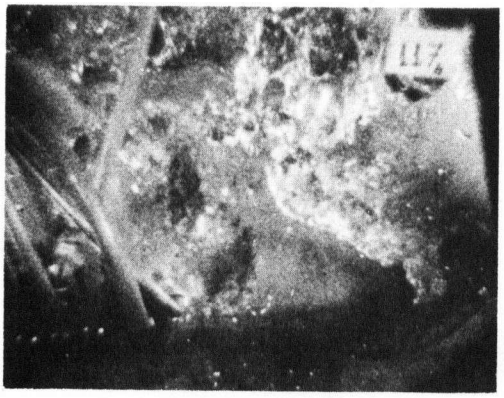

5.- t = 0.066 s

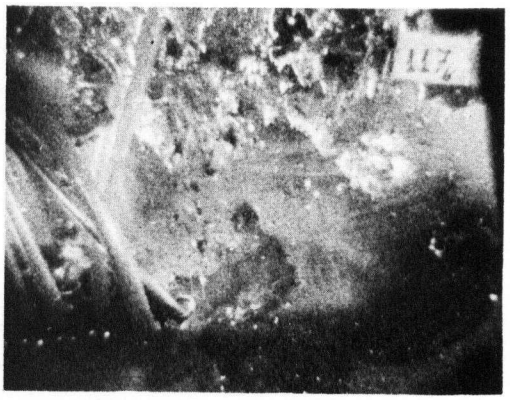

6.- t = 0.083 s

Air in mercury $d_o = 0.476$ cm $Ma_o = 1.2$ $\dot{M} = 74.9$ g/cm^{2}s

Fig. 9 Sequence of Photographs for High-Speed Films, for High Flow of Air into Mercury.

rising bubble breaks down into a number of smaller bubbles.

A transition regime was observed for Mach numbers at the tip between 0.8 and 1.0. This regime consists of periods of jetting, alternating with periods of pulsing. For air injection into mercury, this transition corresponds to a gas mass flux of approximately 50 g cm^{-2} s^{-1}. Similar results were obtained for helium and argon injection into mercury, and they will be discussed later. Appendix I shows sequences of photos taken from high speed films at different gas flows for air, helium and argon injection through a 0.2 cm. diameter half-tuyere into mercury.

3.1.1.2 Pressure Oscillations

The pressure pulses measured at the tip of the nozzle were found to be strongly affected by the flow regime. The influence of gas flow rates on pressure pulsing is shown in Figure 10 for air discharging into mercury from a 0.476 cm. dia. half-tuyere. For a very low flow rate, Mach number = 0.09, Photo 1 shows the pulses to be smooth with small amplitudes. For increased flow rates, Photos 2 and 3, Mach numbers of 0.34 and 0.68 respectively, show the peaks to be much sharper than those observed at low flow rates. The behaviour

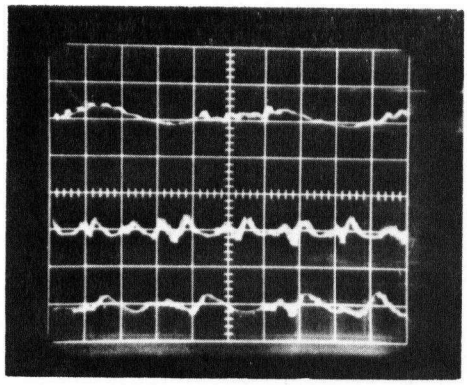

1.- Ma_o=0.091 $\dot{M}$=8.38 g/cm^{2}s

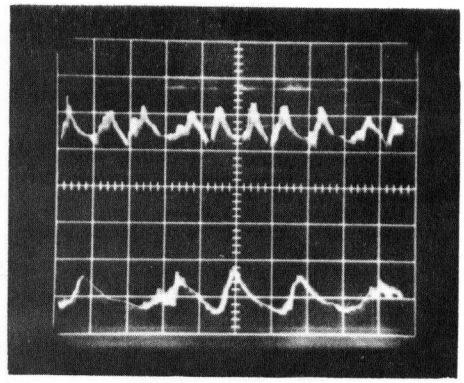

2.-Ma_o=0.336 $\dot{M}$=17.01 g/cm^{2}s

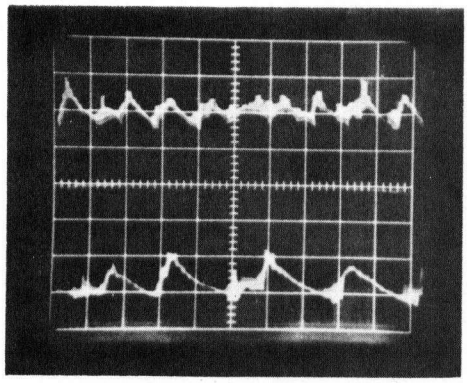

3.-Ma_o=0.675 $\dot{M}$=34.83 g/cm^{2}s

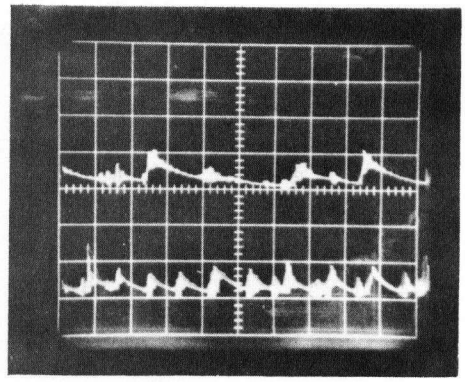

4.-Ma_o=0.937 $\dot{M}$=48.15 g/cm^{2}s

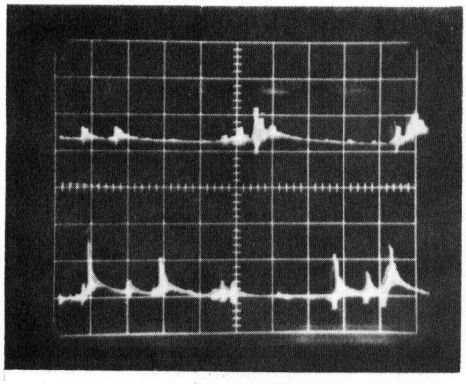

5-Ma_o = 1.205 $\dot{M}$ =67.04 g/cm^{2}s

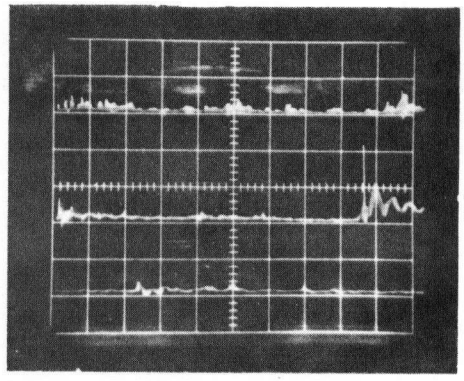

6-Ma_o=1.279 $\dot{M}$ =81.37 g/cm^{2}s

Air in mercury half tuyere d_o=0476cm sensitivity 229 psi/div (vert axis)

Fig. 10 Pressure Pulses for Air-Hg

seen in Photos 2 and 3 is typical of that found for a wide range of subsonic flows between Mach numbers of approximately 0.2 and 0.8. In this region the peaks are characterized by a sharp increase in pressure until a maximum is reached, followed by a more gentle decline. The amplitude of the oscillations is between 2 and 2.5 psi, with frequencies varying from 8 to 15 pulses per second. Photo 4 corresponds to a nominal Mach number of 0.94 which is in the transition regime. As seen in Photo 4, both the amplitude and frequency of the pressure oscillations become more irregular. In the transitional regime the falling part of the pressure pulse is seen to be longer with a smaller slope. Photos 5 and 6 correspond to still higher flow rates, in the steady jetting regime, with nominal Mach numbers of 1.20 and 1.28, respectively. Photo 5 shows the pulses to be less frequent (approximately 4 pulses per second) and more irregular than in the pulsing regime. Almost no pulses are observed in Photo 6, the pressure being practically steady. It is worthwhile mentioning that the relationship between the mass flux and the nominal Mach number at the tip is not linear. In fact, for a case of compressible flow, the continuity equation can be written as

$$\rho \, v = \dot{m}$$

where $\dot{m}$ = mass flux[g cm^{-2} s^{-1}];

ρ = gas density[g cm^{-3}]; and

v = gas velocity[cm s^{-1}]

For a gas, an increase in the back pressure causes both ρ and v to increase. Therefore Photo 6 (Mach number = 1.28) corresponds to a mass flux that is 20% higher than the case for Photo 5 (Mach number = 1.20).

The amplitude of the pressure oscillations was also found to depend on the tuyere diameter and the gas employed, and will be shown later. Appendix II shows pressure traces for different gases injected into mercury, for tuyere diameters of 0.2, 0.325 and 0.476 cm., under a wide range of gas flow rates.

3.1.1.3 Relation between Pressure Oscillations and Gas Dynamics at the Tuyere Tip

In order to correlate the events observed in the jet to the pressure oscillations measured at the tuyere tip, high-speed films were taken with both the jet and the oscilloscope screen in the field of view. Figure 11 summarizes the results for a low flow of air into mercury (Mach = 0.48, 0.476 cm. dia., half-tuyere). The relation

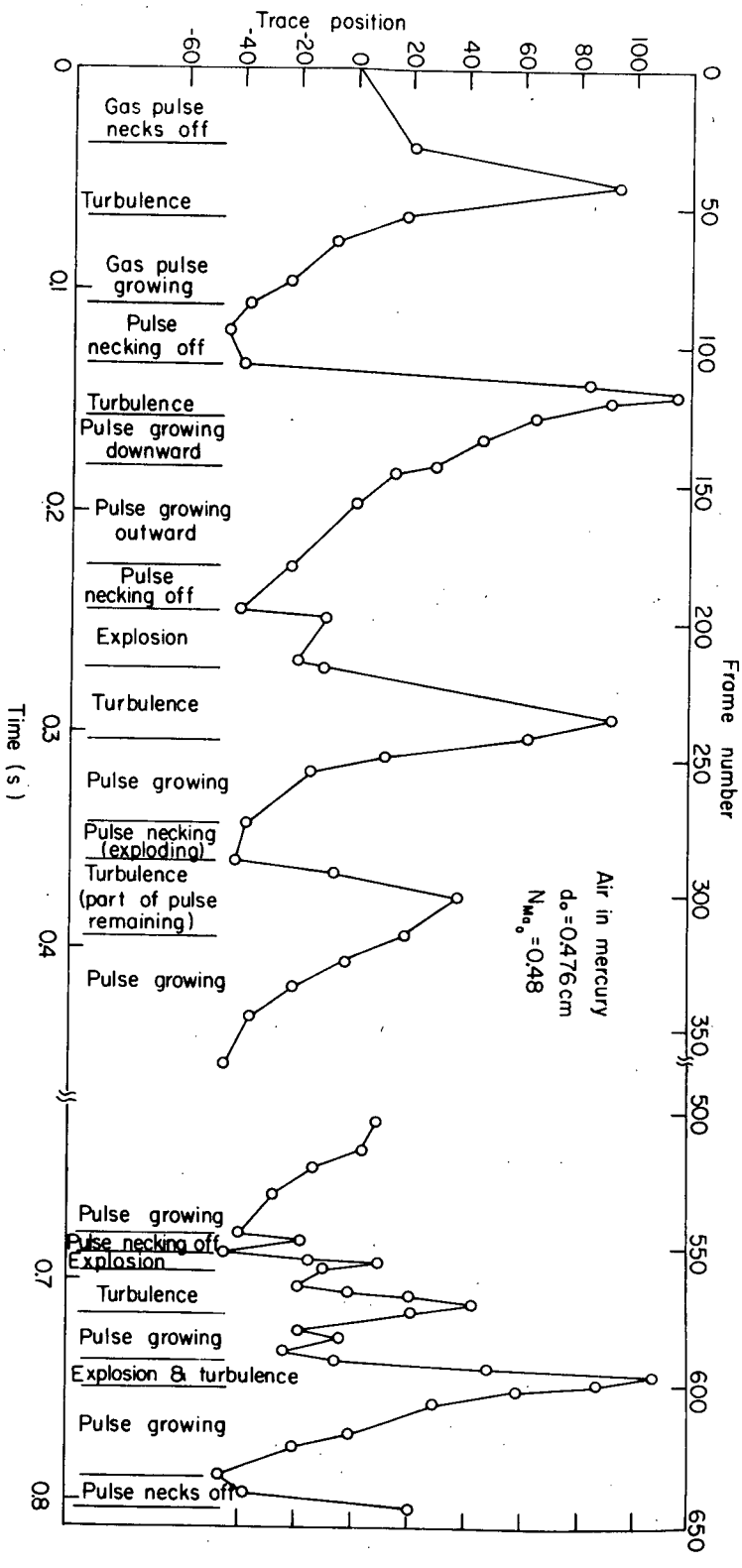

Fig. 11 Relation between Pressure Oscillation and Gas Dynamics at the Tuyere Tip, for Low Flow of Air into Mercury.

between pressure pulses and bubble formation at the tip is evident in that a smooth decrease in pressure corresponds to the growth of a bubble at the tip. As the bubble increases in size, the pressure decreases further until a minimum is reached. This minimum corresponds to the moment when the pulse necks off, and the bubble moves away from the tuyere. This minimum was observed to be followed by a sharp increase in the pressure due to the bath flowing in around the nozzle to replace the volume of the vacating gas pulse. After a maximum is reached the pressure decreases again, while a new bubble is formed at the tip, and the cycle is repeated. Figure 12 shows the results for a high flow of air into mercury (Mach = 1.2; 0.476 cm. dia., half-tuyere). Unlike the pulsing regime, there is no regular pattern in the pressure trace. Oscillations are irregular and of smaller amplitude with no definite relation between them and the bubble formation observed in the jet from the high-speed film. This was observed in what has been termed the steady jetting regime, and corresponds to the conditions of underexpanded jets.

Thus, it can be said that the pressure measurements along the tuyere, especially at the tip, can be used to obtain information about flow regimes in jets for full tuyeres, when it is not possible to view the jet itself.

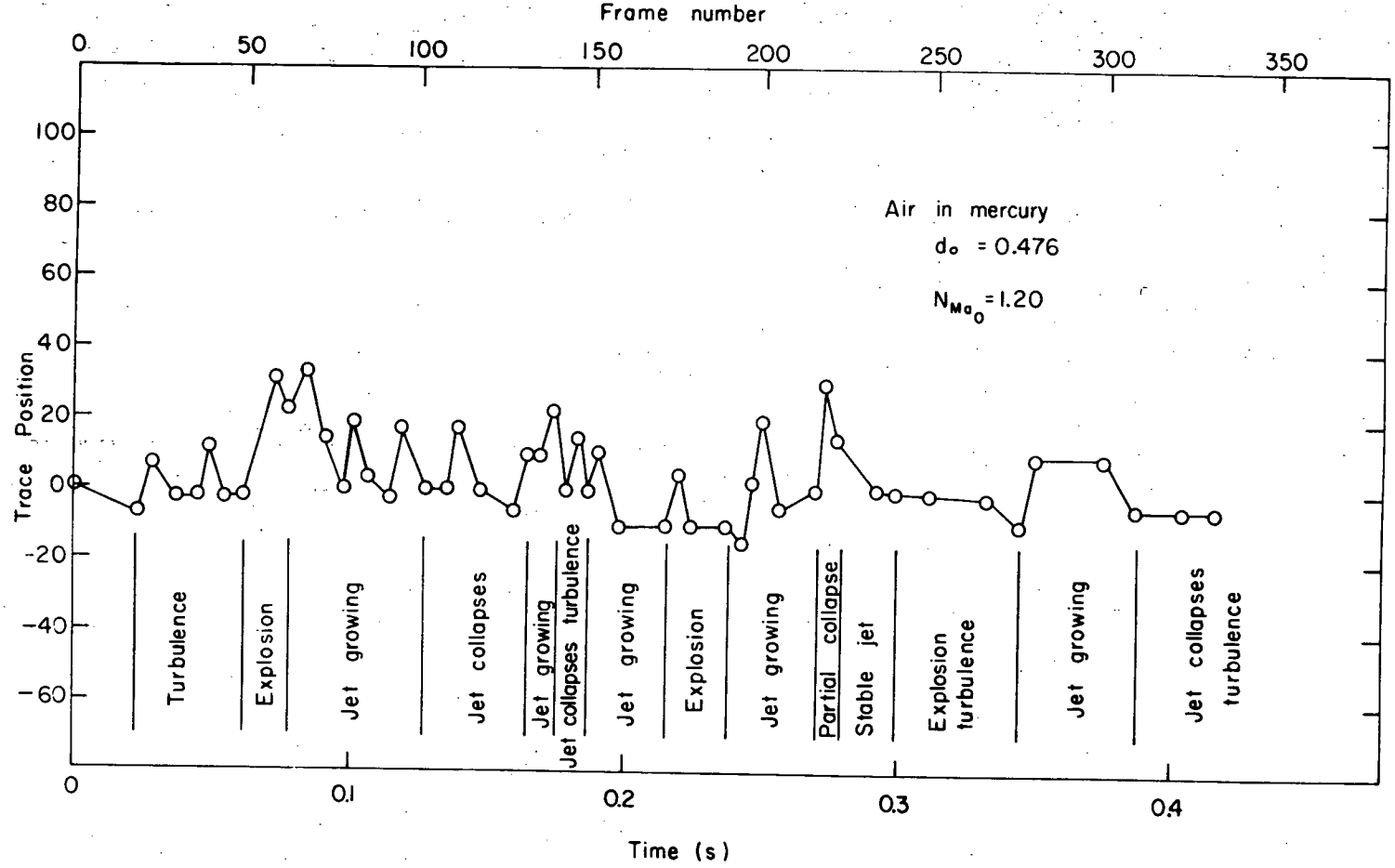

Fig. 12 Relation between Pressure Oscillation and Gas Dynamics at the Tuyere Tip, for High Flow of Air into Mercury.

3.1.1.4 Pressure and Mach Number Profiles

Pressure was measured in different positions along the tuyere, upstream from the tip. Figure 13 shows the pressure profile (relative to atmospheric pressure plus the height of the mercury bath) along a 0.476 cm dia. half-tuyere. In Figure 13 different curves correspond to different mass fluxes of air. It can be seen from these curves that at low flow rates, the pressure decreases steadily along the tuyere, and becomes zero at the tip. This behaviour is observed at gas flows lower than 20 g cm^{-2} s^{-1}. For higher flow rates, 20 to 40 g cm^{-2} s^{-1}, the pressure decrease along the nozzle is sharper, but still remains zero at the tip itself. At even higher mass fluxes the pressure at the tip is no longer zero which corresponds to the transition from fully-expanded to underexpanded jets. For air injection into mercury this transition was observed at a mass flux of approximately 50 g cm^{-2} s^{-1}. The exact mass flux at the transition point is difficult to measure being dependent on the gas that is injected. The pressure at the tip continues to increase with further increase in the gas mass flux. It is worthwhile mentioning that quantitative agreement was observed for pressure profiles in the case of air injection into mercury for the case of half and full tuyeres. Appendix III shows pressure profiles for air injection into mercury, for different tuyere diameters.

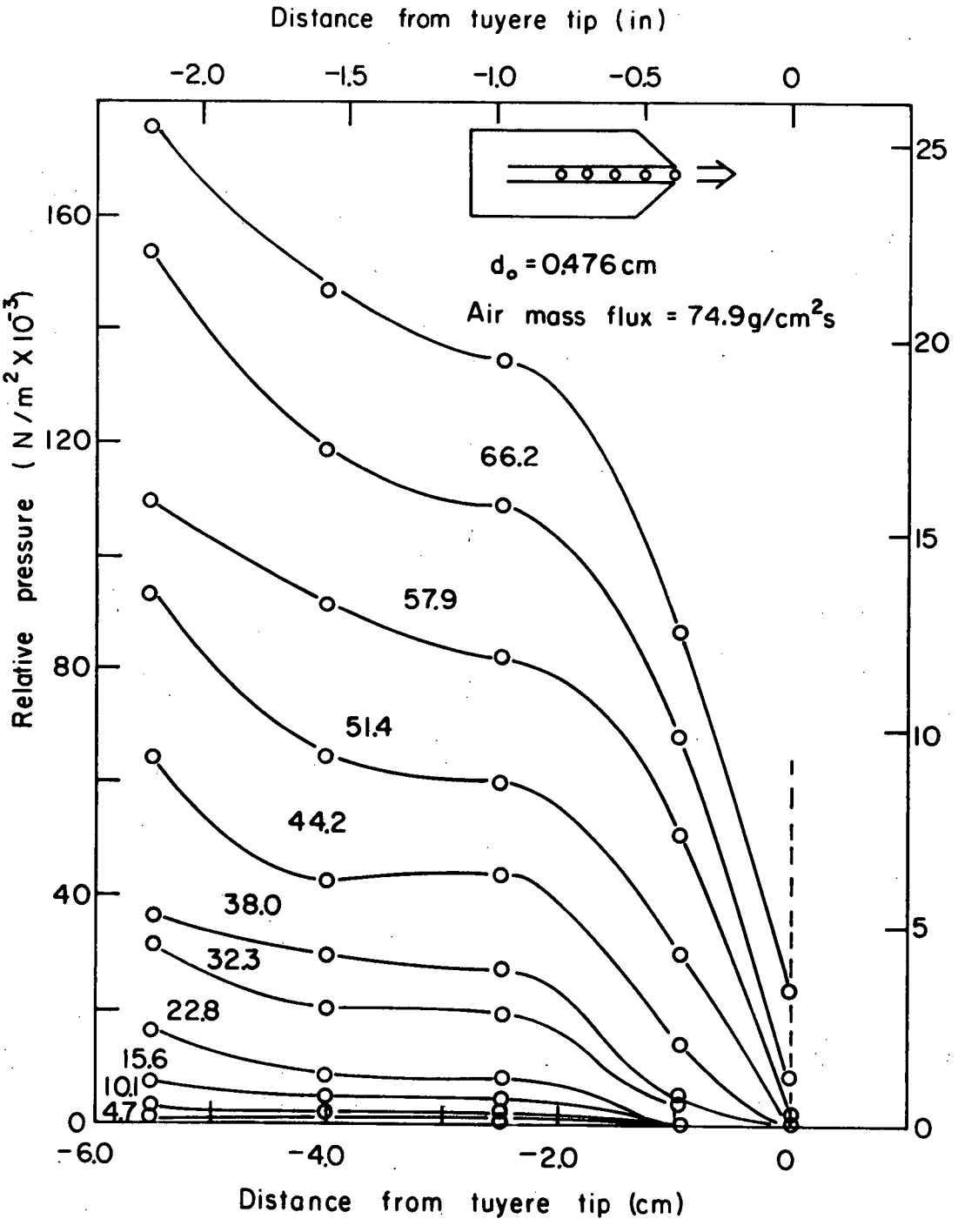

Fig. 13 Pressure Profiles, Air-Hg, 0.476 cm. dia. Half-Tuyere.

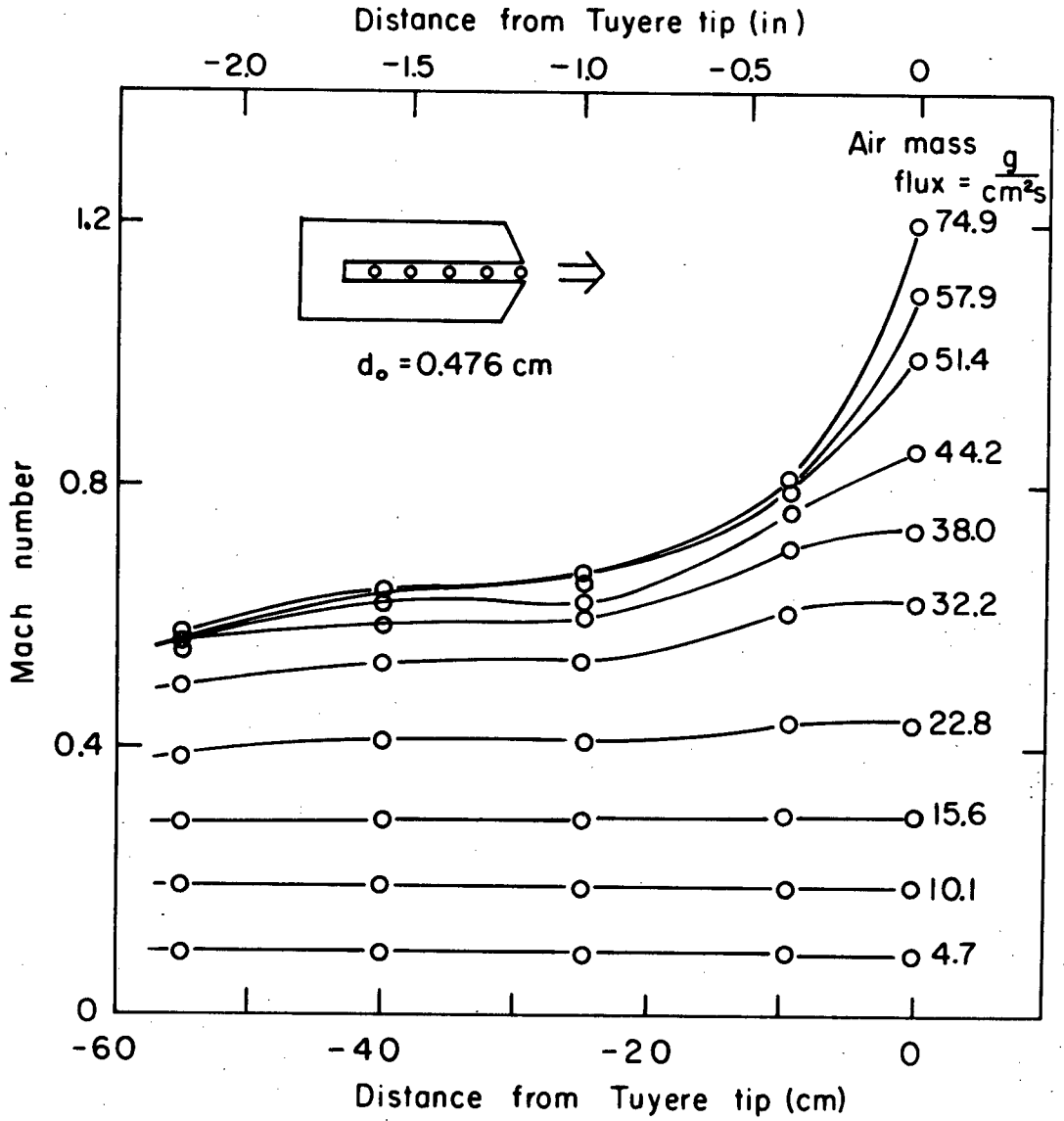

Fig. 14 Mach Number Profiles, Air-Hg, 0.476 cm. dia. Half-Tuyere.

Table III

RESULTS FOR AIR-MERCURY, STRAIGHT-BORE, HALF-TUYERE

Diameter = 0.476 cm

Volumetric Flow at 1 atm. and Room Temp. [$cm^3\ s^{-1}$]	Distance from Tuyere Exit										Froude Number	Gas Speed [$cm\ s^{-1}$]	Mass Flux [$g\ cm^{-2}\ s^{-1}$]	Reynolds Number
	x_1 = 0. cm		x_2 = -0.953cm		x_3 = -2.48 cm		x_4 = -4.00 cm		x_5 = -5.52 cm					
	Press. (psi)	Mach	Press. (psi)	Mach	Press. (psi)	Mach	Press. (psi)	Mach	Press. (psi)	Mach				
323.7	0	0.091	0	0.091	0.048	0.091	0.096	0.091	0.140	0.091	3.88	3227	4.703	6740
691.6	0.048	0.195	0.00	0.196	0.289	0.192	0.289	0.192	0.480	0.190	17.84	6916	10.048	14445
1070.7	0.096	0.301	0.00	0.303	0.630	0.291	0.720	0.290	1.06	0.289	42.50	10675	15.556	22296
1571.7	0.096	0.442	0.096	0.443	1.160	0.415	1.250	0.413	2.41	0.388	91.66	15676	22.837	32741
2218.7	0.00	0.627	0.46	0.610	2.84	0.535	2.96	0.532	4.52	0.492	184.44	22237	32.234	46444
2616.7	-0.289	0.740	0.690	0.710	3.95	0.597	4.30	0.587	5.27	0.561	256.90	26244	38.020	54813
3039.2	-1.440	0.859	2.060	0.764	6.36	0.620	6.18	0.625	9.28	0.550	346.16	30464	44.158	63627
3538.7	-0.096	1.000	4.35	0.792	8.70	0.655	9.39	0.637	13.52	0.550	469.15	35465	51.416	74072
3983.3	0.240	1.110	7.33	0.779	11.91	0.654	13.29	0.623	15.89	0.573	578.03	39366	57.877	82219
4585.2	1.250	1.205	9.85	0.811	15.93	0.669	17.25	0.633	22.25	0.551	681.20	42735	66.621	89256
5092.6	3.470	1.203	12.60	0.825	19.52	0.667	21.34	0.635	25.42	0.573	678.94	42664	74.853	89108

The Mach number can be calculated at the points where the pressure has been measured. Figure 14 shows the Mach number profile for air injection into mercury through a 0.476 cm. dia. half-tuyere. It is observed that at low flow rates, below 20 g cm^{-2} s^{-1}, the Mach number remains almost constant along the tuyere. As the gas mass flux increases, the Mach number begins to show a noticeable increase at positions close to the tip, but it has a fairly flat profile further upstream. For mass fluxes greater than the transition value (approximately 50 g cm^{-2} s^{-1}) from fully expanded to underexpanded jets the Mach number increases very sharply at positions close to the tip, the increase being steeper for higher gas flows. However, at positions upstream from the nozzle tip the Mach number increases slowly along the tuyere, and remains practically unaffected by changes in the mass flux, at a value somewhat smaller than one. Mach number profiles for different test conditions are shown in Appendix III. Table III summarizes the results for air injection into mercury through a 0.476 cm. dia. half-tuyere. Results from tests performed under different conditions are shown in the Tables of Appendix IV.

3.1.2 Effect of Gas Density

The influence of gas density was studied by blowing helium

and argon, which have densities below and above that of air. Table II summarizes the physical properties of these gases together with those of the liquids used as a bath media. With the exception of tuyere diameter, these experiments were performed under similar conditions to those of the air-mercury experiments. For argon and helium tests, a 0.2 cm.dia. half-tuyere was used, to decrease the consumption of bottled gases. Figures in Appendix III show pressure profiles for the argon and helium injection into mercury. As expected, the mass flux is higher for argon than for helium for the same given pressure at any point in the tuyere. For argon the pressure can be seen to be high along most of the tuyere, and decreases sharply only at a short distance from the tip. For helium the pressure decreases steadily along the tuyere. In the regimes of underexpanded jetting the terminal pressure at the tip is higher for argon than for helium, at the same upstream pressure values.

Oscilloscope traces of pressure oscillations measured at the tip of the nozzle show that the shape of the pulses for helium and argon under conditions of pulsing or steady jetting are similar to those found for air injection into mercury. However, the amplitude of the oscillations was observed to be dependent on the gas type, being larger for a lower density gas. Figure 15 shows pressure traces for helium and argon injected into mercury through the 0.2 cm.

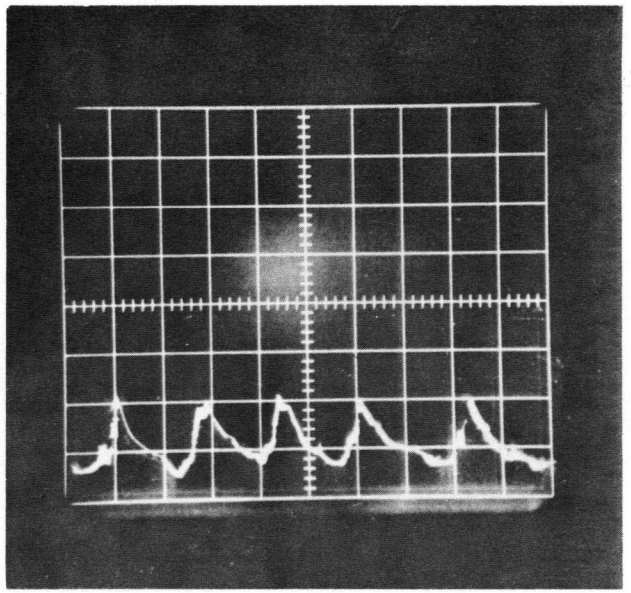

1.- Helium-Mercury, 2.29 psi/div,
Mach=0.681

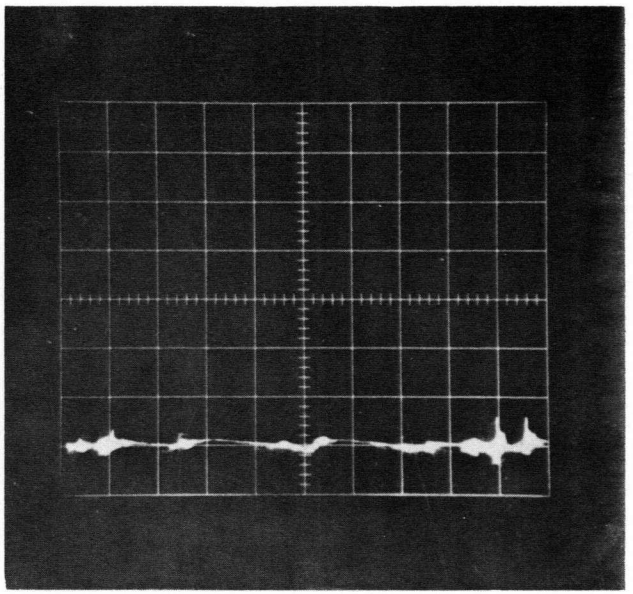

2.- Argon-Mercury, 9.08 psi/div,
Mach=0.698

Pressure Oscillations, He-Hg and Ar-Hg,
0.2 cm dia., Half-tuyere

Fig. 15 Pressure Pulses, A-Hg and
He-Hg, 0.2 cm. dia. Half-Tuyere.

dia. half-tuyere. Pressure traces for a wide range of flow rates of the different gases injected into mercury are shown in Appendix II.

The results from the high-speed films confirmed the dissimilar characteristics of the jets obtained when blowing different gases into mercury. For the case of helium, the pulses consist of a rather violent gas expansion at the tip, at low flow rates. At high gas flows, a steady jetting regime was attained, but it appears to be unstable even at high Mach numbers. For argon the amplitudes of the pulses are smaller than for helium, and at high gas flows a very smooth jetting regime was observed.

The transition from the pulsing to the jetting regime was found to depend on the gas injected. For helium it occurs at a mass flux of about 28 g cm^{-2} s^{-1}; in the case of argon this value is approximately 65 g cm^{-2} s^{-1}, while for air it is between 50 and 55 g cm^{-2} s^{-1}.

Sequences of photographs taken from high-speed films of the air, helium and argon jets in mercury are shown in Appendix I.

3.1.3 Effect of Tuyere Diameter

The influence of the tuyere diameter on the jet was studied by blowing air into mercury using straight-bore half-tuyeres. Figures of Appendix III show pressure profiles along the tuyere for nozzle diameters of 0.2 and 0.375 cm, and different mass fluxes of gas. It is observed that for a smaller diameter the pressure remains high along most of the tuyere and drops sharply near the tip. For a larger tuyere diameter the pressure drop is more evenly distributed along the tuyere. For a given mass flux, the overall pressure drop in the tuyere is larger for a smaller nozzle diameter, and thus the terminal pressure at the tip is lower when underexpanded jet conditions are obtained.

3.1.4 Effect of Tuyere Design

The behaviour of jets produced by blowing through a convergent-divergent nozzle was also studied. The main objective was to observe the flow regimes that can be obtained when a high speed, supersonic gas is injected into the liquid bath. The tuyere employed is shown in Figure 5, while the design characteristics

have been specified in Section 2.1.1.2.

Although the design of the nozzle is specific to particular values of gas flow and pressure, it was decided to study a range of gas flows, as the presence of the mercury bath introduces some uncertainty in the design parameters. Figures 16 and 17 show the pressure and Mach number profiles, respectively, that were obtained using this nozzle.

From the pressure profiles it can be seen that at very low mass fluxes, less than 15 g cm^{-2} s^{-1}, the pressure reaches a minimum at the constriction. Because the pressure drop in the divergent portion of the tuyere is small, this minimum does not differ much from the ambient pressure at the tip. This also means that the gas moves at subsonic speed all along the tuyere. At intermediate gas flows, 23 to 55 g cm^{-2} s^{-1}, the minimum in the pressure is noticeably lower than the ambient pressure at the tip and appears to occur not at the constriction, but rather at a point downstream from

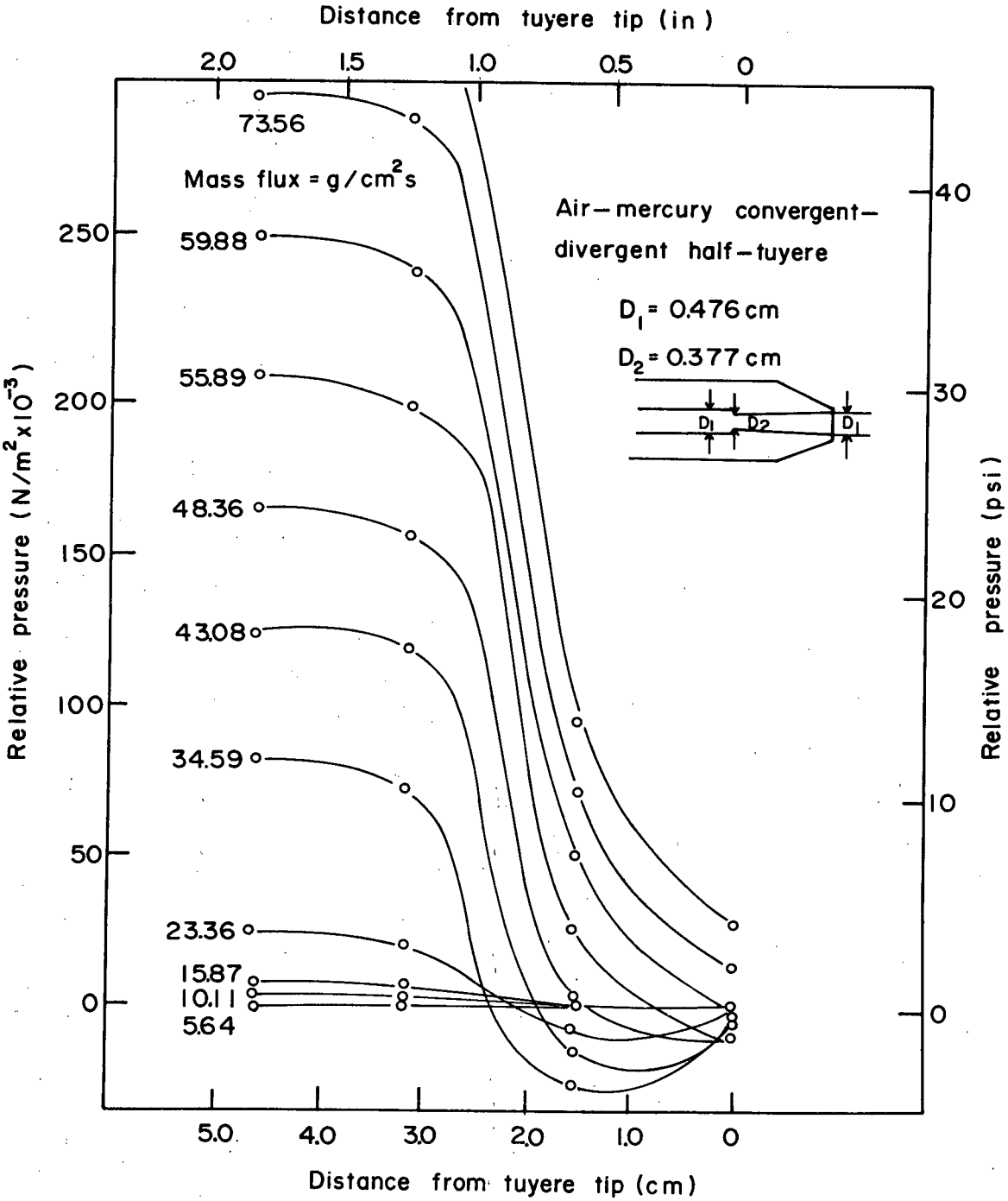

Fig. 16 Pressure Profiles, Air-Hg, Convergent-Divergent Tuyere.

it, in the divergent section of the nozzle. This indicates that the gas has been accelerated after passing through the constriction,which can happen only if sonic velocity has been reached at that point. However, for gas flows in the range of 23 to 55 g cm^{-2} s^{-1}, the difference between the pressures before the constriction and at the exit of the nozzle is not large enough, and a shock wave is produced in the divergent part of the tuyere. Therefore, the pressure rises at this point, reaching a value close to ambient pressure. At high mass fluxes, greater than 55 g cm^{-2} s^{-1}, the pressure decreases steadily along the tuyere indicating that the gas is continuously accelerated, resulting in supersonic flow in the divergent section of the nozzle. There is a sharp pressure drop at the constriction and the minimum is reached at the tip itself. At mass fluxes greater than 60 g cm^{-2} s^{-1}, this minimum is higher than the ambient pressure, meaning that underexpanded jets are attained in this case of supersonic flow.

A similar analysis can be made from the Mach number profiles. At low mass fluxes there is a maximum less than one at the constriction beyond which the Mach number decreases smoothly. For intermediate Mach numbers, mass fluxes between 23 and 55 g cm^{-2} s^{-1}, Mach = 1 is attained at the constriction and the flow becomes supersonic in the

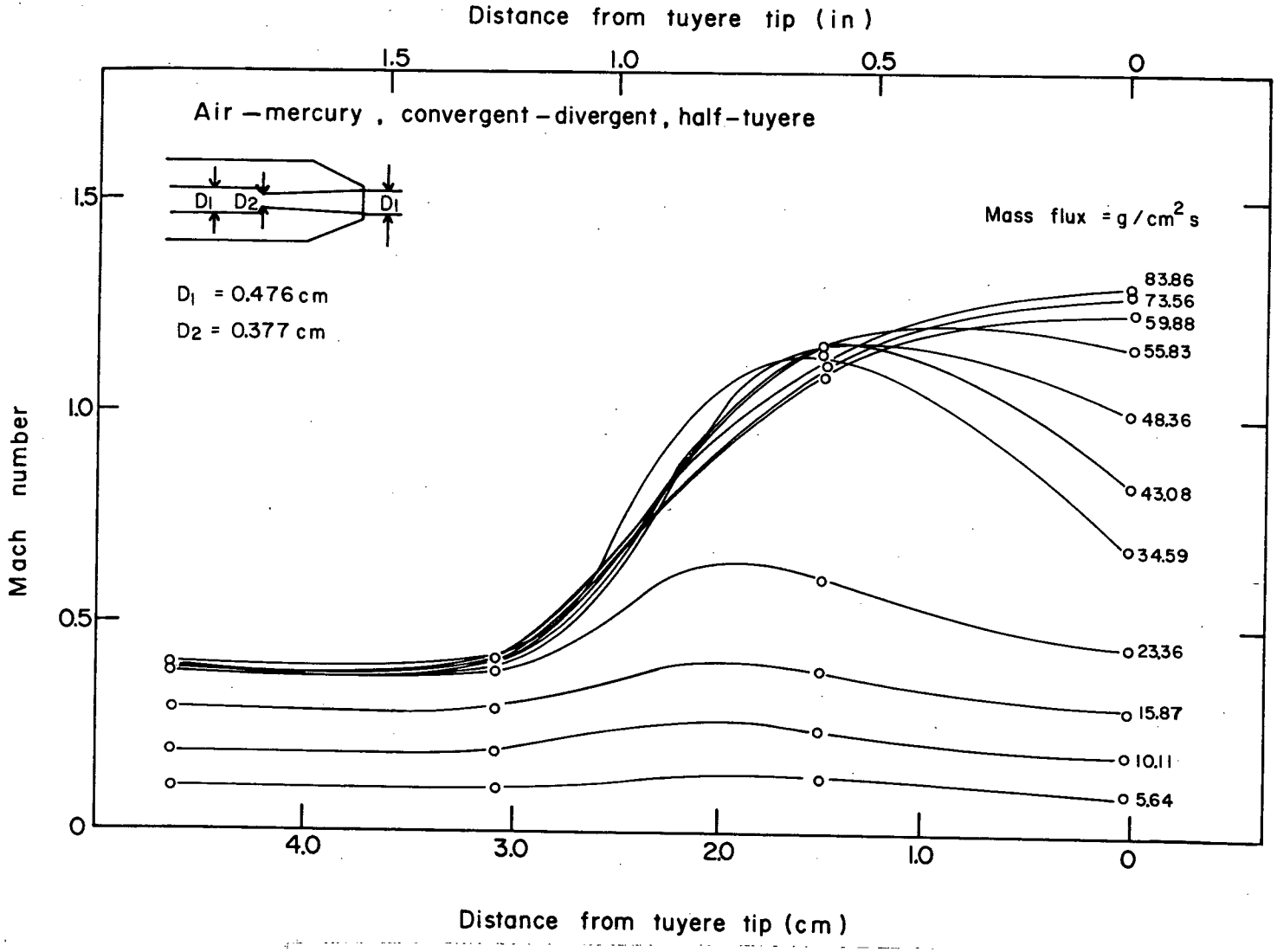

Fig. 17 Mach Number Profiles.

divergent part of the tuyere. However, the regime is not stable and the Mach number becomes subsonic after the shock wave is produced, resulting in a lower Mach number at the tip. Since the pressure was not measured continuously, the exact position of the shock wave could not be determined. Hence, the profiles in the divergent section of the nozzle are only approximate. At high mass fluxes the Mach number increases steadily along the tuyere, to values greater than one downstream of the constriction, and a maximum is reached at the tip itself.

From the pressure traces and the high-speed films it was observed that both the pulsing and the jetting regimes were similar for both the convergent-divergent and the straight-bore nozzles. The pulsing regime is obtained when the Mach number is subsonic in the latter part of the divergent section of the tuyere. The jetting regime is achieved at higher pressure and flows, when the Mach number is greater than one throughout the divergent section.

3.1.5 Penetration of the Jet into the Bath

The dimensionless penetration of the jet, ℓ/d, has been plotted as a function of the jet Froude number. Figure 18 shows average and maximum penetrations for the air-mercury system. A substantial increase

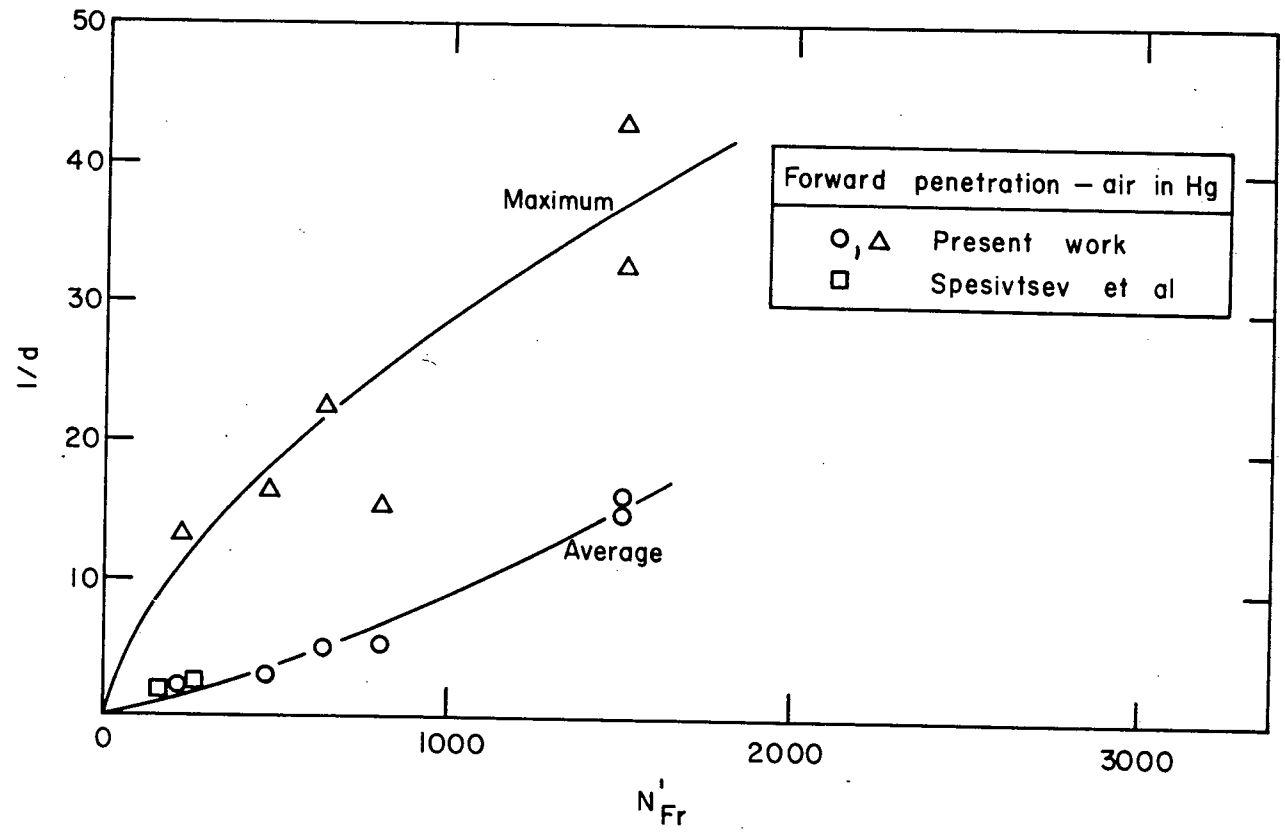

Fig. 18 Forward Penetration as a Function of the Froude Number for Air-Hg System.

in the jet penetration is observed as the Froude number becomes larger. Also included are two points obtained from the work by Spesivtseev et al[6], which are in good agreement with the data from this work, although they correspond to a low Froude number.

Back penetration of the jet behind the nozzle was also measured. Figure 19 shows average and maximum back penetrations as a function of the Froude number. It can be observed that the average back penetration first increases, and then reaches a plateau as the Froude number is increased. It must be kept in mind that at low gas flows the pulsing regime produces bubbles that rise almost vertically, and that in these circumstances backward expansion of the gas is a frequent event. On the other hand, the steady jetting regime at high flows causes the jet to penetrate deeply into the bath. In this case, the back penetration is caused by instabilities of the jet that cause large bubbles to expand behind the nozzle. This occurs with a lower frequency as the mass flux increases within the jetting regime, and is much less frequent than the pressure oscillations in the pulsing regime. Therefore, although at larger flows the gas expands a greater distance behind the nozzle, the amount of gas that actually expands backward, measured as a fraction of the total gas injected, is smaller than in the pulsing regime.

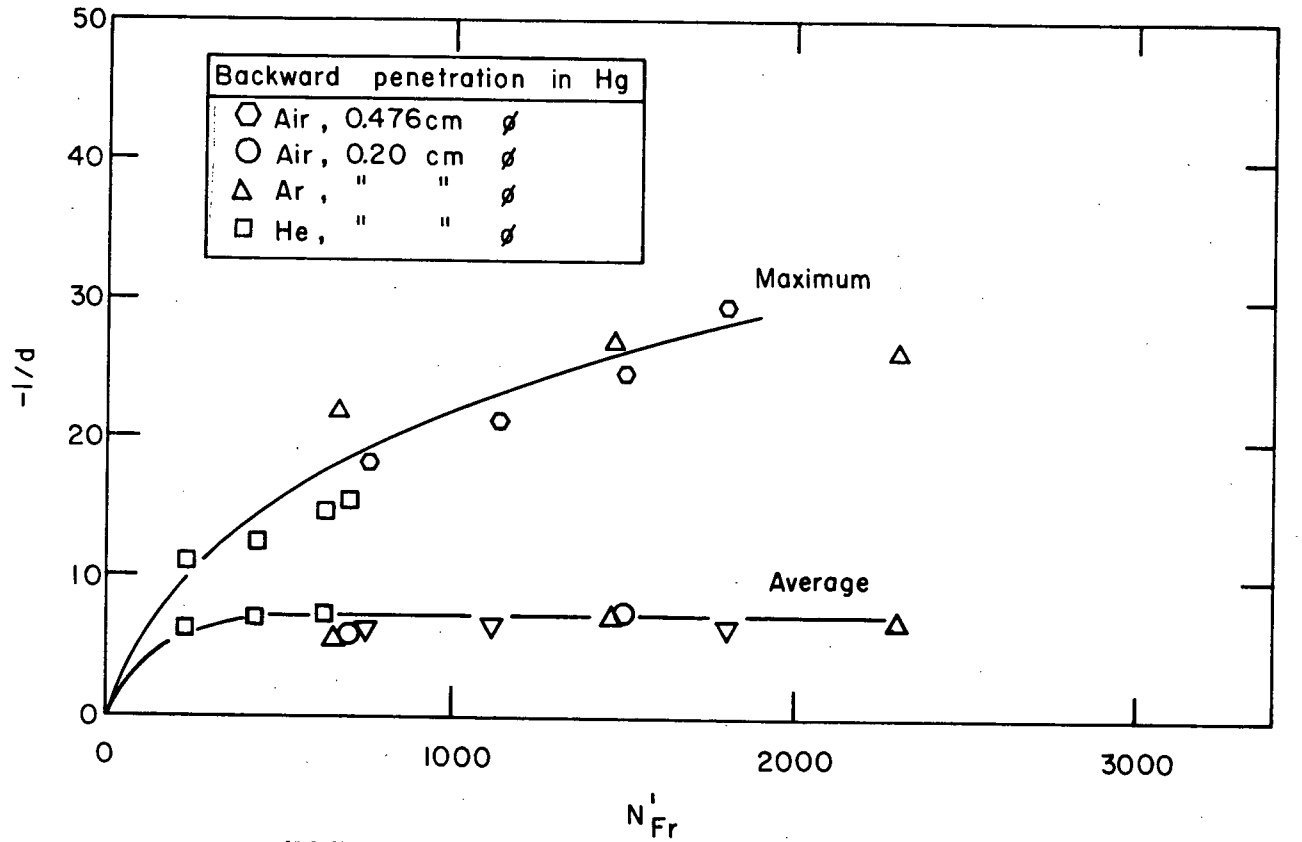

Fig. 19 Backward Penetration as a Function of the Froude Number, for Several Gases Injected into Mercury.

3.2 Jets in Water and in $ZnCl_2$ Solution

Gas jets in water and $ZnCl_2$ solution were studied to obtain information concerning the effect of liquid density on jet behaviour. The systems investigated were air-$ZnCl_2$ solution, helium-$ZnCl_2$ solution, and air-water. For these experiments, the diameter was 0.476 cm. for the $ZnCl_2$ solution, and 0.325 cm. for the water tests. Both high-speed films of the jets and pressure measurements were made as previously described.

3.2.1 Effect of Gas Flow

The gas flow rates used covered the same range as for the tests in mercury. However, due to the lower density of these solutions, a higher Froude number is attained under similar gas flow conditions.

3.2.1.1 Observations from High Speed Films

Figures 32 to 37 of Appendix I show sequences of photographs taken from the high speed films of the three systems studied. The films of the helium-$ZnCl_2$ solution, (Figures 32 and 33 of Appendix I), show the greatest similarity to the air-mercury system, particularly

at low gas flow rates. For both systems, the penetration of the jet into the bath is short, the jet rises almost vertically, and the gas penetrates behind the nozzle to a considerable extent. Unlike the air-mercury system, where bubbles form at the tip, for the case of He-$ZnCl_2$ solution the bubbles form further into the bath, with a less constant frequency of formation. The He-$ZnCl_2$ solution also differs from the air-mercury system in that at high helium flow rates, a long, steady walled jet was seen to penetrate deeply into the bath, with little back penetration. Both the air-$ZnCl_2$ solution and the air-water systems show a behaviour that is increasingly dissimilar to that observed for the gas-mercury systems, as the ratio of gas density to liquid density becomes larger. For the air-$ZnCl_2$ solution, as observed in Figures 34 and 35 of Appendix II, the jet shows a larger penetration into the bath, while the bubbles are formed further away from the nozzle tip. Among all the systems investigated, the air-water films show characteristics that differ the most from the gas-mercury systems studied, as can be observed in Figures 36 and 37 of Appendix II. For the air-water system, bubble formation close to the tip can be observed only at very low air flow rates. At high air flow rates a narrow, steady-walled jet can be observed. Unlike the case for air-mercury, the air-water system shows a clearly conical shape, which penetrates

deeply into the bath, bending upwards at a considerable distance from the tuyere tip.

3.2.1.2 Pressure Measurements

The pressure measurements performed in a similar manner as in the mercury tests revealed pressure oscillations for all the aqueous systems. However, as can be seen in Figures 43 to 45 of Appendix II, these pulses are weak, compared to those found with mercury. Note that a higher sensitivity on the oscilloscope was necessary to reveal noticeable changes in the pressure. For example, when injecting air through a 0.325 cm. dia. half-tuyere, under similar flow conditions, the amplitude is about 1.1 psi with mercury, compared to 0.2 to 0.4 psi for water. The frequency of the oscillations with water is higher than for mercury, ranging from 16 to 20 pulses per second.

3.2.1.3 Effect of Gas and Liquid Density

When comparing the jet behaviour of gases injected into mercury with that when using an aqueous liquid media, it was observed that the He-$ZnCl_2$ solution more closely resembles the air-mercury system, especially at low gas flow rates. However, both the air-

Table IV

GAS DENSITY/LIQUID DENSITY RATIOS

System	Gas Density at 20°C [g cm^{-3}] x 10^3	Liquid Density [g cm^{-3}]	Gas Density/ Liquid Density (x 10^4)
Argon-Mercury	1.7828	13.6	1.31
Air-Mercury	1.2928	13.6	0.99
Helium-Mercury	0.1769	13.6	0.13
Argon-$ZnCl_2$ Solution	1.7828	1.9	9.38
Air-$ZnCl_2$ Solution	1.2928	1.9	6.80
Helium-$ZnCl_2$ Solution	0.1769	1.9	0.93
Air-Water	1.2928	1.0	12.93
Air-Matte	1.2928	5.5	2.35
Air-Molten Iron	1.2928	7.1	1.82

$ZnCl_2$ solution and particularly the air-water system differ considerably from the air-mercury system, showing a more steady jetting regime, bubble formation far from the tuyere tip, and large penetration of the jet into the bath.

Table IV presents the ratios of gas to liquid density for the systems that were investigated. For comparison estimates of the densities for the air-matte and air-iron systems are also included. As can be observed from these values, the density ratio for the systems air-mercury and He-$ZnCl_2$ solution are very close. Therefore it appears that this ratio has a significant influence on the behaviour of the jet. It is worthwhile to mention that the density ratio for the air-water system is 5 to 7 times greater than for the air-matte and air-iron systems, and 13 times the value for the air-mercury system.

CHAPTER 4

INDUSTRIAL CONVERTER TESTS

4.1 Introduction

The injection of gases into liquids of different densities, as reported in Chapters II and III, differs from industrial practice in the following ways:

i) Isothermal Conditions

The gases injected in the laboratory were approximately the same temperature as the bath (room temperature). In industry this is not usually the case since the baths are much hotter than the gas, and thus industrial jets are non-isothermal.

ii) Chemical Reaction

The gases injected in this work did not react with the bath. In industrial practice, on the other hand, one of the main objectives of submerged gas injection is to produce chemical reactions between the gas and the melt. These reactions are frequently exothermic and produce a substantial change in the volume and composition of the jet, and to a lesser extent, of the

liquid bath.

iii) Reactor Design

The laboratory tests were performed using a simplified single-tuyere vessel. Industrial reactors usually have multiple tuyeres, and the different jets interact with one other. Thus different flow patterns are produced in the melt, and in turn can affect the jet behaviour.

iv) Liquid Bath

Mercury is a homogeneous melt, and its density is at least two-fold larger than that of industrial baths.

Due to these differences between the laboratory and the industrial systems, and to translate the laboratory results to metallurgical processes, it was desirable to perform some industrial tests under realistic operating conditions. To achieve this, an agreement was made to carry out some experiments in a nickel converter at the INCO Smelter in Thompson, Manitoba. Technical support to perform the tests was provided by the Process Technology group of the Thompson Smelter. It was expected that these experiments might help to establish the usefulness of the results obtained in the laboratory experiments in addition to shedding further light on the fundamentals

of process jets.

4.2 Experimental Procedure

In a similar manner to the laboratory tests, the industrial tests consisted of measuring pressures and recording pressure oscillations since it was again not possible to view the jets. The industrial tests were divided into two parts. The first set of experiments were performed using regular tuyeres blowing air at low pressure. The second set of tests involved the injection of high-pressure air using a pipe introduced into the bath through a tuyere.

4.2.1 Low-Pressure Tests

During a maintenance period, pressure taps were placed in two tuyeres of an industrial nickel converter. The tuyeres equipped with pressure taps were located at the end and centre of a bank of tuyeres. These locations were chosen to detect any noticeable effect of adjacent tuyeres on the flow regimes.

Two pressure taps were placed in each tuyere, as shown in Figure 20. The first pressure tap was placed in the tuyere guide,

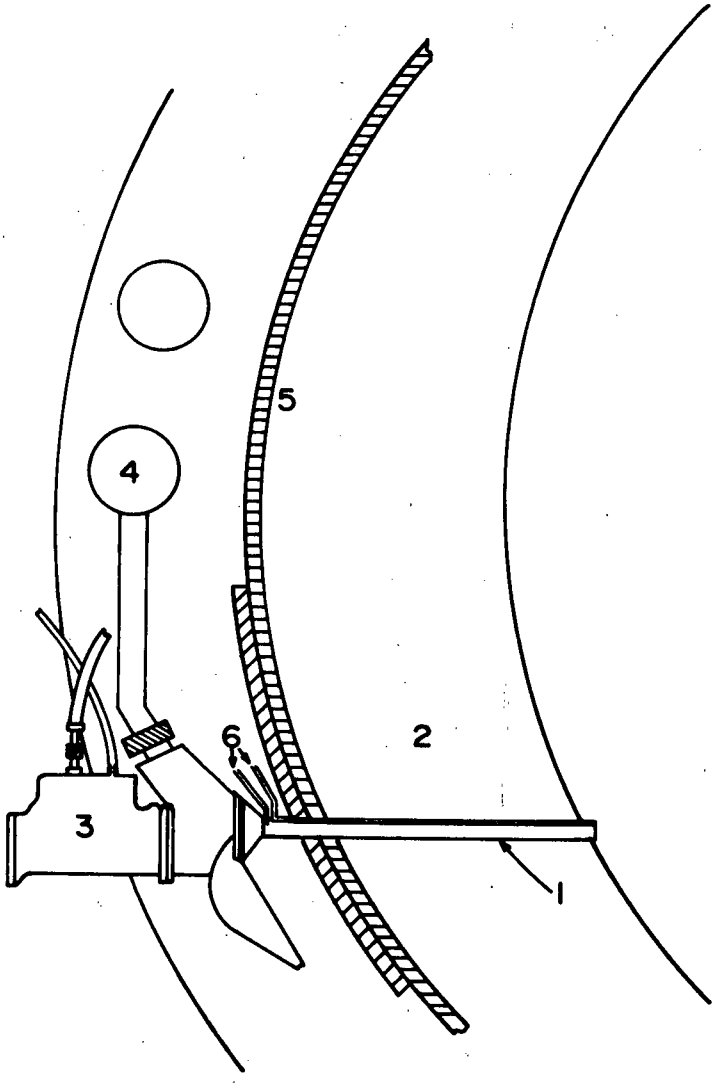

1 Tuyere
2 Refractory wall
3 Tuyere puncher
4 Header
5 Iron shell
6 Pressure taps

Fig. 20 Location of Pressure Taps,
Low-Pressure Industrial Tests.

near the outer end of the tuyere, while the second tap was installed in the tuyere itself, close to the tip. To avoid excessive heating of the transducer when the converter was turned, a fast disconnect device was employed to couple the transducer to the pressure tap. The signal from the transducer was amplified and recorded in a storage oscilloscope, and Polaroid photographs of the screen were taken, as described in the laboratory tests. In this way pressure traces were obtained in all four of the pressure taps at different stages of the nickel-matte converting process. The pressure measurements were made during the first charge of the converter campaign, since the pressure taps could be destroyed by the punching rods. The pressure was monitored for periods as long as several punching cycles, to observe any differences caused by a change in the diameter of the tip of the nozzle.

4.2.2 High-Pressure Tests

High-pressure tests were also performed in order to obtain a wide range of air flow rates. However, since the air pressure available is not higher than 0.105 MPa (15 psi), a different technique had to be employed. A 1.905 cm. (3/4 in.) I.D. iron pipe with an overall length of 102 cm. (approximate length of the tuyere was 61 cm.) was connected to the 0.63 MPa (90 psi) high-pressure line used normally

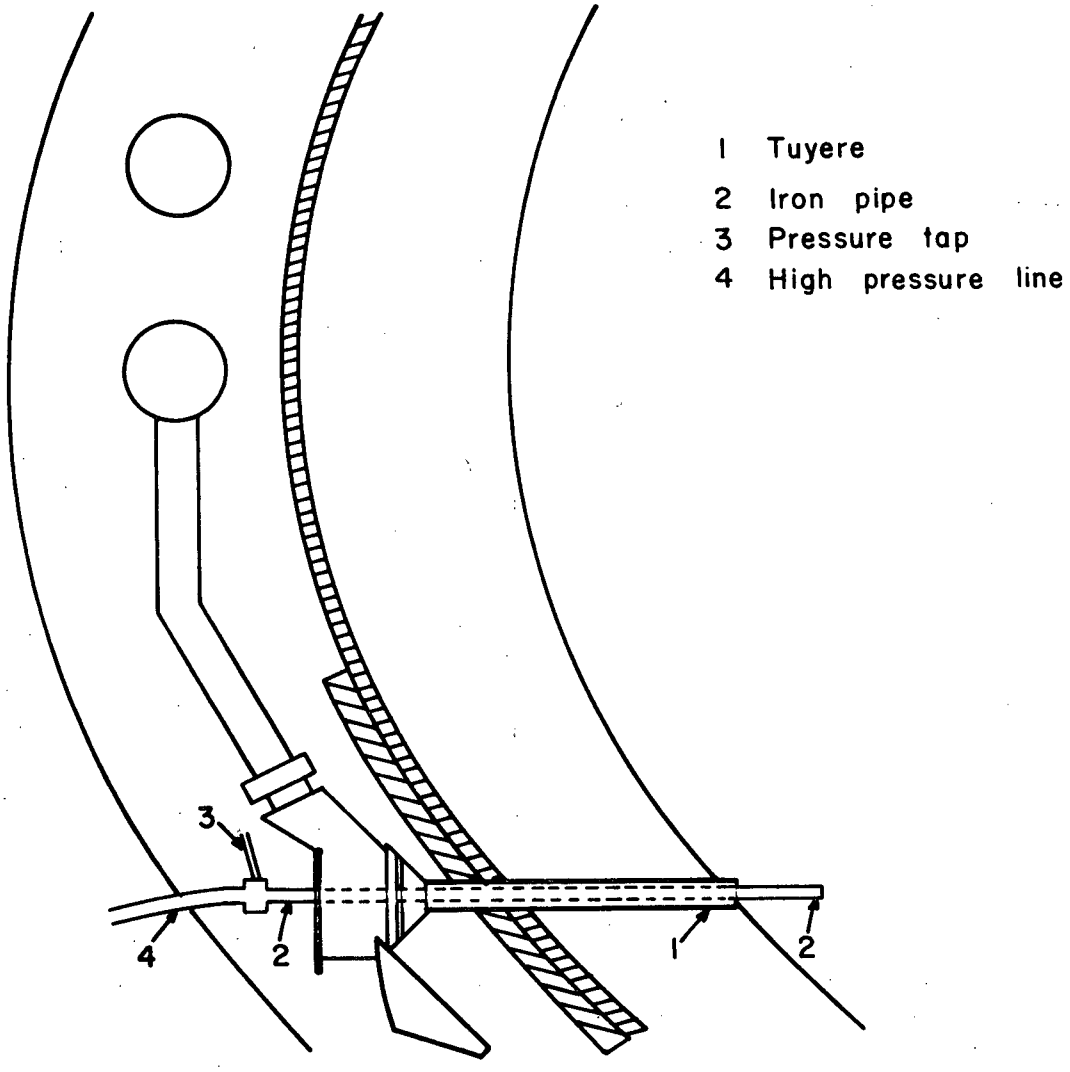

Fig. 21 Location of Pipe and Pressure Taps, High-Pressure Industrial Test.

to operate the pneumatic tuyere punchers. A pressure tap, coupled to the pressure transducer, was placed in the pipe, as depicted in Figure 21. The pneumatic puncher was removed from its position behind the tuyere, and the iron pipe was introduced through the nozzle into the bath.

The procedure employed to record the pressure was similar to that used for the low-pressure tests. Four values were used for the back pressure: 0.105, 0.21, 0.35 and 0.56 MPa (15, 30, 50 and 80 psi, respectively).

4.3 Results

4.3.1 Low-Pressure Tests

The conditions for and results from the low-pressure tests are summarized in Table V. The number of tests was limited due to the difficult conditions that are typical of a smelter. However, the results were consistent with what was expected from the results for the laboratory tests. Figure 22 shows pressure traces obtained for the low pressure experiments (test numbers 1 to 6). Photos 1 and 2 were obtained as a reference by blowing air into an empty converter. As expected the pressure was constant, both at the tuyere (Photo 1)

Table V

LOW-PRESSURE TESTS

Run #	Position #*	Overall Air Flow (scfm)	Pressure, psi		
			In the Header	In the Tuyere Guide	In the Tuyere
1	1	n.a.	-	-	0.91
2	2	n.a.	-	0	-
3	1	25000	12	-	1.35
4	2	20000	10	2.7	-
5	3	22500	10.5	-	2.2
6	4	22500	10.5	2.7	-
7	1	23000	12.5	-	3.5
8	2	22500	13	8.3	-
9	3	22500	13.9	-	8.9
10	4	21500	14	9.6	-

* Positions #1 and 2 at end of tuyeres bench; positions #3 and 4 in the middle of tuyeres bench.

Positions #1 and 3 in the tuyere; positions #2 and 4 in the tuyere guide.

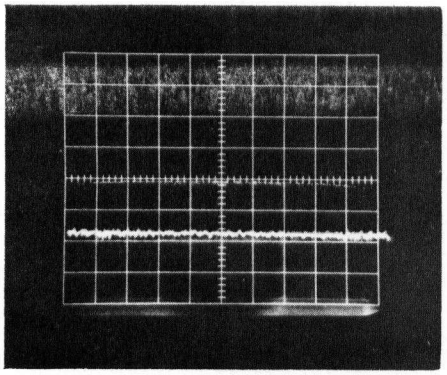

Test 1–Empty Converter

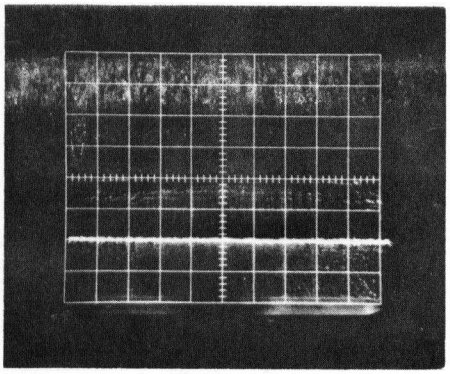

Test 2– Empty Converter

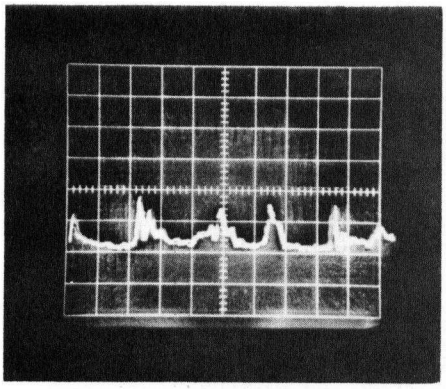

Test 3–Blowing matte, end of tuyere bank

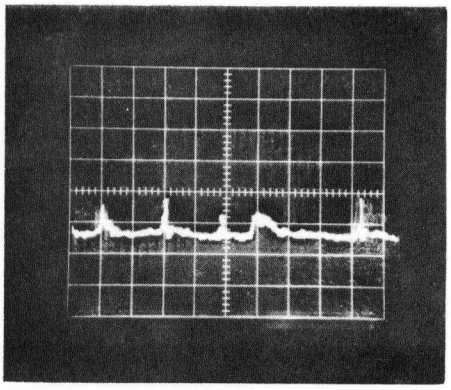

Test 4–Blowing matte, end of tuyere bank

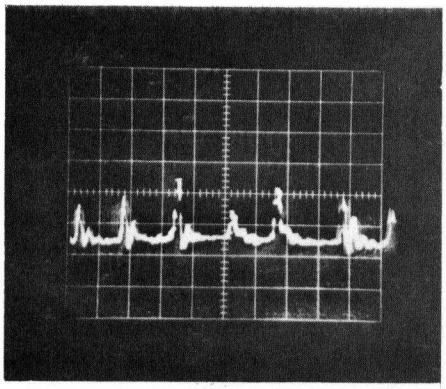

Test 5–Blowing matte, middle of tuyere bank

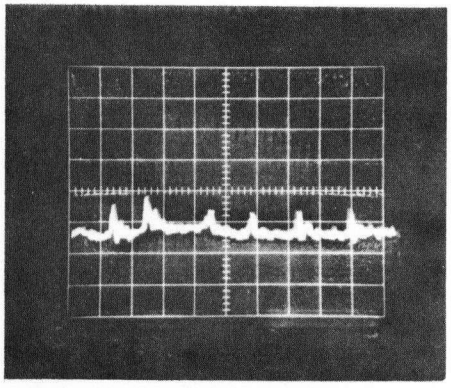

Test 6–Blowing matte, middle of tuyere bank

Low Pressure Tests. Sensitivity: 4.54 psi/div, 50 ms/div

Fig. 22 Pressure Pulses, Low-Pressure Industrial Tests.

and at the tuyere guide (Photo 2). Photos 3 and 4 show pressure oscillations while blowing into the nickel matte, through the tuyere located at the end of the bank of tuyeres. It can be observed that there are clear, regular pulses in both positions (Photo 3 in the tuyere; Photo 4 in the tuyere guide). As expected the amplitude was seen to be larger near the tuyere tip than in the tuyere guide. The frequency of the pulses is 10 to 12 per second.

Compared to the pressure traces obtained in the laboratory tests, the industrial signals were "noisier". It is believed that there was some interference due in part to other electrical equipment operating in the vicinity of the oscilloscope, and also a converter is a more complex system than the mercury tank used in the laboratory experiments. Nonetheless the pressure pulses were clear and had approximately the same frequency and shape as those observed in the laboratory tests.

It is important to notice the effect of the tuyere punching on the pressure pulses. Immediately after punching the pressure pulses had a greater amplitude, which then decreased (although the pulses never disappear) as the next punching cycle was approached. This can be explained by the fact that a decreasing diameter at the tip of the nozzle due to accretion build-up will cause a smaller perturbation

along the constant diameter tuyere, upstream from the tip.

For a tuyere located in the centre of the bank, Photos 5 and 6 of Figure 22 show pressure pulses in the tuyere and in the tuyere guide, respectively. The results are very similar to those obtained for a nozzle at the end of the set of tuyeres, and no noticeable effect was observed due to the presence of the neighbouring tuyeres.

4.3.2 High-Pressure Tests

Table VI summarizes the conditions for and results from the high-pressure tests. Figure 23 shows pressure traces obtained for back pressures of 15, 30, 50 and 80 psi, respectively. Photo 1 shows pressure pulses obtained for a back pressure of 15 psi. Marked similarity between these pressure traces and those found with a regular tuyere is evident. The shape, frequency and amplitude of the pulses correspond closely. Photo 2 shows pressure traces for a back pressure of 30 psi. Pressure pulses are visible. However, the frequency is irregular and the amplitude is small. This case would correspond to the transition from fully expanded to under-expanded jets, as was described earlier. Photos 3 and 4 were obtained with back pressures of 50 and 80 psi, respectively. It is

Table VI

HIGH-PRESSURE TESTS

Run #	Line Pressure (psi)	Tuyere Pressure (psi)
12	80	57.8
13	50	37.8
13b	50	37.8
14	30	13.3
15	15	0
15b	15	0

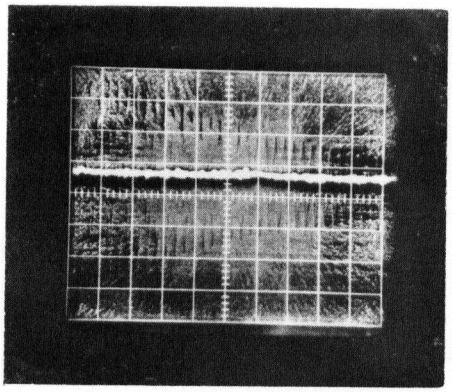

Test 12 — 80 psi

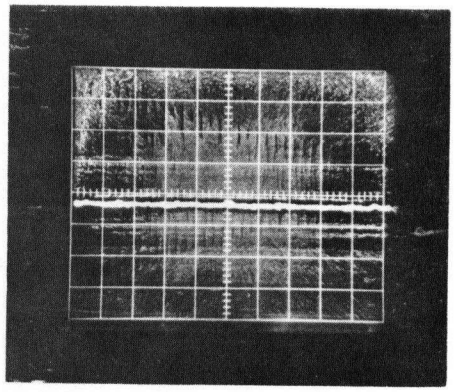

Test 13 — 50 psi

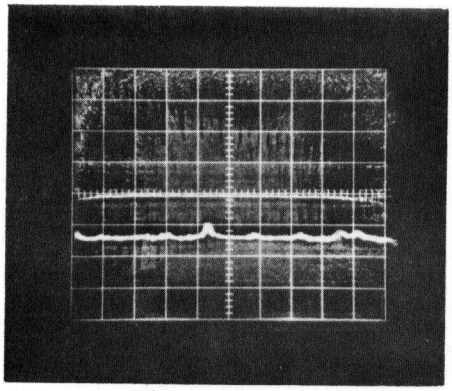

Test 14 — 30 psi

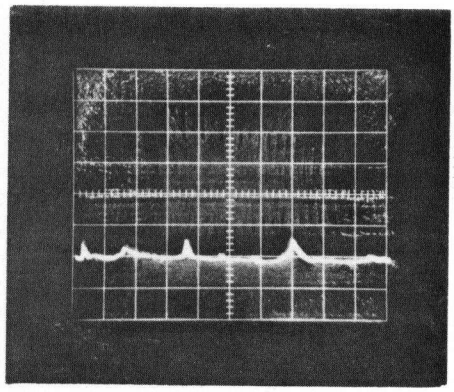

Test 15 — 15 psi

High Pressure Tests. Sensitivity: 22.23 psi/div, 50 ms/div.

Fig. 23 Pressure Pulses, High-Pressure Industrial Tests.

observed that the pressure is practically constant, as was found earlier for the case of underexpanded jets obtained in the laboratory tests.

For the high-pressure tests, a lower sensitivity had to be used for the oscilloscope. This low sensitivity was kept the same for all pressures used, in order to be able to compare the results obtained directly. At this reduced sensitivity, little background noise was seen.

CHAPTER 5

DISCUSSION

5.1 Description of Gas Injection into a Liquid

From this study, it has been observed that depending on the gas flow, two different regimes can be distinguished. The first is the fully-expanded jet obtained at relatively low gas flow rates, in which the pressure decreases steadily along the tuyere, reaching ambient pressure at the nozzle tip. The second regime is the underexpanded jet at higher gas flow rates in which the pressure also decreases along the tuyere, but at the tip is higher than the surrounding pressure of the bath. The transition from one regime to the other depends on the gas flow rate and on the type of gas that is injected.

5.1.1 Fully-Expanded Jets

A fully-expanded jet in mercury exhibits a pulsing behaviour, as was seen in Figure 8. Basically it consists of large irregular shaped bubbles that grow at the exit of the tuyere. After a bubble has reached a certain size, it rises almost vertically,

detaches from the tuyere, and liquid flows in to occupy the vacated space. These flow events generate a pressure pulse that can be detected in the nozzle upstream from the tip. With this type of behaviour, the cone angle, trajectory and envelope of the jet can best be described on a time-averaged basis, as was done in the work by Oryall[1]. The data from the present study shows a wide angle of expansion, an almost vertical trajectory, and a very short penetration of the gas into the bath, in confirmation of Oryall's work for an air jet into mercury.

5.1.2 Underexpanded Jets

For an underexpanded jet, the pressures measured along the tuyere are relatively steady, with no regular pulsing behaviour being observed. From the high-speed films this jetting regime was seen to consist basically of a short, stable jet that protrudes into the bath from the tip of the nozzle. Occasional instabilities that were observed can be attributed to the liquid flow pattern in the small vessel. Due to the presence of this stable jet, there is little contact between the liquid and the tuyere tip. Bubbles are formed not at the tip of the nozzle, but slightly downstream, at the end of the stable jet. These bubbles have very irregular shapes, and frequently break down into smaller bubbles, providing a large

area of contact between the gas and the liquid. Bubble formation at the end of the jet is accompanied by a considerable expansion of the gas. This produces some back penetration of the gas behind the tuyere. Figure 9 shows a sequence of high-speed photographs for a wider-expanded jet of air into mercury.

5.1.3 Transition from Fully-Expanded to Underexpanded Jets

The transition from fully-expanded to underexpanded jetting occurs when the nominal Mach number at the tuyere tip is greater than 1. While nominal Mach numbers at the tuyere exit are larger than 1 at the transition point, Mach numbers along the tuyere are always less than 1, and do not increase with further increases in the back pressure after the transition has been reached. Factors that produce a greater pressure drop along the tuyere such as a decrease in the tuyere diameter, cause the values of the transitional Mach numbers along the tuyere to be even lower. This can be observed comparing Figures 51 and 53 of Appendix III.

The transition from pulsing to steady jetting regime is related to both the gas mass flux, and the type of gas that is injected. For injection of helium, air and argon into mercury, the

transition occurs at mass fluxes of about 28,50 and 65 g cm^{-2} s^{-1}, respectively. Not surprisingly these values are directly proportional to the square root of the molecular weight of the gas, in a manner similar to the speed of sound in gases (See Appendix V).

The transition from fully-expanded to underexpanded jetting can be explained in terms of compressible flow theory. For small Mach numbers (< 0.2 for a perfect gas) the effects of compressibility are negligible, and the gas in the tuyere behaves as an incompressible fluid. In this regime the pressure drop is small, the average speed of the gases is almost constant along the tuyere, and the relative pressure at the tip is zero. Under such conditions a very regular pulsing regime is achieved. For higher Mach numbers (0.2 < Mach < 1.0) the flow is compressible due to the higher back pressure at the entrance to the tuyere. In this regime the relative pressure decreases steadily along the tuyere, and is again zero at the tip. To produce this continuous pressure profile, the gas is accelerated as it moves along the tuyere. The fact that the pressure at the tip is zero, together with the high density of the liquid bath, helps to explain the bubble formation at the tip and the extent of penetration of the gas into the bath. In the case of mercury, the large difference in density between the gas and the bath causes the gas to decelerate rapidly, immediately as it leaves the tuyere. Buoyancy then acts

on the gas, causing it to rise almost vertically and detach from the tuyere tip. Because the pressure of the gas at the tip is equal to the ambient pressure of the bath, the liquid moves back to the orifice, displacing the departing gas. In this way the liquid periodically washes against the tuyere as the momentum of the gas in the nozzle is too small to reverse the flow. Thus the jet necks off regularly at the tip of the nozzle, and a pressure pulse that can be measured upstream from the tip is produced.

In the case of water and $ZnCl_2$ solution, the lower density of the liquid allows the jet to penetrate further into the bath, and since buoyancy effects are not as strong as for those present in mercury, the jet curves upwards at a greater distance from the tip. Therefore the bubbles are produced not at the tip, but well into the bath. As observed in Figures 43 to 45 of Appendix II irregular weak pressure pulses can be detected under these conditions. It appears that bubble formation at the tip of the nozzle in these low-density liquids can only be attained at lower Mach numbers than those studied in this work. This strongly suggests that results obtained from water models cannot be accurately extrapolated to metallurgical melts of higher densities.

For higher back pressures and mass fluxes, the Mach number reaches a value that is close to 1 along the tuyere. It is well known that in a straight-bore tuyere, under conditions of compressible flow without friction, the maximum attainable Mach number is 1, and that if friction is considered, this value has to be less than 1. Further increases in the back pressure (considering it to be a driving force) cause an increase in the mass flux by increasing the density, but not the velocity of the gas. Therefore the pressure drop between the high back pressure in the tuyere and the ambient pressure in the bath cannot be produced by an acceleration of the gas inside the tuyere, and the pressure at the tip is higher than that outside the tuyere. The excess pressure is then released by a multidirectional expansion of the gas as it leaves the nozzle. This pressure gradient is steep and has to occur at a very short distance from the tip. Because the pressure at the tuyere tip is now higher than the pressure of the surrounding bath, the liquid metal is prevented from touching the tip of the nozzle, and a short, but stable jet is produced (Figure 9). This behaviour was named the steady-jetting regime. In this regime bubbles are formed inside the bath, at a short distance downstream from the tip of the nozzle, where the horizontal speed of the gas becomes small, and buoyancy forces become more predominant. The decrease of gas speed added to the buoyancy causes

the jet to neck off. Pressure pulses generated by bubble formation cannot, under these circumstances, be detected inside the tuyere. This can be explained by the fact that the bubbles are formed outside the tuyere, and also that the underexpanded jet may become supersonic after expansion at the exit of the nozzle; it is well known that shock waves travel at the speed of sound, so that the pressure pulses would not be observed upstream of their point of origin. Evidence to this effect is the steady pressure measured in the divergent portion of a convergent-divergent tuyere under conditions of supersonic flow and slight underexpansion. Therefore in the steady jetting regime a relatively steady pressure is expected at any point along the tuyere.

The transition from a fully-expanded to an underexpanded jet is determined by the flow conditions within the tuyere, particularly the gas flow rate. However, the pulsing and steady jetting regimes obtained for the jet within the bath appear to be strongly influenced by the physical properties of the liquid, especially the density. Underexpanded flows are necessary to obtain jetting regimes in a high-density liquid such as mercury. However a fully-expanded jet can produce a steady jetting regime in a liquid of lower density, such as water.

5.1.4 Forward and Backward Penetration of the Gas

Forward and backward penetrations of jets of different gases in a mercury bath have been plotted in Figures 18 and 19. The increase in penetration into the bath with larger jet Froude numbers is explained by the greater momentum of the jet, which allows the gas to better overcome the fluid flow resistance of the liquid. A higher density of the gas causes the jet to penetrate deeper into the bath. However this effect was found to be small.

The method employed in this work was not suitable for making accurate measurements of the expansion angle, since the jet was viewed only in a vertical plane. However qualitative observations agree with the results obtained by Oryall[1] in that a very rapid expansion of the gas was observed for all gases injected into mercury. It also appears that the type of gas has an influence on the expansion angle, with greater values being obtained for gases of low density. A more important variable affecting the expansion angle is liquid density, with higher densities giving rise to greater expansions. This finding is consistent with the observed effect of bath density on jet penetration. Figure 2 shows the results from the work by Spesivtsev et al[6], for air injected into different liquid media.

It can be observed that the penetration of the jet into the bath decreases for an increase in the density of the liquid, for the same value of the Froude number. It is obvious that smaller jet penetrations would be expected with larger expansion angles of the gas.

5.2 Effect of the Tuyere on Jet Behaviour

As has been already discussed, the most important factors that influence jet behaviour are the gas mass flux and the density of the liquid. However tuyere parameters also affect the flow regimes and are discussed in this section.

5.2.1 Tuyere Diameter

The influence of the tuyere diameter can be best understood by considering its effect on the modified Froude number,

$$N'_{Fr} = \frac{\rho_G V_o^2}{g(\rho_L - \rho_G)d_o}$$

where the velocity V_o of the gas is inversely proportional to the cross-sectional area of the nozzle.

Thus, for a given overall gas flow rate, an increase in the diameter of the nozzle produces a sharp decrease in the Froude number of the jet. Correspondingly the transition from a fully-expanded to an underexpanded jet requires a larger gas flow. It is clear that in order to achieve an underexpanded jet without an excessive pressure drop, it is convenient to employ a short tuyere of small diameter.

5.2.2 Tuyere Design

From the pressure traces and high-speed films of the jet, similar jet behaviour was found for straight-bore and convergent-divergent tuyeres. Both types of tuyeres exhibited pulsing and steady jetting regimes at low and high gas flow rates. The main purpose of employing a convergent-divergent nozzle was to study the jet behaviour when supersonic flow is attained inside the tuyere. This was achieved at high flow rates as shown in Figures 16 and 17. However, for a high-density bath, the transition from pulsing to the steady jetting regime appears to be determined by the existence of conditions of fully-expanded or underexpanded jets along the tuyere- and not by the exit velocity of the gases.

It is worthwhile mentioning that the results for the convergent-divergent tuyere agree with compressible flow theory. Using

this design, the pressure profiles along the tuyere, the transition from subsonic to supersonic flow and the existence of shock waves in the divergent section of the nozzle were observed in agreement with theory, even though the gases were being injected into a high-density liquid.

5.3 Industrial Process Jets

Results from the tests performed on the industrial nickel converter agree well with those obtained in the laboratory tests, as was seen in Chapter 4 of the present work. Based on this comparison, the current practice of gas injection in matte converting can be discussed.

5.3.1 Jetting Regimes in Process Jets

Pressure measurements in the industrial converter have revealed that a pulsing regime is present when air is injected into matte under the current blowing practice. In Figure 22 regular pressure oscillations are clearly observed. The shape and frequency of the pressure pulses is similar to those for jets in mercury. In the higher pressure tests, a transition from pulsing to the steady

jetting regime was observed, when increasing the back pressure from 15 to 80 psi, in close agreement with the laboratory tests.

In comparing both sets of results, it can be said that for conventional nickel-matte converting, a pulsing regime is obtained at the tuyeres, corresponding to a fully-expanded gas flow with a low Mach number. As the pressure is increased, the pulsing regime changes to a transitional regime, and then to a steady jetting regime, whereupon an underexpanded jet is attained at the tip of the tuyere. Thus it appears that under non-isothermal conditions, the existence of chemical reactions and the presence of the neighbouring tuyeres do not have a substantial effect on the flow conditions at the tip of the tuyeres. Furthermore, as was mentioned in other works[1,6], the thermal expansion of the gas, as it contacts the high temperature bath, enhances the pulsing nature of the jet, causing it to behave like a jet injected into a higher density liquid such as mercury.

5.3.2 Process Jets in Matte Converting

Based on the information obtained from this work, several facts associated with the current blowing practice in matte converting

can be explained.

i) Tuyere Plugging

During blowing tuyeres frequently become plugged by liquid from the bath that solidifies in the interior of the nozzle. This necessitates frequent punching of the tuyeres which in turn decreases the efficiency of the process, and ties up additional equipment and labour. Back flow of melt inside the tuyere can be explained considering that a pulsing regime is obtained under the current blowing practice. If the liquid washes regularly against the tip of the nozzle, part of it can penetrate inside the tuyere and solidify due to the cooling effect of the injected air.

ii) Tuyere Erosion

During a converter campaign, the length of a tuyere is reduced from its original length of 60 cm to about 24 to 30 cm in a period of few months. The causes of tuyere erosion can be understood by considering the pulsing regime that is present in conventional blowing. The periodical washing of the

liquid against the exit of the nozzle, detected as pressure pulses in the tuyere, causes a fluctuating strain on the tip of the nozzle. Since the reaction between the gas and the melt is exothermic, a high temperature zone alternates between the tip and the interior of the bath. This causes thermal shock to the tuyere. In addition, punching required to remove the solidified material at the tuyere exit enhances erosion. Therefore it appears that the pulsing regime is highly detrimental to tuyere life.

iii) Back-Wall Erosion

Under pulsing conditions the gas penetrates only a short distance into the melt, and rises almost vertically. Due to the wide angle of expansion of the jet, there is extensive back penetration of the gas behind the tip of the nozzle. Since the tuyeres are installed flush with the inside wall of the converter, the jet impinges directly on the refractory wall, and erodes it. Since the tuyere is also being eroded, this zone of the refractory wall shows even more pronounced wear. One way of minimizing this problem would be to move the gas stream away from the refractory wall.

CHAPTER 6

CONCLUSIONS

6.1 Summary

From the results obtained from both the laboratory and the industrial experiments, the following can be concluded:

i) A novel technique has been developed to study gas jets injected into opaque, room temperature melts. This technique, consisting of a half-tuyere attached to a transparent wall, gives good agreement with results obtained for full jets at short distances from the tuyere exit. Qualitative agreement with a full jet was observed at distances greater than 10 to 15 times the diameter of the nozzle. It has also been shown that pressure measurements in the tuyere give valuable information concerning the behaviour of a gas jet in high density melts at any temperature.

ii) Two different flow regimes were observed when blowing a gas into a high density liquid: a pulsing regime at low gas flows, and a steady jetting regime at high gas flows. For a given liquid bath, the transition

depends on the type of gas that is blown. The pulsing regime causes pressure oscillations along the tuyere, due to the washing of the liquid against the tip of the nozzle. The steady jetting regime produces a fairly steady pressure in the tuyere, and the contact of the liquid bath with the tip of the nozzle is greatly reduced. A jetting regime can be obtained (when the gas-liquid system has already been fixed) by increasing the back pressure to achieve conditions of underexpanded jets.

iii) Results from injecting gases into lower density liquids such as water and zinc chloride solution show a strong effect of the density of the liquid media on the jet behaviour. The expansion of the gas is smaller and the penetration of the gas is greater for a liquid of lower density, and a steady jetting regime with bubble formation not at the tuyere tip, but in the interior of the bath, can be observed even at low gas flow rates, under conditions of fully-expanded jets. It seems clear that results obtained from tests performed in water models cannot be accurately extrapolated to metallurgical melts.

iv) Results from tests performed in a nickel matte converter show that in conventional blowing a pulsing regime is obtained at the tuyeres, corresponding to a fully-expanded flow with a low Mach number. This regime changes to steady jetting when the back pressure is increased so that under-expanded conditions are attained at the tip of the nozzle. The results obtained for a high temperature nickel matte are very similar to those for a low temperature mercury bath.

v) A jetting regime appears to be more convenient than the pulsing regime currently used in conventional converting practice. It provides smoother conditions for the tuyeres, and a deeper penetration of the gas into the bath, minimizing the contact between the liquid bath and the tuyere. This would increase tuyere and backwall service life, and reduce tuyere plugging.

6.2 Suggestions for Future Work

Further studies on the behaviour of jets into high density liquids are necessary. These studies can be made in the laboratory and on an industrial scale.

i) Laboratory Tests

It seems necessary to conduct a more complete study on the effect of a high temperature melt on jet behaviour for densities of the liquid intermediate between those of water and mercury. Inert gases such as argon or nitrogen can be injected into aluminum or alloys of low-melting temperature. Pressure measurements in the nozzle and X-ray photography could provide useful information about flow regimes and jet characteristics.

ii) Industrial Tests

Long term tests involving the injection of air into a matte converter under steady jetting conditions appear very appealing. Selected tuyeres in a converter could be operated at a high gas flow. The remaining tuyeres could be left under conventional blowing conditions for comparison (The overall gas flow in the converter would be left constant). In this way, more definitive information can be obtained about the effect of the gas flow regime on tuyere plugging and on backwall and tuyere erosion. Also additional information can be obtained about other

aspects of jetting, such as the effect of the gas speed on the spilling of material outside the converter, and on the slopping of the bath inside the reactor.

REFERENCES

1. Oryall, G.N.: M.A.Sc. thesis, Dept. of Metallurgy, University of British Columbia, 1975.

2. Themelis, N.J., Tarassoff, P. and Szekely, J.: J. Trans. Met. Soc. AIME, vol. 249, 1969.

3. Oryall, G.N. and Brimacombe, J.K.: Met. Trans., 1976, 7B, pp. 391 - 403.

4. Engh, T.A. and Bertheusen, H.: Scan. J. Met., 1975, 4, pp. 241 - 249.

5. McKelliget, J.W., Cross, M. and Gibson, R.D.: private communication.

6. Spesivtsev A.V. et al: Tsvetnye Metally, UDC 669.046.53, pp. 10 - 12.

7. Hansen, A.G.: Fluid Mechanics, Chapter 7, John Wiley and Sons, editors.

APPENDIX I

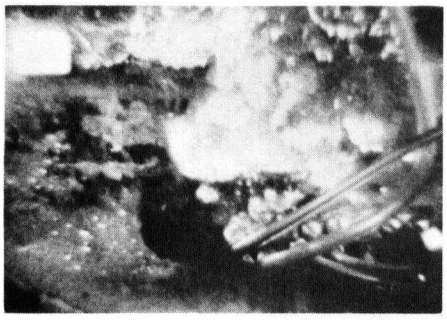

1.- t = 0.00 s

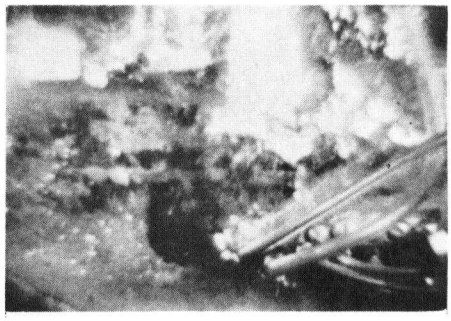

2.- t = 0.02 s

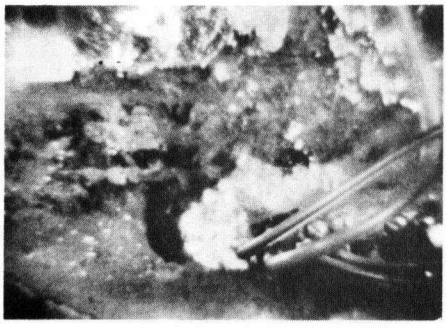

3.- t = 0.04 s

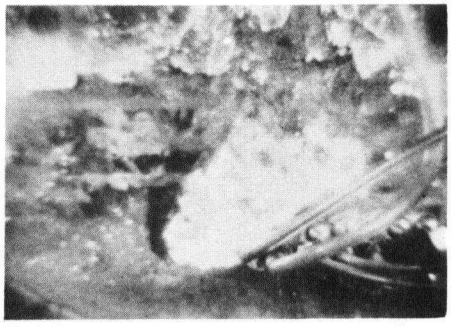

4.- t = 0.06 s

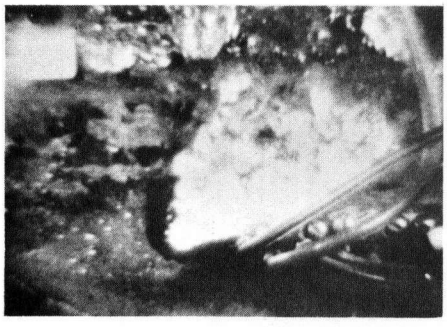

5.- t = 0.08 s

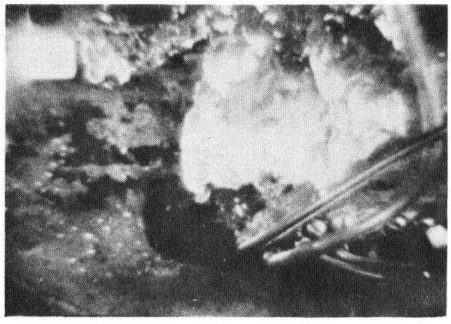

6.- t = 0.10 s

Air - Hg, 0.325 cm diam , half - tuyere

Mass flux = 34.0 g cm^{-2} s^{-1} N'_{Fr} = 248 Nominal Mach = 0.601

Fig. 24 Air-Hg, Low Flow, 0.325 cm. dia.

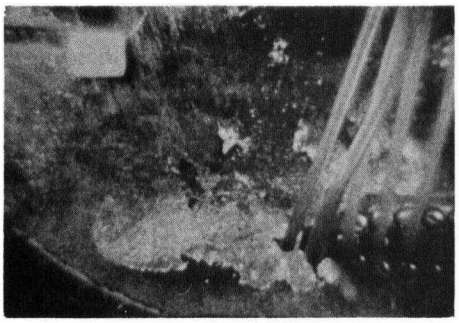

1.- t = 0.00 s

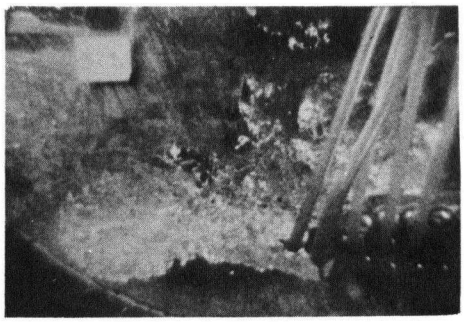

2.- t = 0.02 s

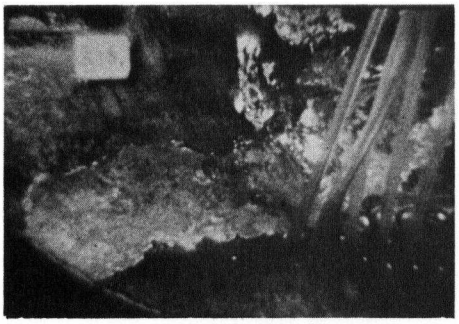

3.- t = 0.04 s

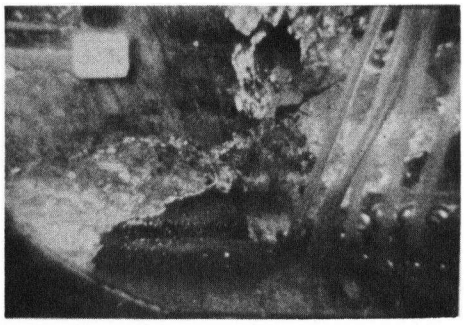

4.- t = 0.06 s

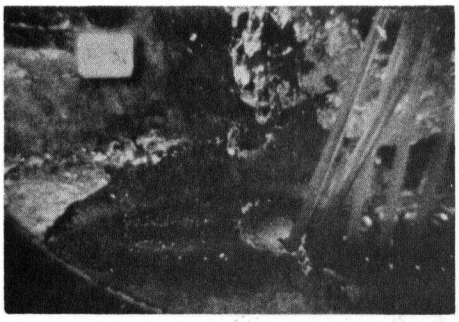

5.- t = 0.08 s

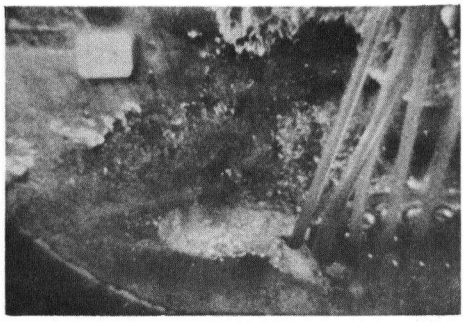

6.- t = 0.10 s

Air - Hg, 0.325 cm dia, half-tuyere

Mass flux = 193.0 $g\,cm^{-2}s^{-1}$ N'_{Fr} = 1457 Nominal Mach = 1.456

Fig. 25 Air-Hg, High Flow, 0.325 cm. dia.

1.- t=0.00 s

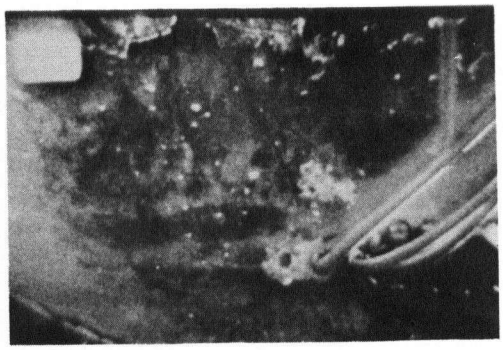

2.- t=0.02 s

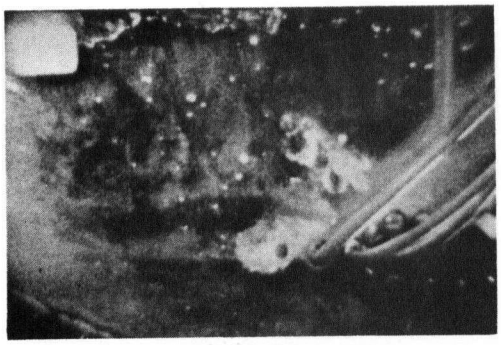

3.- t =0.04 s

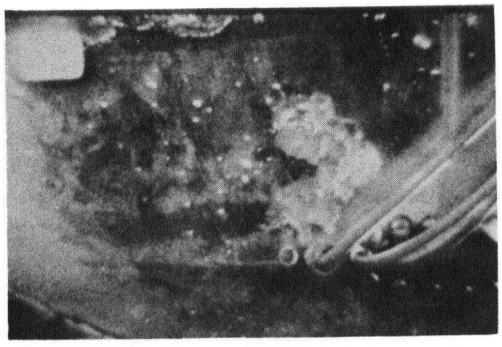

4.- t =0.06 s

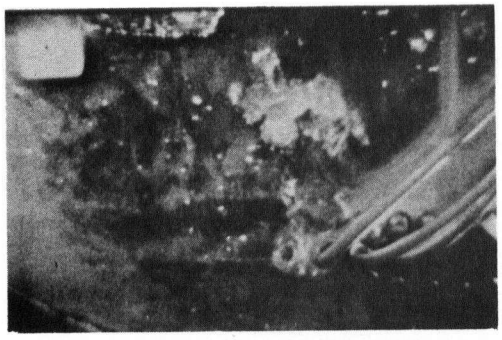

5.- t=0.08 s

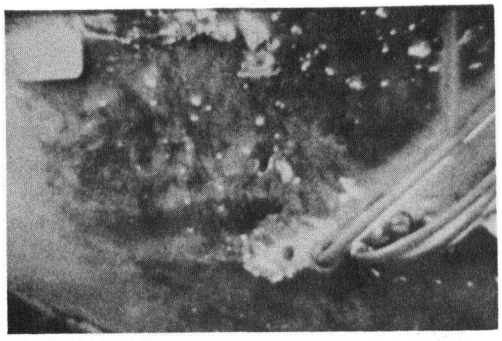

6.- t =0.10 s

Air in Mercury , 0.2 cm. dia., Half-tuyere.

Mass Flux = 45.99 $g cm^{-2} s^{-1}$ N'_{Fr} = 906 Nominal Mach=0.901

Fig. 26 Air-Hg, Low Flow, 0.2 cm. dia.

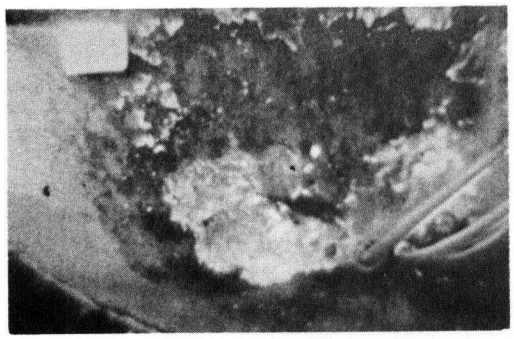

1.- t=0.00 s

2.- t=0.02 s

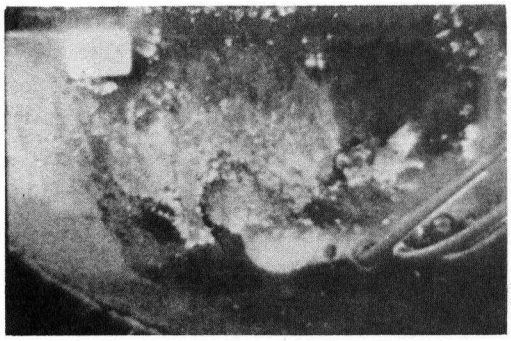

3.- t=0.04 s

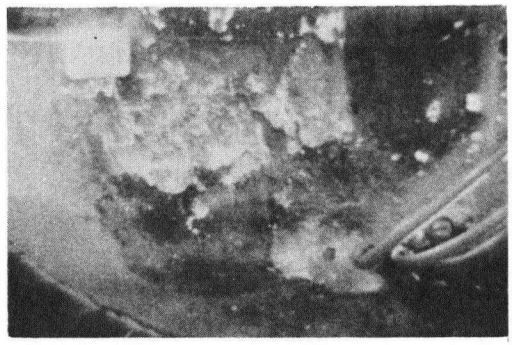

4.- t=0.06 s

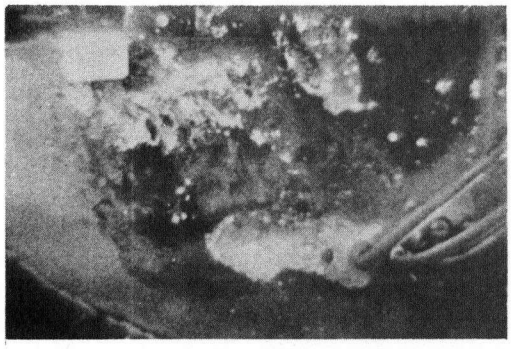

5.- t=0.08 s

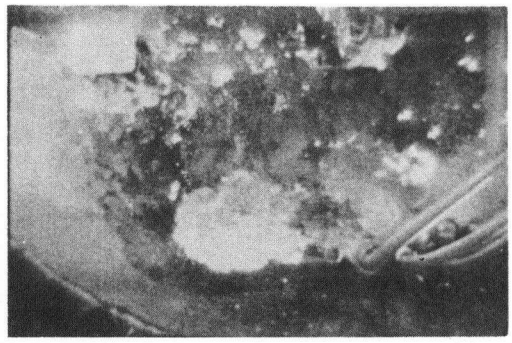

6.- t=0.10 s

Air-Hg, 0.2 cm. dia., Half-tuyere,

Mass flux= 153.88 g $cm^{-2}s^{-1}$ N'_{Fr}= 4122 Nominal Mach= 1.923

Fig. 27 Air-Hg, High Flow, 0.2 cm. dia.

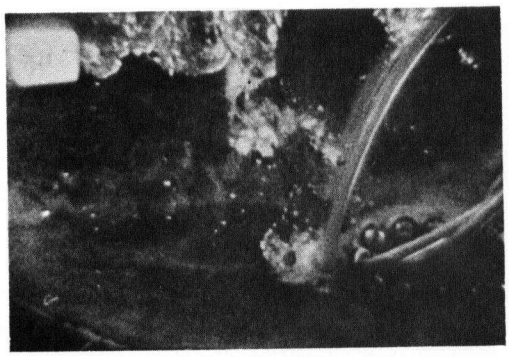

1.- t=0.00 s

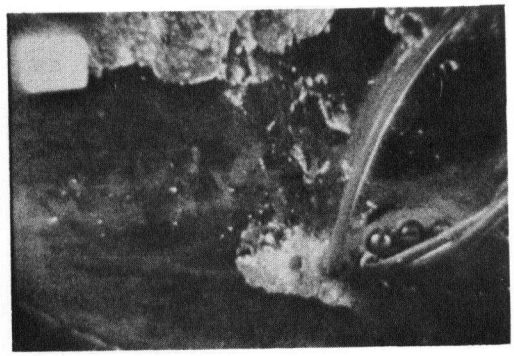

2.- t=0.02 s

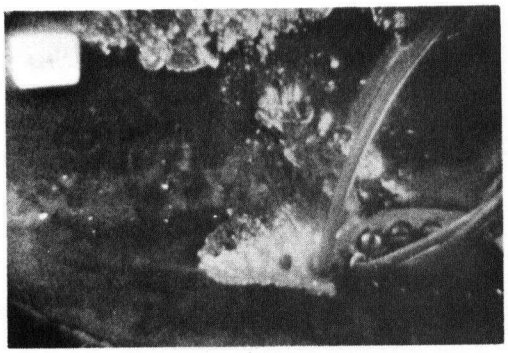

3.- t=0.04 s

4.- t=0.06 s

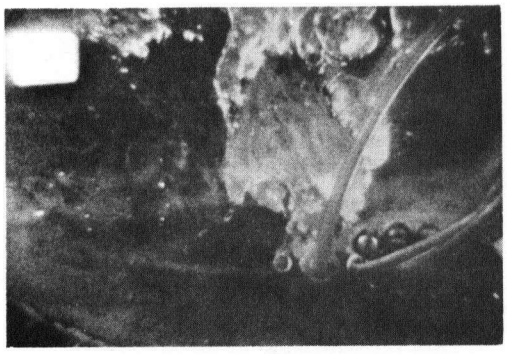

5.- t=0.08 s

6.- t=0.10 s

He-Hg, 0.2 cm. dia., Half-tuyere.

Mass flux= 17.62 g $cm^{-2}s^{-1}$ N'_{Fr} = 919 Nominal Mach=0.850

Fig. 28 He-Hg, Low Flow, 0.2 cm. dia.

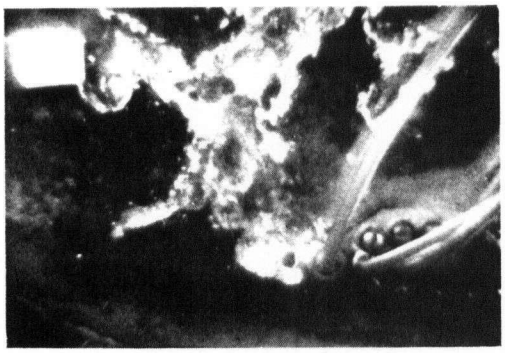

1.- t=0.00 s

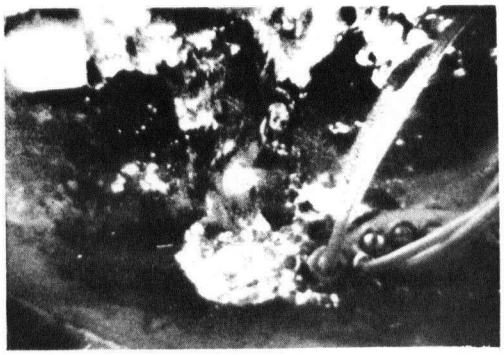

2.- t=0.02 s

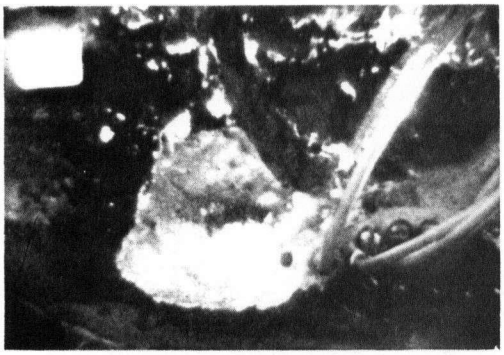

3.- t=0.04 s

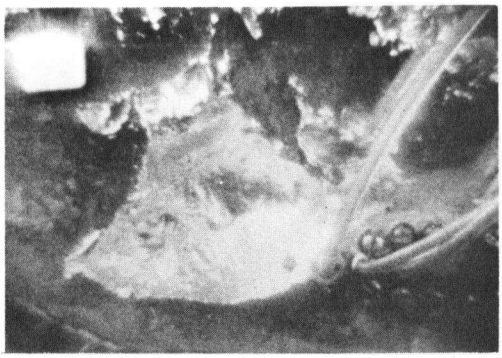

4.- t=0.06 s

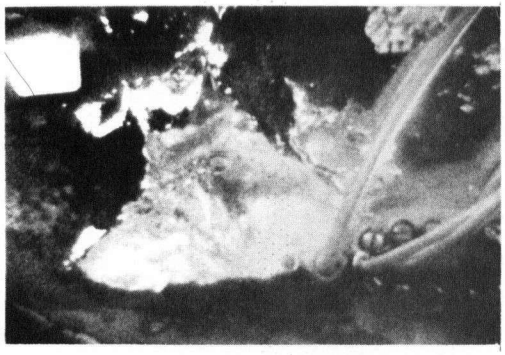

5.- t=0.08 s

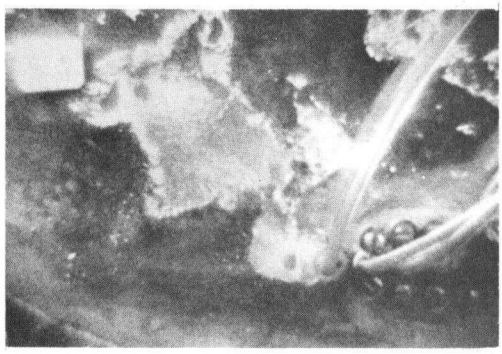

6.- t=0.10 s

He-Hg, 0.2 cm. dia., Half-tuyere.

Mass flux = 55.34 g $cm^{-2}s^{-1}$ N'_{Fr} = 4606 Nominal Mach = 1.903

Fig. 29 He-Hg, High Flow, 0.2 cm. dia.

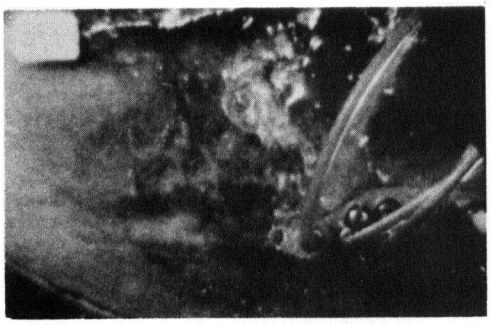

1.- t=0.00 s

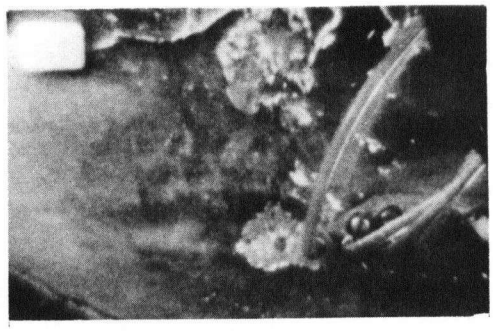

2.- t=0.02 s

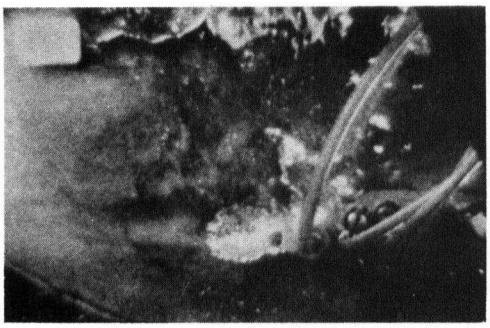

3.- t=0.04 s

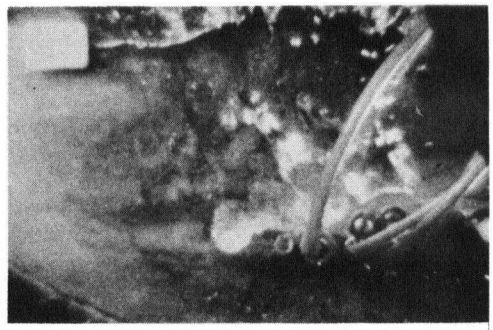

4.- t=0.06 s

5.- t=0.08 s

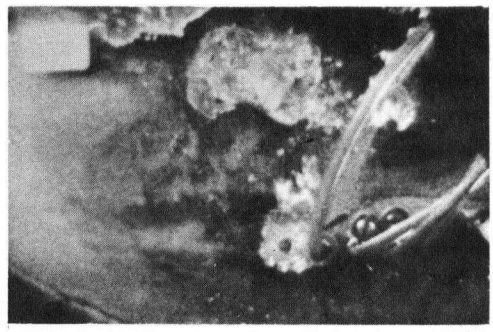

6.- t=0.10 s

Ar-Hg, 0.2 cm. dia., Half-tuyere,

Mass flux=30.93 $g cm^{-2} s^{-1}$ N'_{Fr} = 262.4 Nominal Mach=0.831

Fig. 30 Ar-Hg, Low Flow, 0.2 cm. dia.

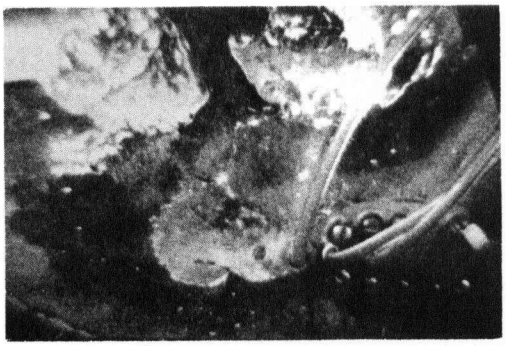

1.- t=0.00 s

2.- t=0.02 s

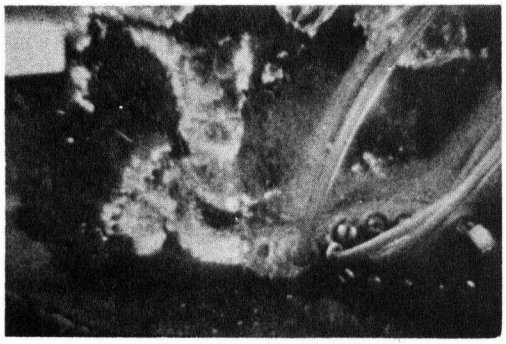

3.- t=0.04 s

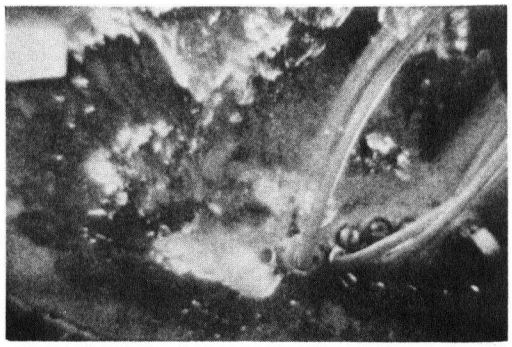

4.- t=0.06 s

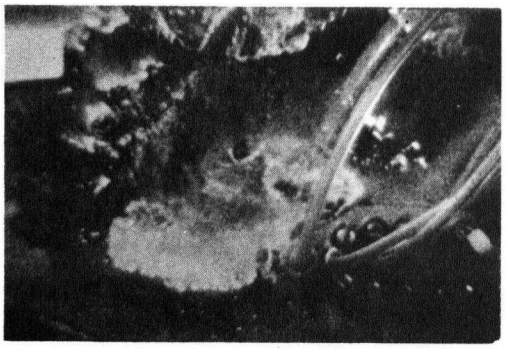

5.- t =0.08 s

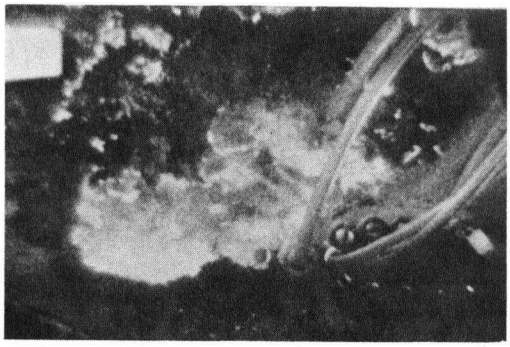

6.- t =0.10 s

Ar-Hg, 0.2 cm. dia., Half-tuyere,

Mass flux = 180.41 g $cm^{-2}s^{-1}$ N'_{Fr} = 17373 Nominal Mach = 1.163

Fig. 31 Ar-Hg, High Flow, 0.2 cm. dia.

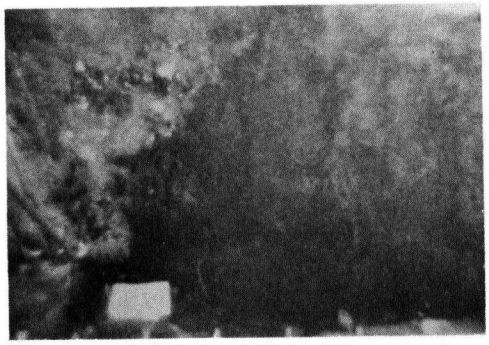

1.- t = 0.00 s

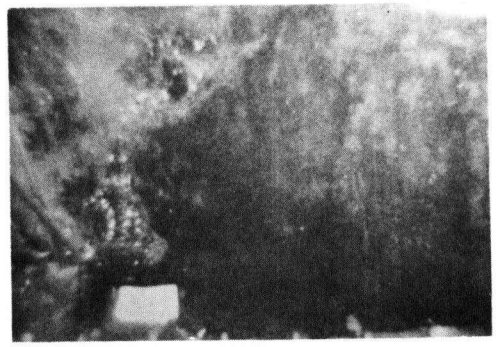

2.- t = 0.02 s

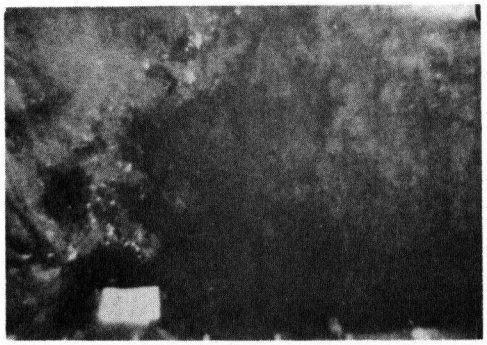

3.- t = 0.04 s

4.- t = 0.06 s

5.- t = 0.08 s

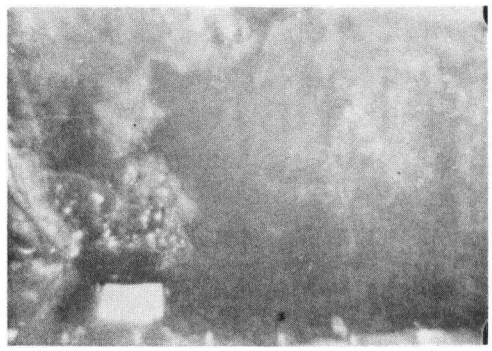

6.- t = 0.10 s

Helium - $ZnCl_2$ soln., 0476 cm. diam., half-tuyere.

Mass flux = 5.26 g/cm^{2}s N'_{Fr} = 259 Nominal mach = 0.267

Fig. 32 He-$ZnCl_2$ Solution, Low Flow, 0.476 cm. dia.

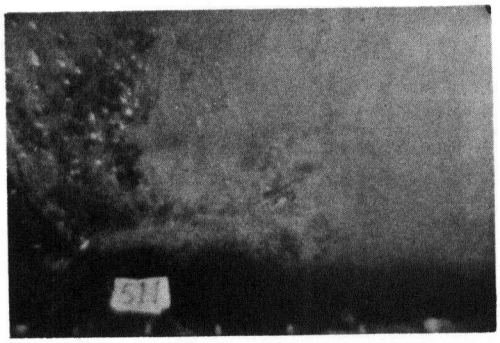

1.- t = 0.00 s

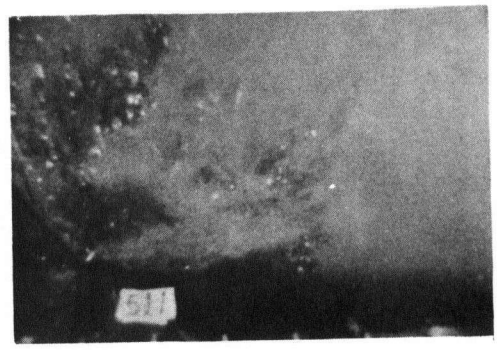

2.- t = 0.02 s

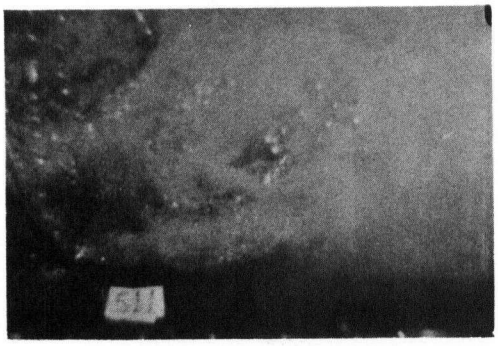

3.- t = 0.04 s

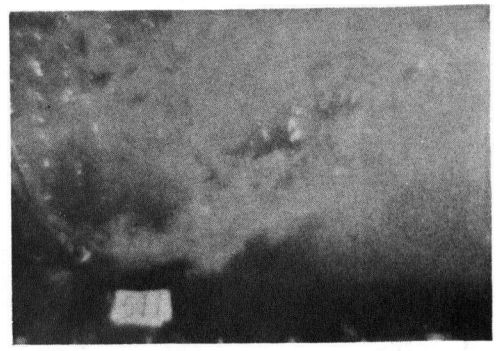

4.- t = 0.06 s

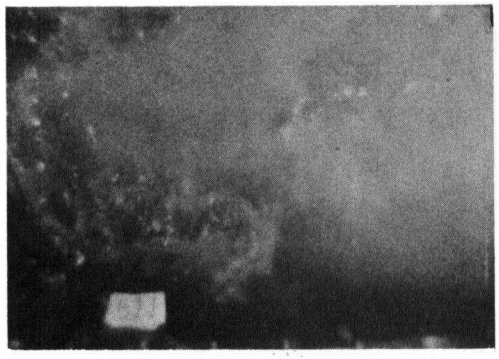

5.- t = 0.08 s

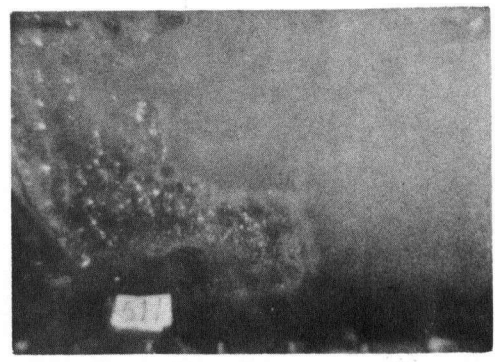

6.- t = 0.10 s

Helium - $ZnCl_2$ soln., 0.476 cm. diam., half-tuyere

Mass flux = 20.10 g/cm^{2}s N'_{Fr} = 4050 Nominal mach = 1.050

Fig. 33 Air-$ZnCl_2$ Solution, Low Flow, 0.476 cm. dia.

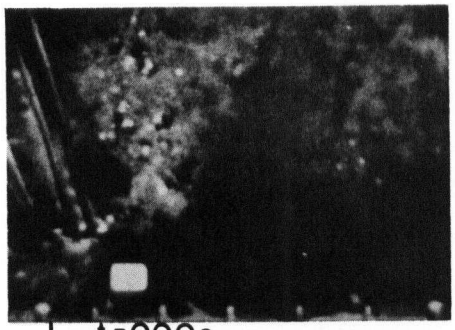

1.- t = 0.00 s

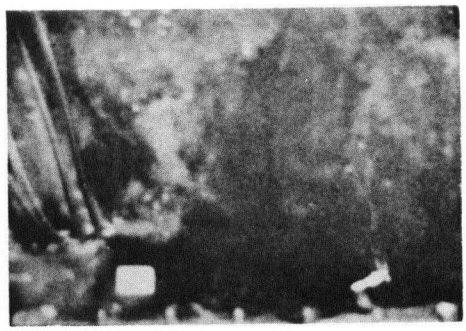

2.- t = 0.02 s

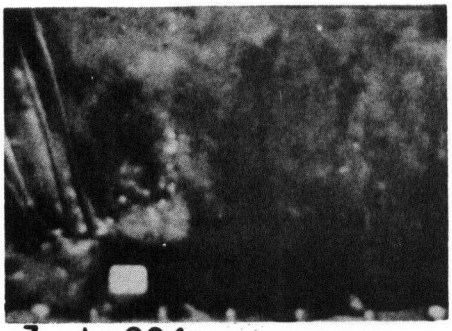

3.- t = 0.04 s

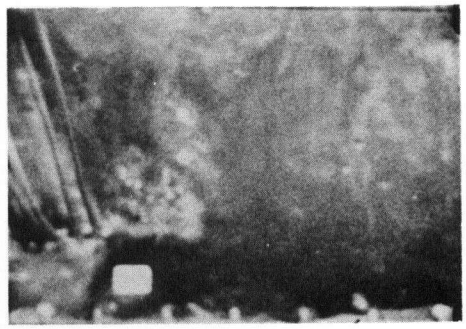

4.- t = 0.06 s

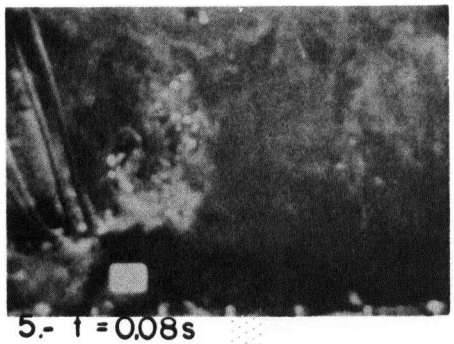

5.- t = 0.08 s

6.- t = 0.10 s

Air - $ZnCl_2$ soln., 0.476 cm. diam., half - tuyere

Mass flux = 13.89 g/cm^{2}s , N'_{Fr} = 277 , Nominal mach = 0.295

Fig. 34 Air-$ZnCl_2$ Solution, High Flow, 0.476 cm. dia.

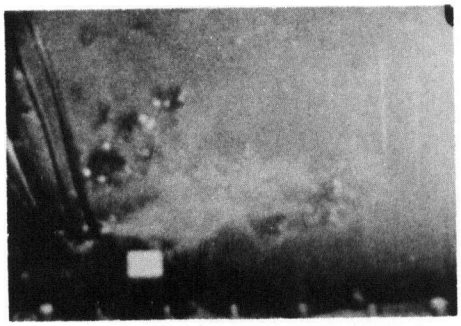

1.- t = 0.00 s

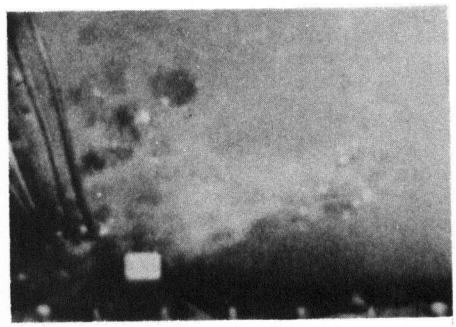

2.- t = 0.02 s

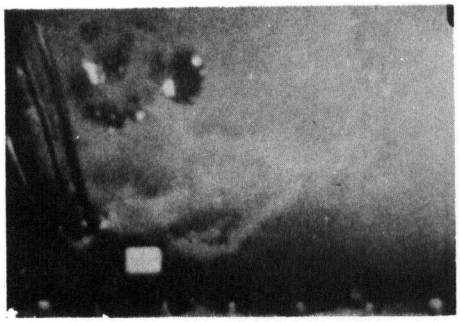

3.- t = 0.04 s

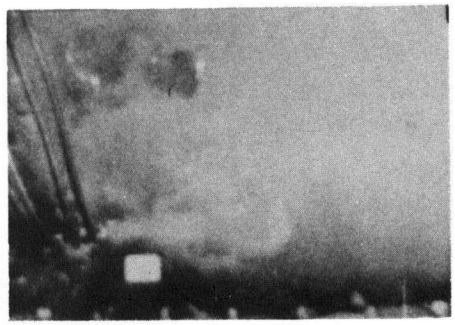

4.- t = 0.06 s

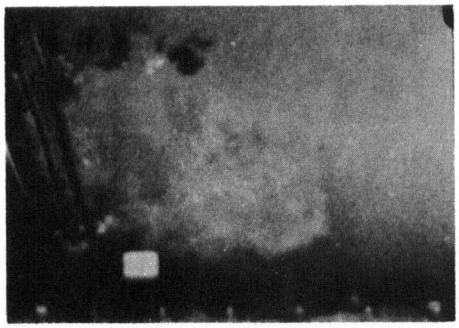

5.- t = 0.08 s

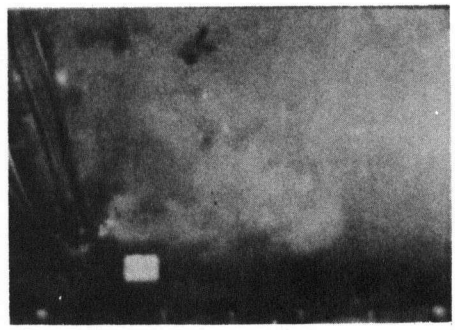

6.- t = 0.10 s

Air-ZnCl soln, 0.476 cm diam, half-tuyere

Mass flux = 52.81 g/cm^{2}s N'_{Fr} = 4210 Nominal mach = 1.150

Fig. 35 Air-$ZnCl_2$ Solution, High Flow, 0.476 cm. dia.

1.- t = 0.00s

2.- t=0.02 s

3.- t = 0.04s

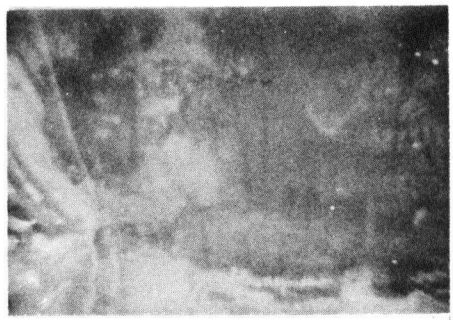

4.- t=0.06 s

5.- t = 0.08s

6.- t = 0.10s

Air - water, 0.476cm diam, half-tuyere

Mass flux = 26.13 g/cm^{2}s N'_{Fr} = 21 03 Nominal mach = 0.510

Fig. 36 Air-H_2O, Low Flow, 0.476 cm. dia.

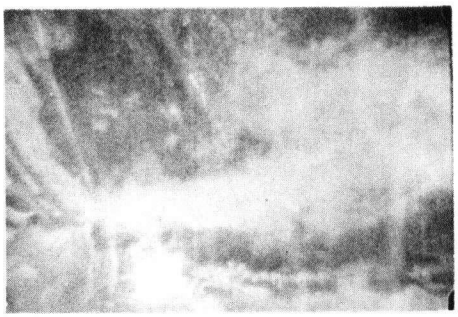

1.- t = 0.00 s

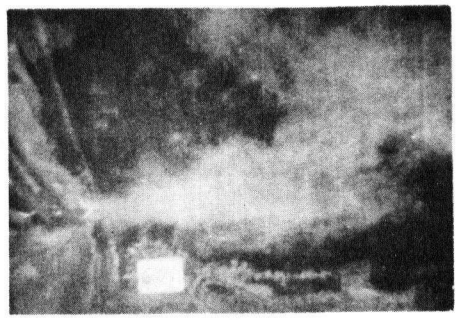

2.- t = 0.02 s

3.- t = 0.04 s

4.- t = 0.06 s

5.- t = 0.08 s

6.- t = 0.10 s

Air-water, 0.476cm diam, half-tuyere

Mass flux = 57.51 N'_{Fr} = 8520 Nominal mach = 1.250

Fig. 37 Air-H_2O, High Flow, 0.476 cm. dia.

APPENDIX II

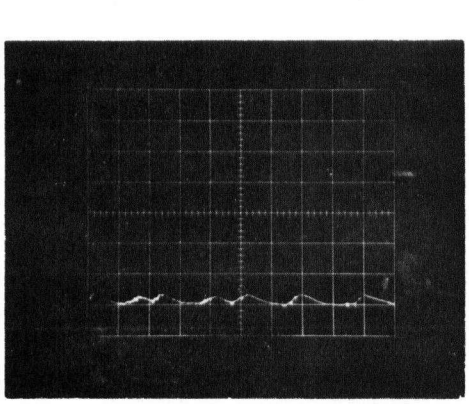

1.- $Ma_o = 0.205$, $\dot{M} = 10.51\ g/cm^2s$

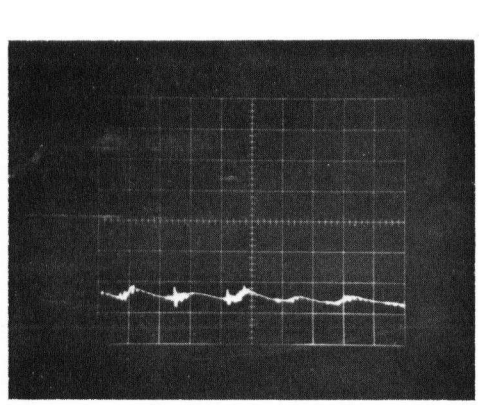

2.- $Ma_o = 0.464$, $\dot{M} = 23.84\ g/cm^2s$

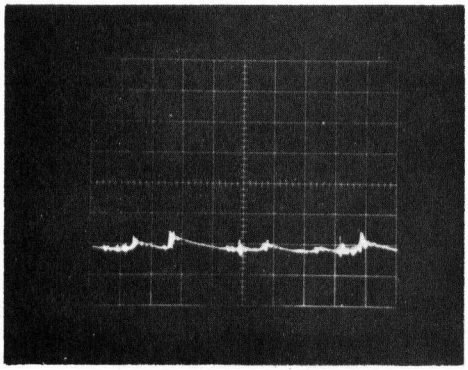

3.- $Ma_o = 0.815$, $\dot{M} = 47.69\ g/cm^2s$

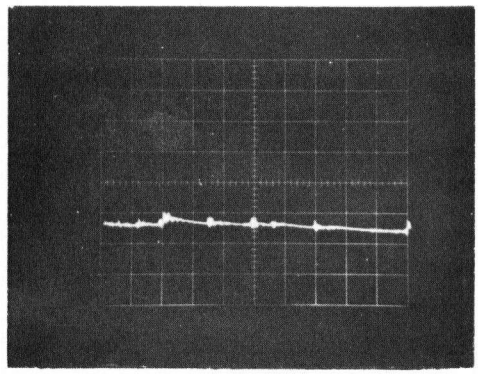

4.- $Ma_o = 0.873$, $\dot{M} = 56.69\ g/cm^2s$

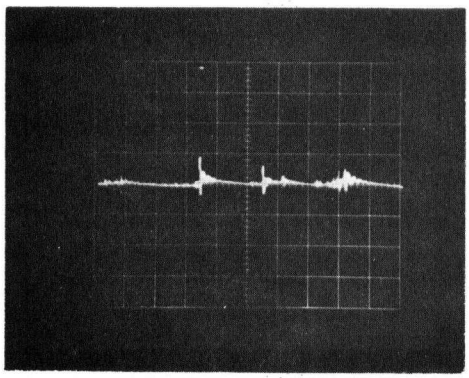

5.- $Ma_o = 0.877$, $\dot{M} = 64.48\ g/cm^2s$

Air - Mercury, 0.325 cm. diam., half-tuyere

vert. axis: sensitivity = 2.29 psi/div

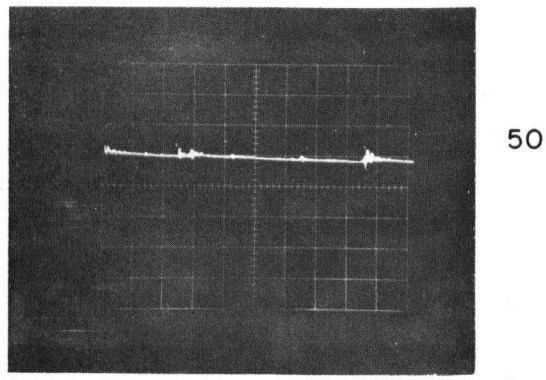

6.- $Ma_o = 0.878$, $\dot{M} = 72.07\ g/cm^2s$

Fig. 38 Air-Hg, 0.325 cm. dia., Half-Tuyere.

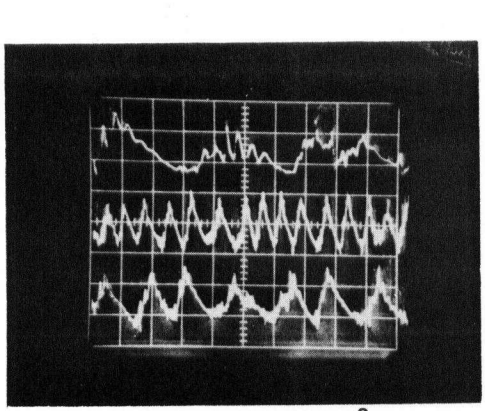

1.- $Ma_0 = 0.208, \dot{M} = 10.78\ g/cm^2s$

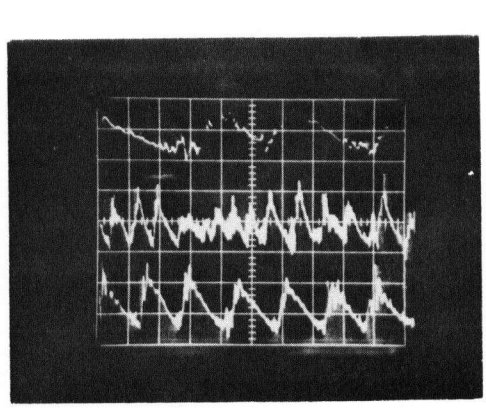

2.- $Ma_0 = 0.317, \dot{M} = 16.52\ g/cm^2s$

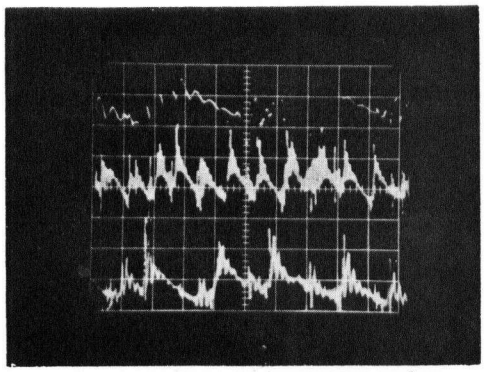

3.- $Ma_0 = 0.666, \dot{M} = 34.68\ g/cm^2s$

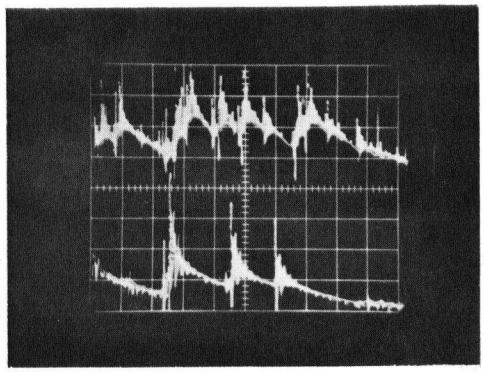

4.- $Ma_0 = 0.937, \dot{M} = 55.25\ g/cm^2s$

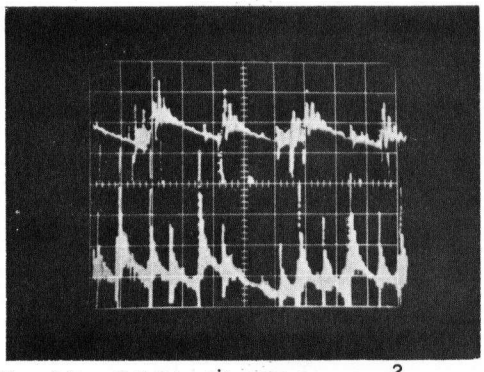

5.- $Ma_0 = 0.961, \dot{M} = 63.01\ g/cm^2s$

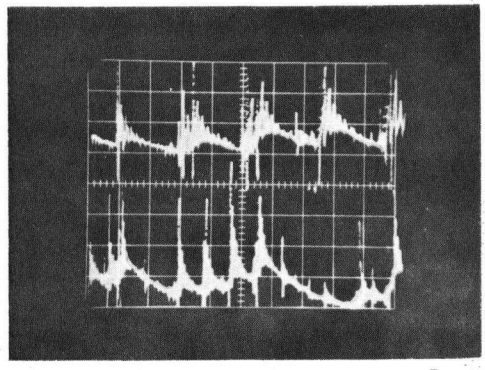

6.- $Ma_0 = 0.972, \dot{M} = 71.86\ g/cm^2s$

Air–Mercury, 0.325 cm. diam, full tuyere
vert. axis: sensitivity = 0.963 psi/div

Fig. 39 Air-Hg, 0.325 cm. dia., Full-Tuyere.

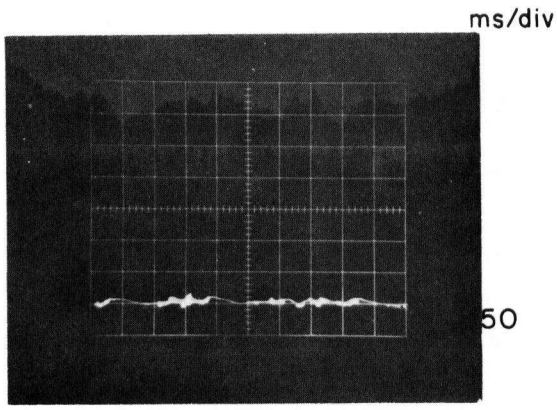

1.- $Ma_o = 0.516$, $\dot{M} = 26.14\ g/cm^2s$

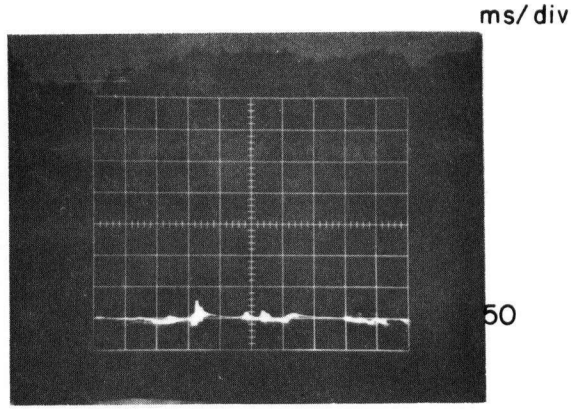

2.- $Ma_o = 0.901$, $\dot{M} = 45.99\ g/cm^2s$

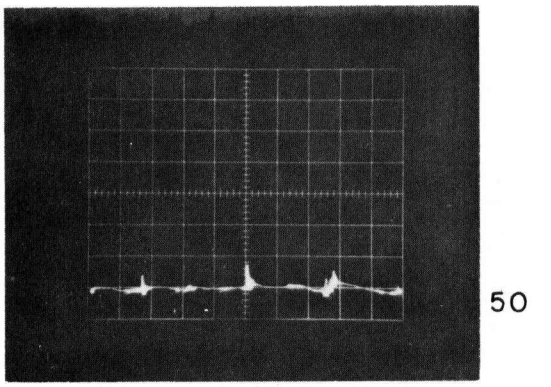

3.- $Ma_o = 1.340$, $\dot{M} = 68.87 g/cm^2s$

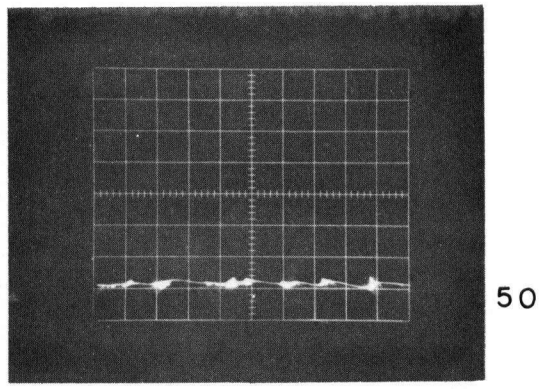

4.- $Ma_o = 1.777$, $\dot{M} = 98.17 g/cm^2s$

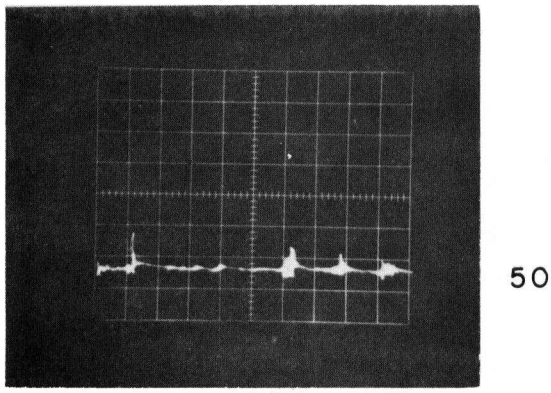

5.- $Ma_o = 1.876$, $\dot{M} = 113.87 g/cm^2s$

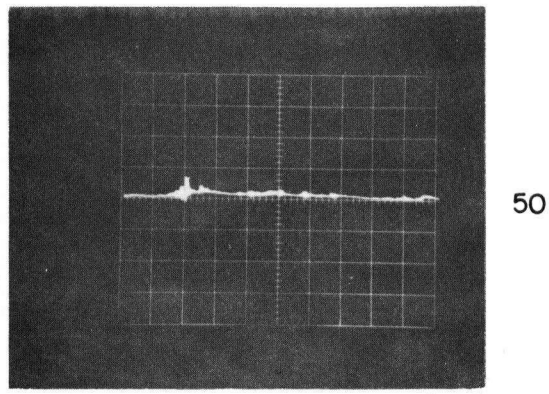

6.- $Ma_o = 1.923$, $M = 153.88 g/cm^2s$

Air-Mercury, 0.2 cm. diam., half-tuyere
vert. axis sensitivity = 2.29 psi/div

Fig. 40 Air-Hg, 0.2 cm. dia., Half-Tuyere.

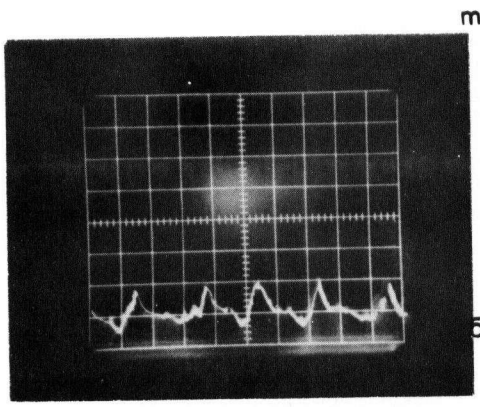

1.- $Ma_o = 0.498$, $\dot{M} = 10.32\ g/cm^2s$

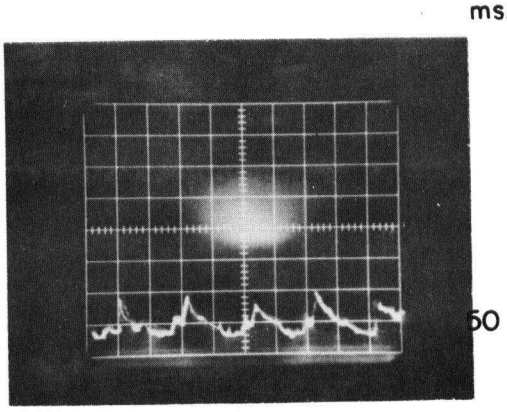

2.- $Ma_o = 1.173$, $\dot{M} = 24.31 g/cm^2s$

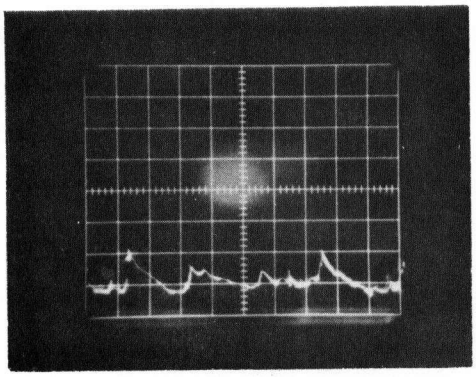

3.- $Ma_o = 1.519$, $\dot{M} = 32.35\ g/cm^2s$

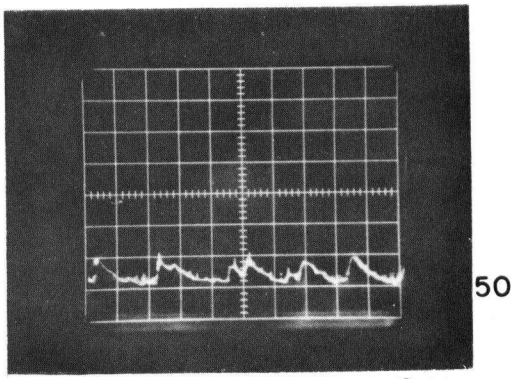

4.- $Ma_o = 1.716$, $\dot{M} = 38.52\ g/cm^2s$

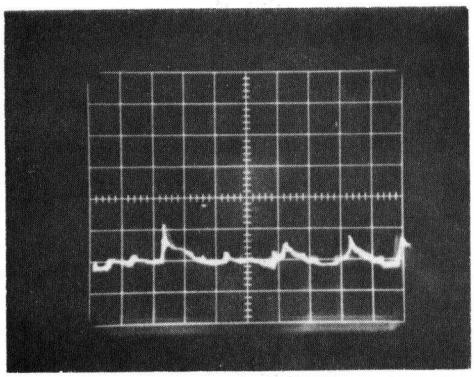

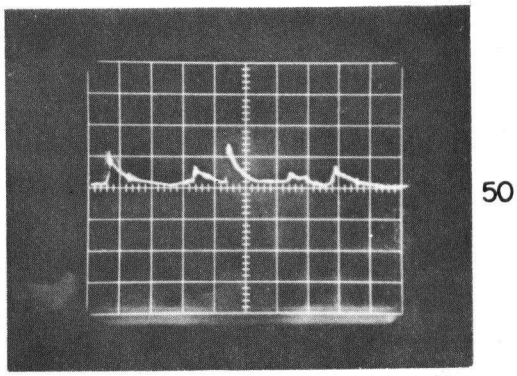

5.- $Ma_o = 1.803$, $\dot{M} = 44.69\ g/cm^2s$

Helium - Mercury, 0.2 cm. diam., half-tuyere
Vert. axis sensitivity = 2.23 psi / div

Fig. 41 He-Hg, 0.2 cm. dia., Half-Tuyere.

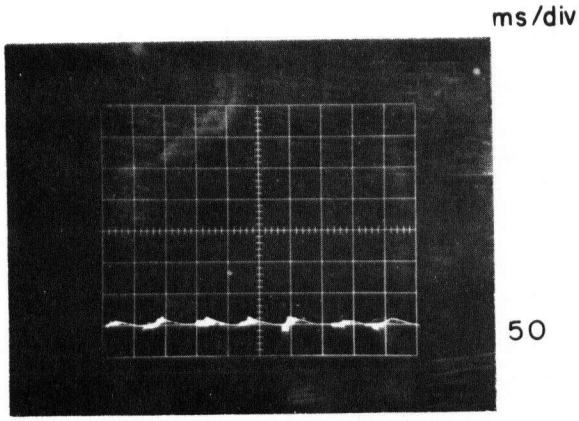

1.- $Ma_o = 0.452$, $\dot{M} = 30.93\ g/cm^2 s$

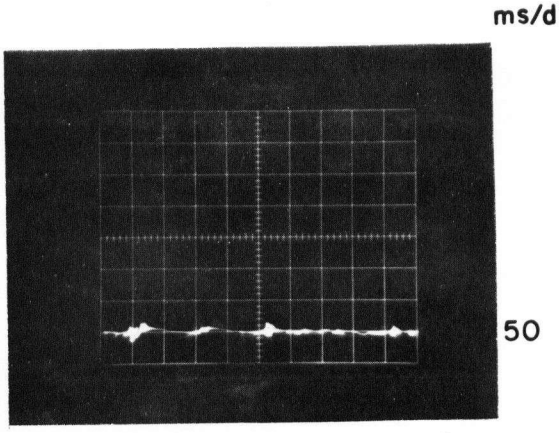

2.- $Ma_o = 0.831$, $\dot{M} = 53.75\ g/cm^2 s$

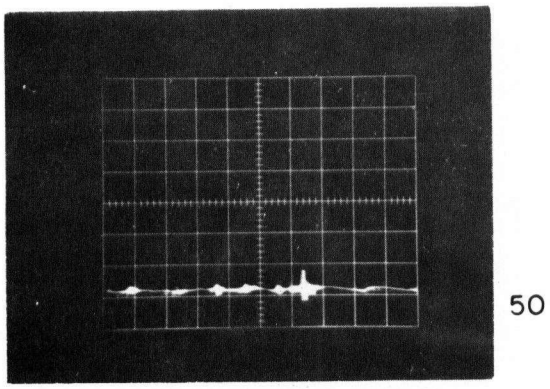

3.- $Ma_o = 1.874$, $\dot{M} = 107.5\ g/cm^2 s$

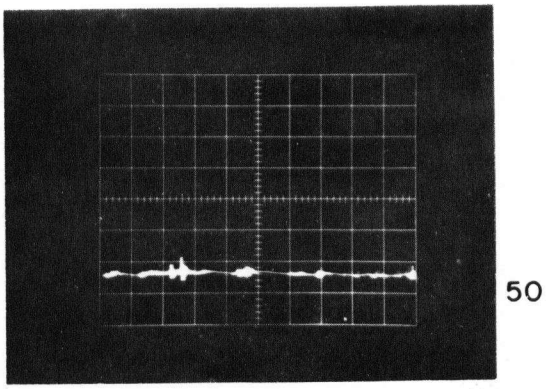

4.- $Ma_o = 1.828$, $\dot{M} = 125.09\ g/cm^2 s$

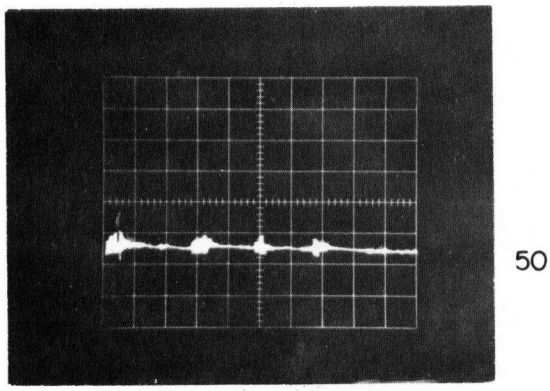

5.- $Ma_o = 1.589$, $\dot{M} = 144.66\ g/cm^2 s$

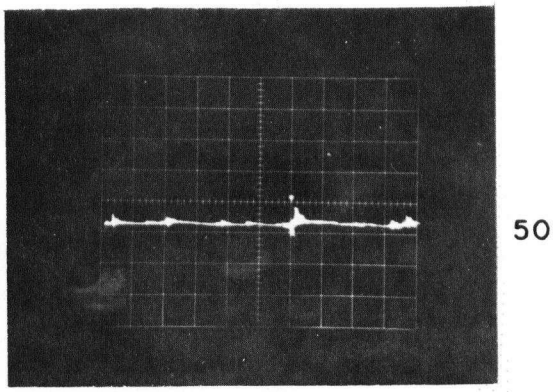

6.- $Ma_o = 1.163$, $\dot{M} = 180.41\ g/cm^2 s$

Argon - Mercury 0.2 cm. diam., half-tuyere

Vert. axis sensitivity = 9.04 psi/div

Fig. 42 Ar-Hg, 0.2 cm. dia., Half-Tuyere.

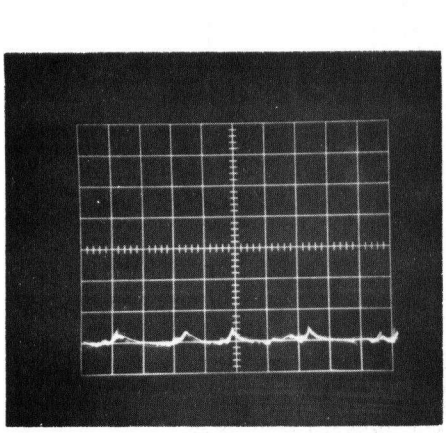

1.- $Ma_0 = 0.156$ $\dot{M} = 3.08 g/cm^2 s$

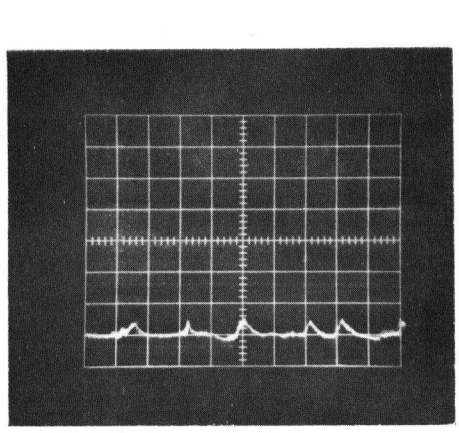

2.- $Ma_0 = 0.267$ $\dot{M} = 5.26 g/cm^2 s$

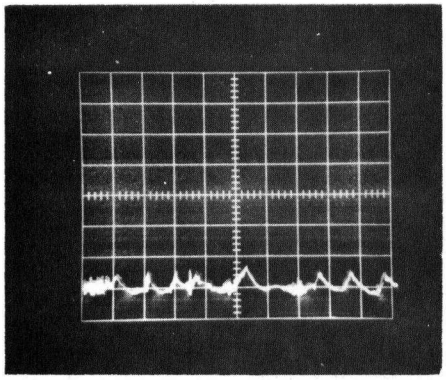

3.- $Ma_0 = 0.433$ $\dot{M} = 8.55 g/cm^2 s$

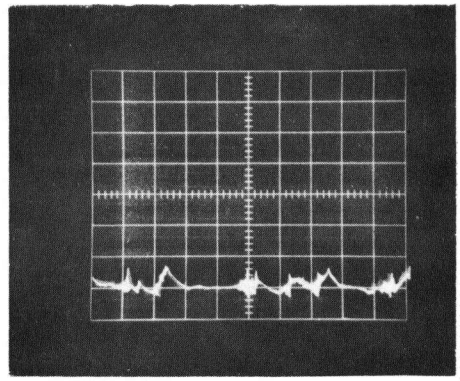

4.- $Ma_0 = 0.648$ $\dot{M} = 12.76 g/cm^2 s$

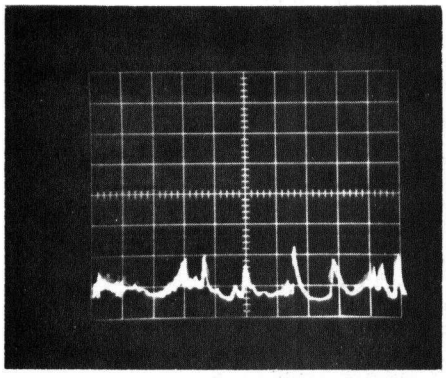

5.- $Ma_0 = 0.897$ $\dot{M} = 17.67 g/cm^2 s$

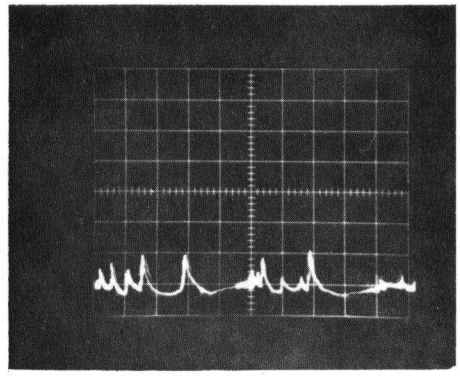

6.- $Ma_0 = 1.117$ $\dot{M} = 22.02 g/cm^2 s$

Helium – $ZnCl_2$ soln., 0.476 cm. diam., half-tuyere
Vert. axis sensitivity = 0.963 psi/div

Fig. 43 He-$ZnCl_2$ Solution, 0.476 cm. dia., Half-Tuyere.

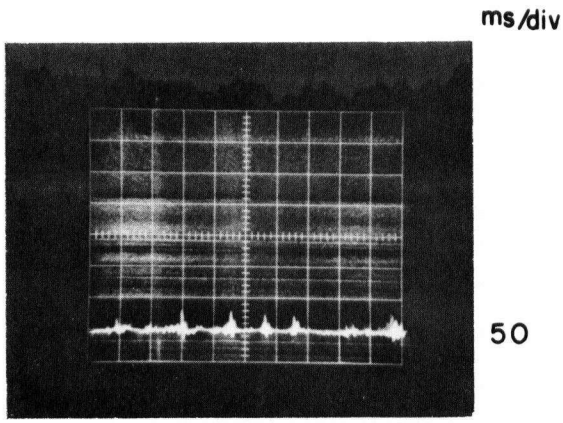

1.- $Ma_0 = 0.295$, $\dot{M} = 13.89\ g/cm^2\ s$

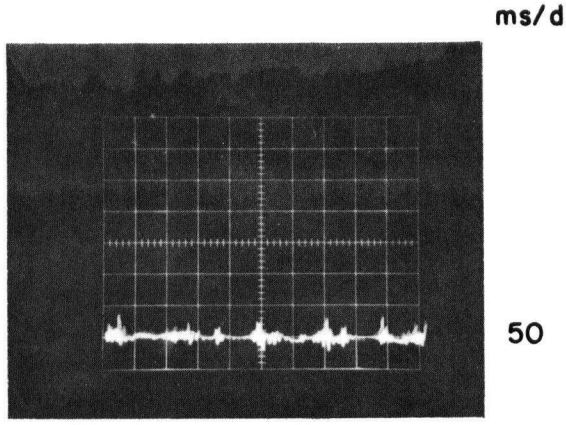

2.- $Ma_0 = 0.464$, $\dot{M} = 21.87\ g/cm^2 s$

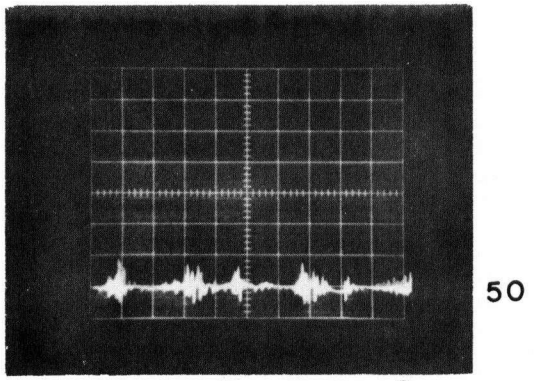

3.- $Ma_0 = 0.700$, $\dot{M} = 32.97\ g/cm^2 s$

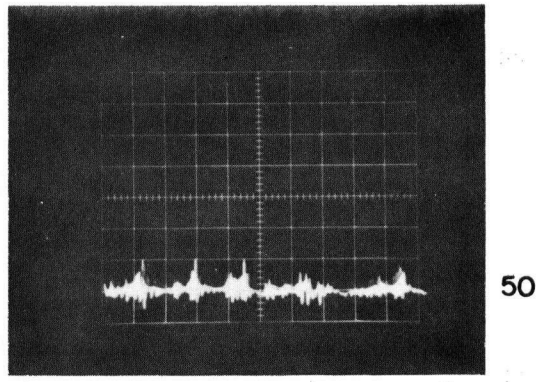

4.- $Ma_0 = 0.840$, $\dot{M} = 39.54\ g/cm^2 s$

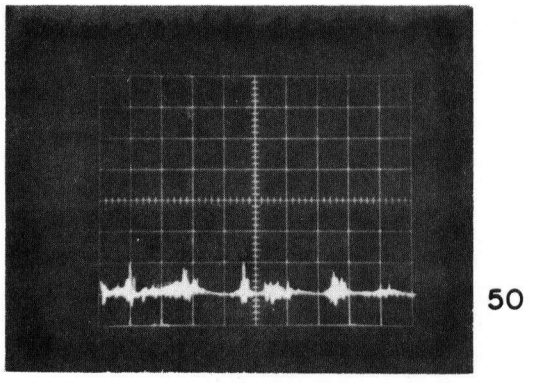

5.- $Ma_0 = 0.964$, $\dot{M} = 45.44\ g/cm^2\ s$

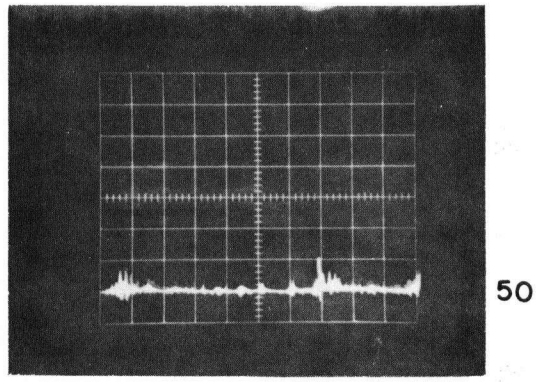

6.- $Ma_0 = 1.164$, $\dot{M} = 54.81\ g/cm^2 s$

Air – $ZnCl_2$ soln. 0.476 cm. diam., half-tuyere
Vert. axis: sensitivity = 0.963 psi / div

Fig. 44 Air-$ZnCl_2$ Solution, 0.476 cm. dia., Half-Tuyere.

ms/div

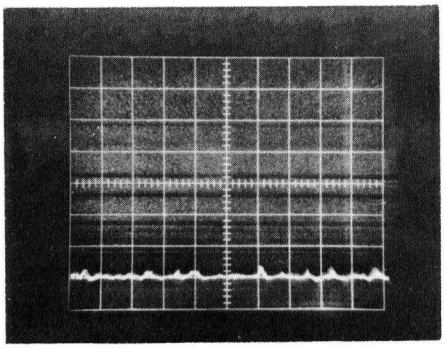

1.- $Ma_o = 0.198$, $\dot{M} = 9.942\ g/cm^2 s$

ms/div

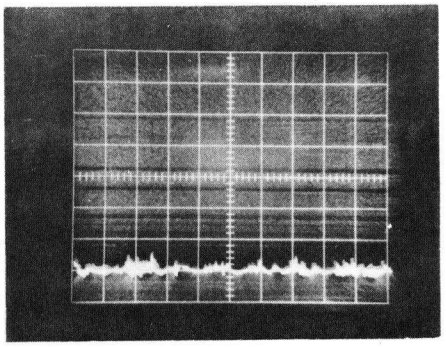

2.- $Ma_o = 0.372$, $\dot{M} = 18.709\ g/cm^2 s$

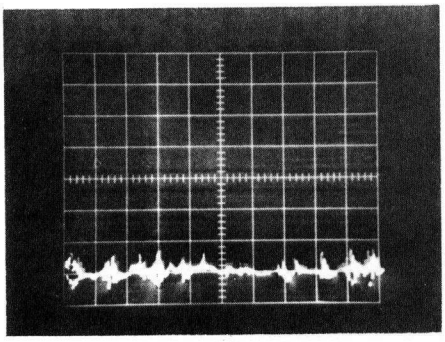

3.- $Ma_o = 0.660$, $\dot{M} = 33.168\ g/cm^2 s$

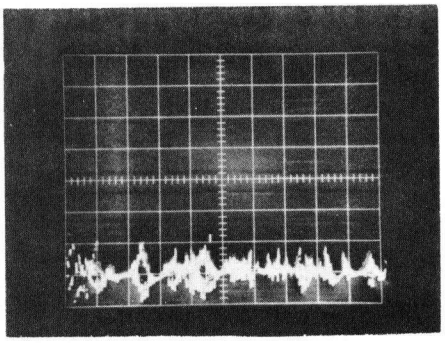

4.- $Ma_o = 1.336$, $\dot{M} = 68.70\ g/cm^2 s$

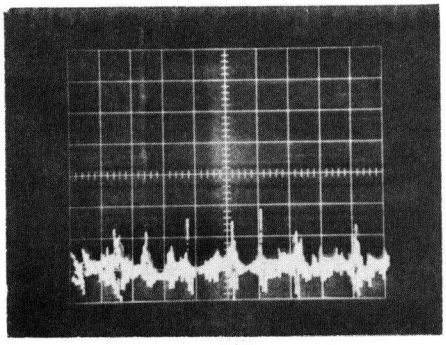

5.- $Ma_o = 1.598$, $\dot{M} = 83.38\ g/cm^2 s$

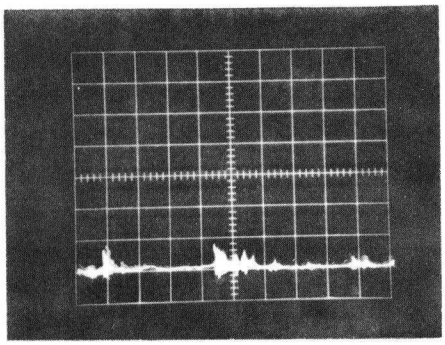

6.- $Ma_o = 1.879$, $\dot{M} = 98.75\ g/cm^2 s$

Air- water, 0.476 cm. diam., half-tuyere
Vert. axis sensitivity = 0.232 psi / div

Fig. 45 Air-H_2O, 0.476 cm. dia., Half-Tuyere.

APPENDIX III

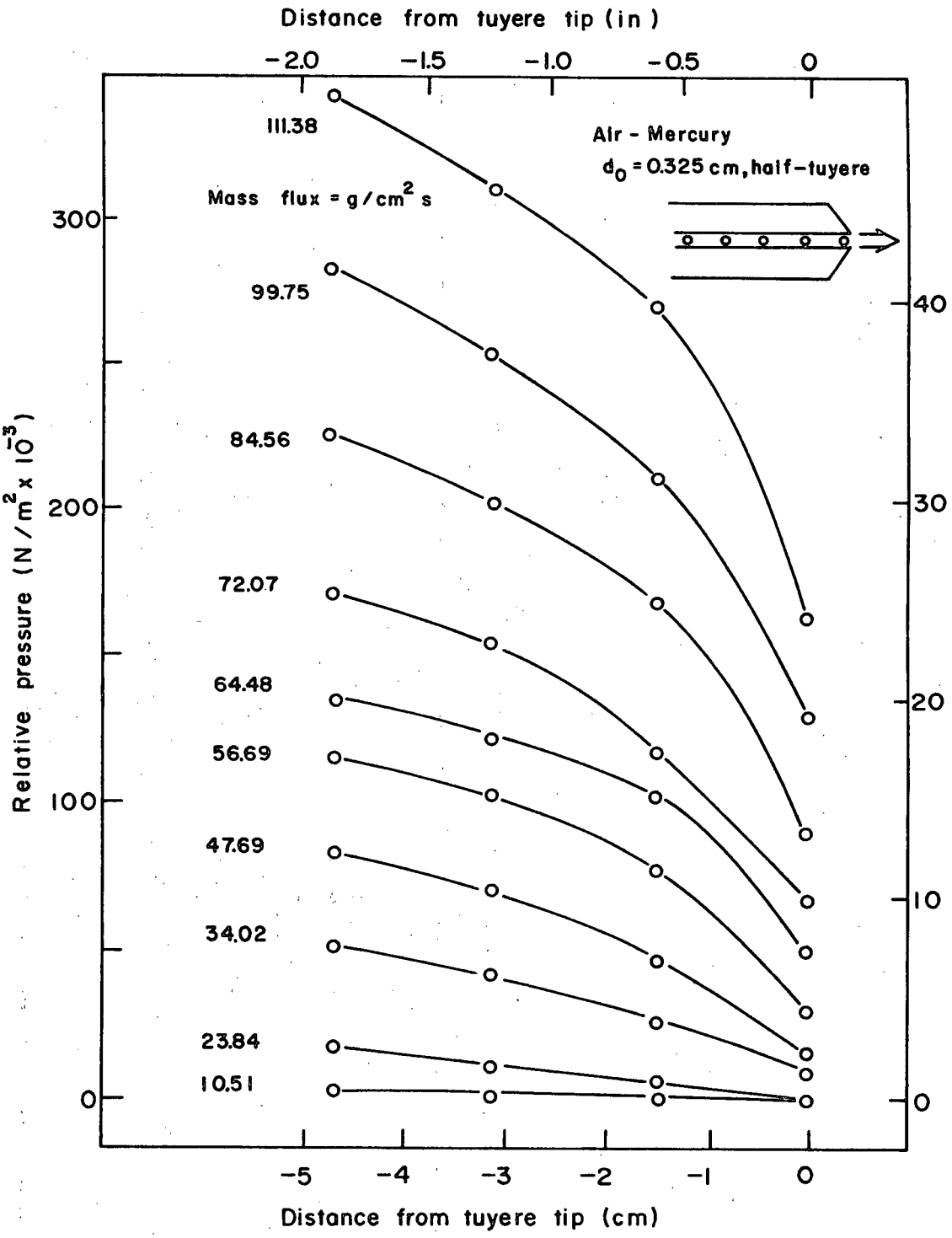

Fig. 46 Pressure Profiles, 0.325 cm. dia., Half-Tuyere.

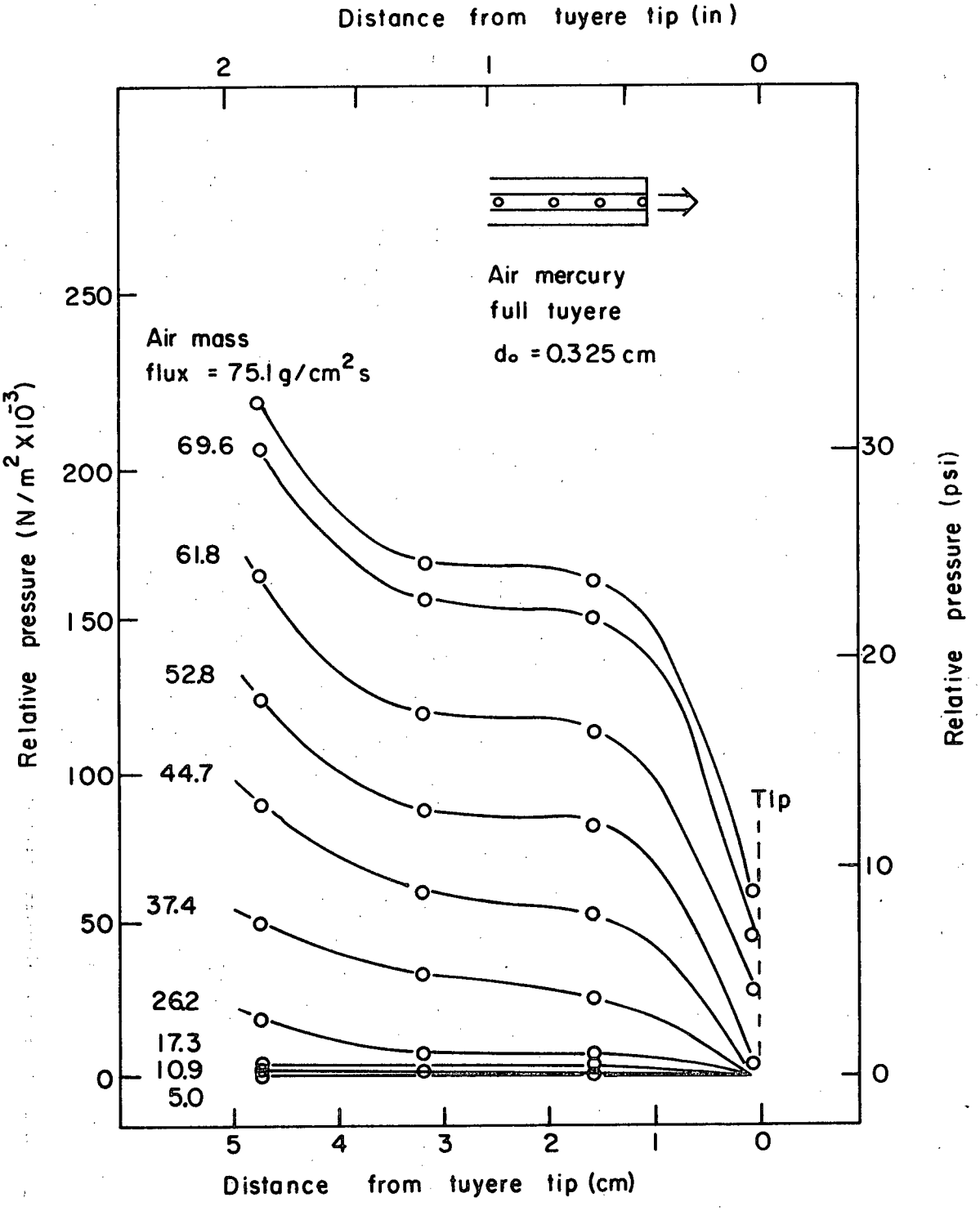

Fig. 47 Pressure Profiles, 0.325 cm. dia., Full-Tuyere, Air-Hg.

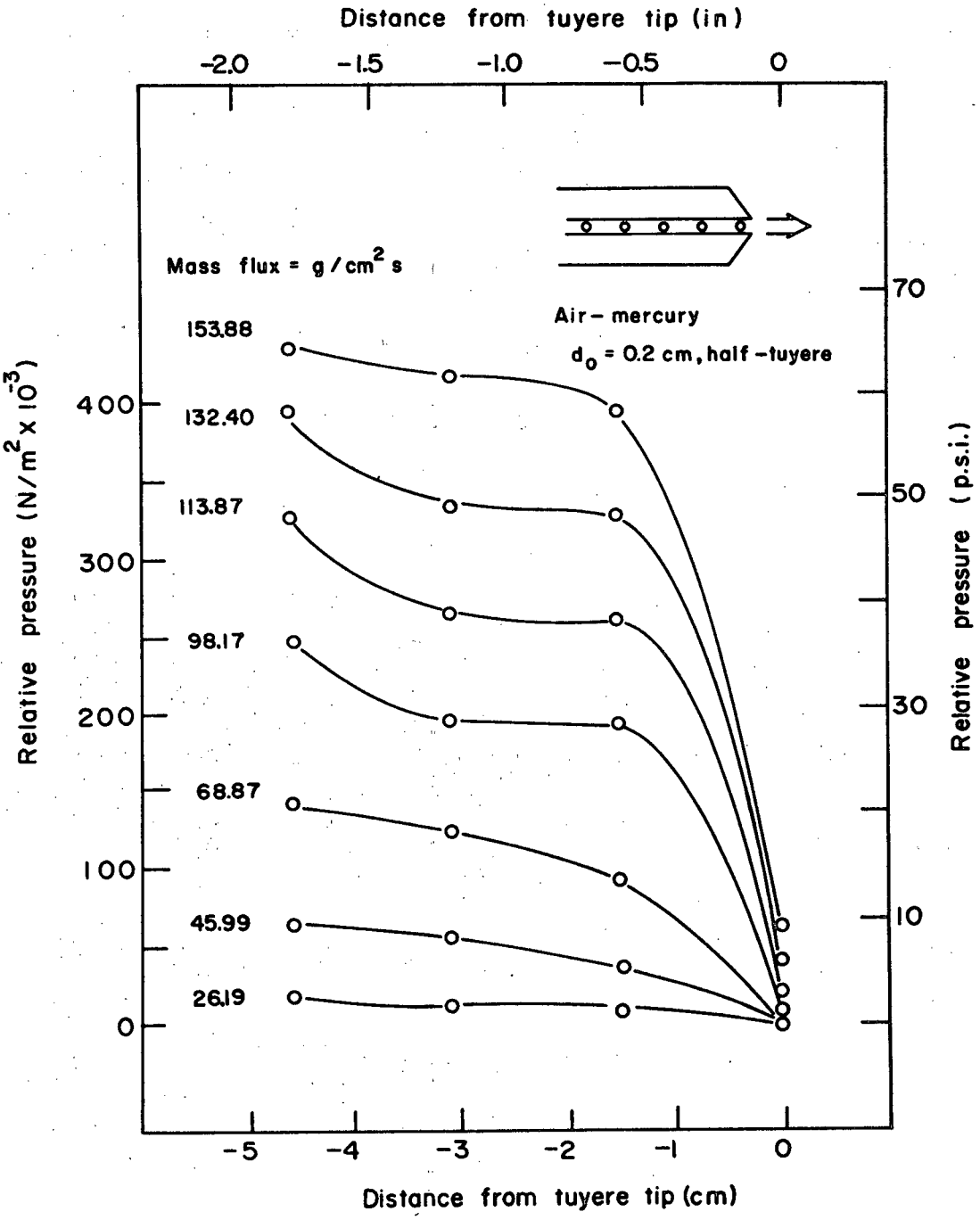

Fig. 48 Pressure Profiles, 0.2 cm. dia., Half-Tuyere, Air-Hg.

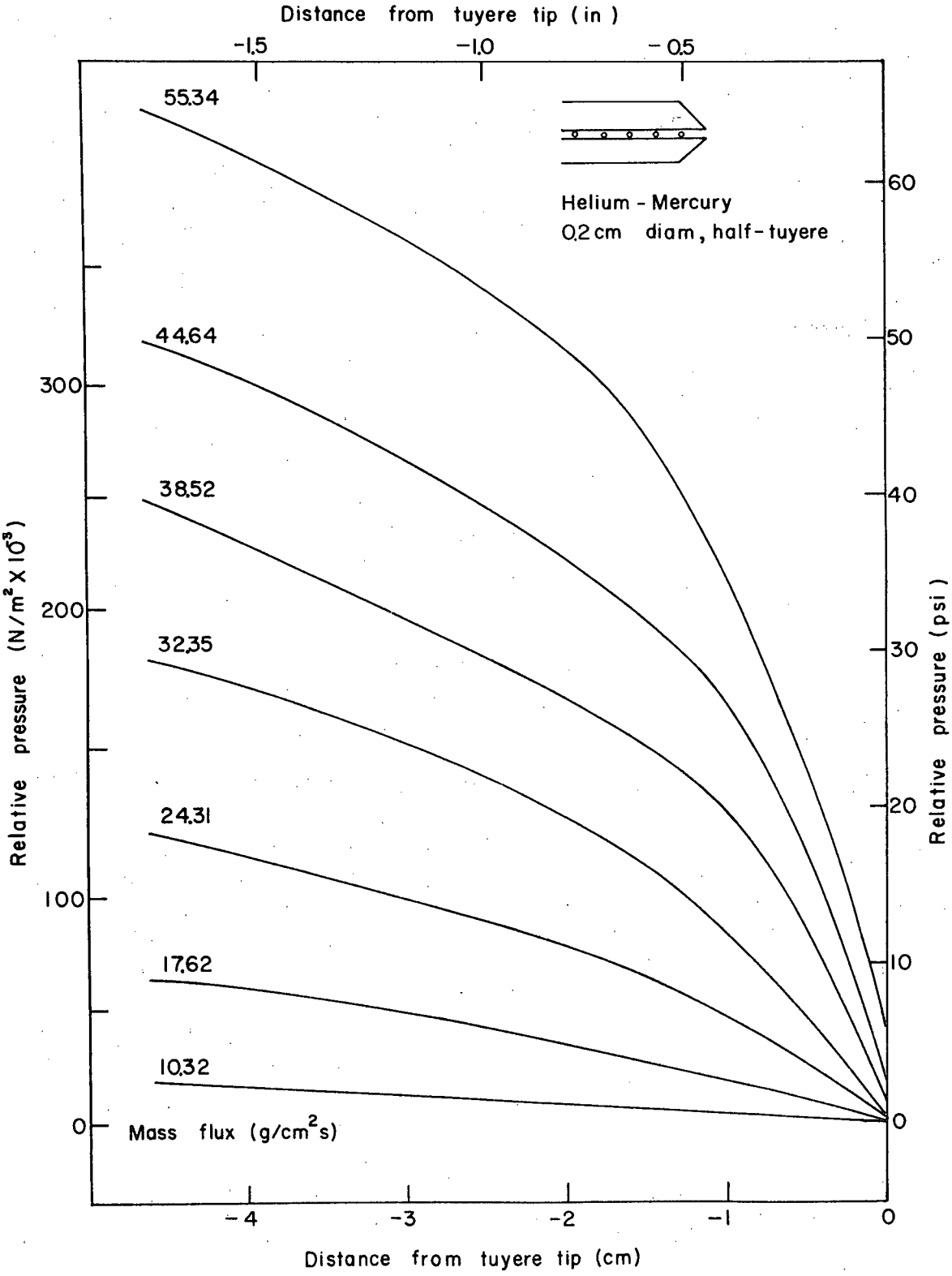

Fig. 49 Pressure Profiles, 0.2 cm. dia., Half-Tuyere, He-Hg.

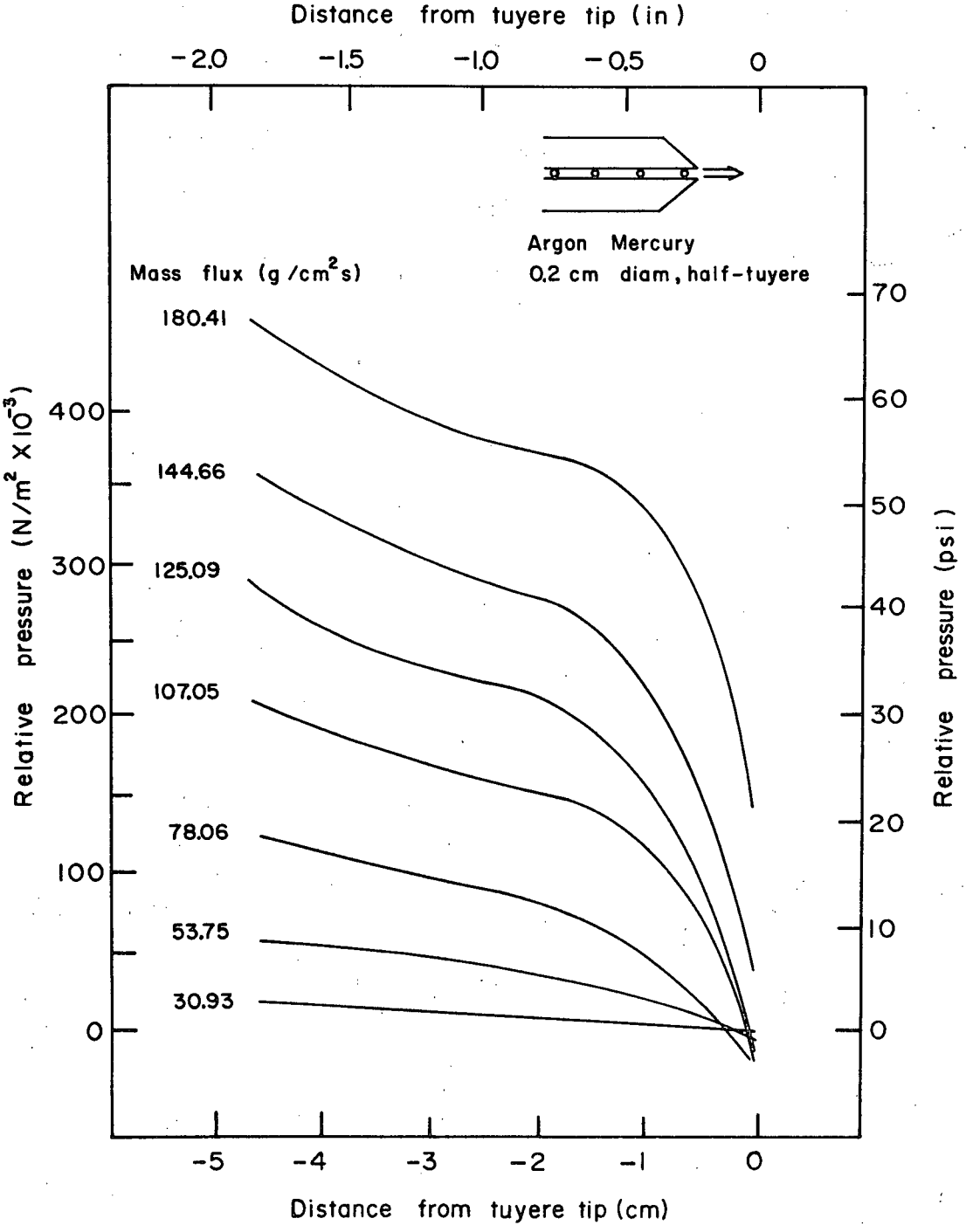

Fig. 50 Pressure Profiles, 0.2 cm. dia., Half-Tuyere, A-Hg.

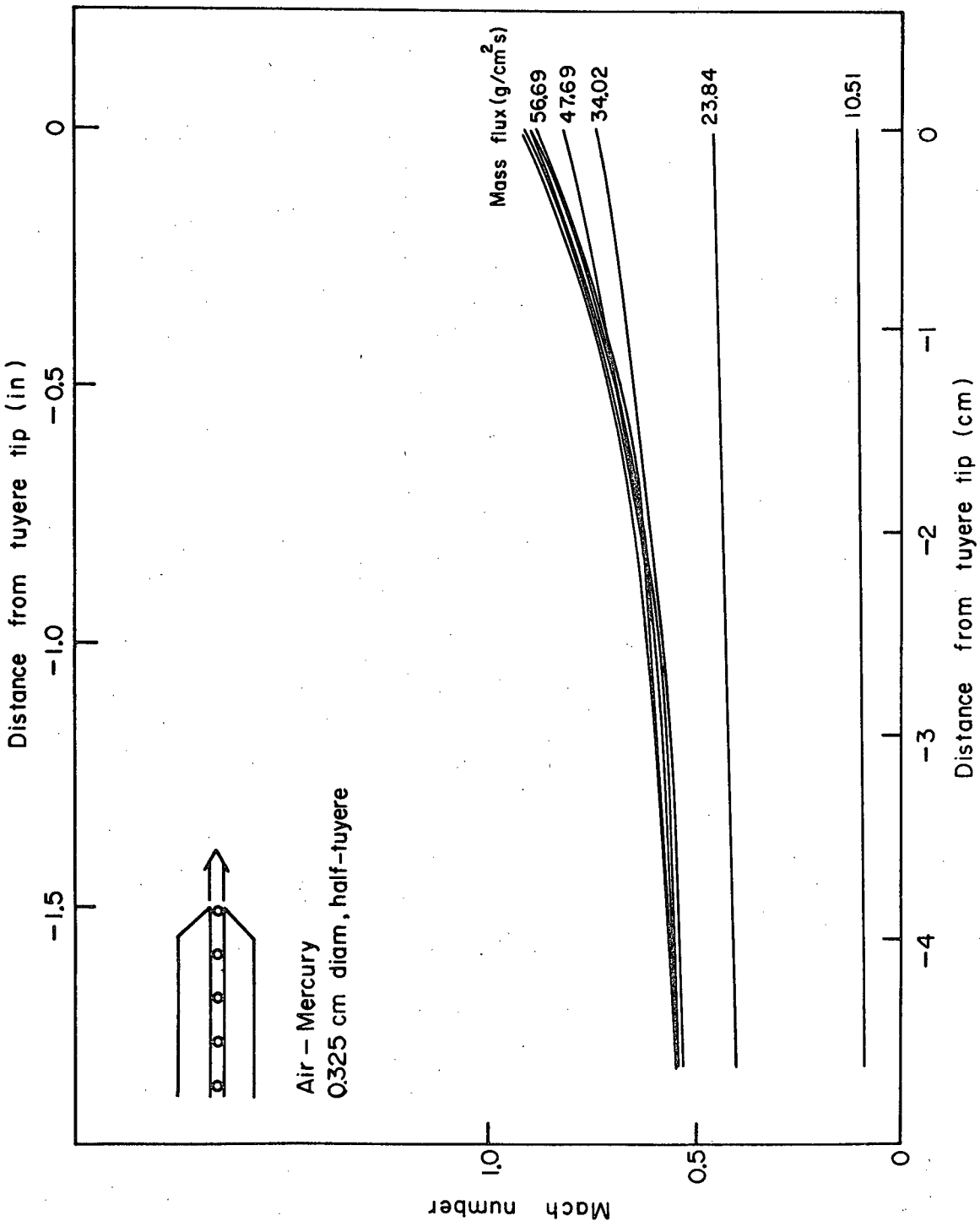

Fig. 51 Mach Number Profiles, 0.325 cm. dia., Half-Tuyere, Air-Hg.

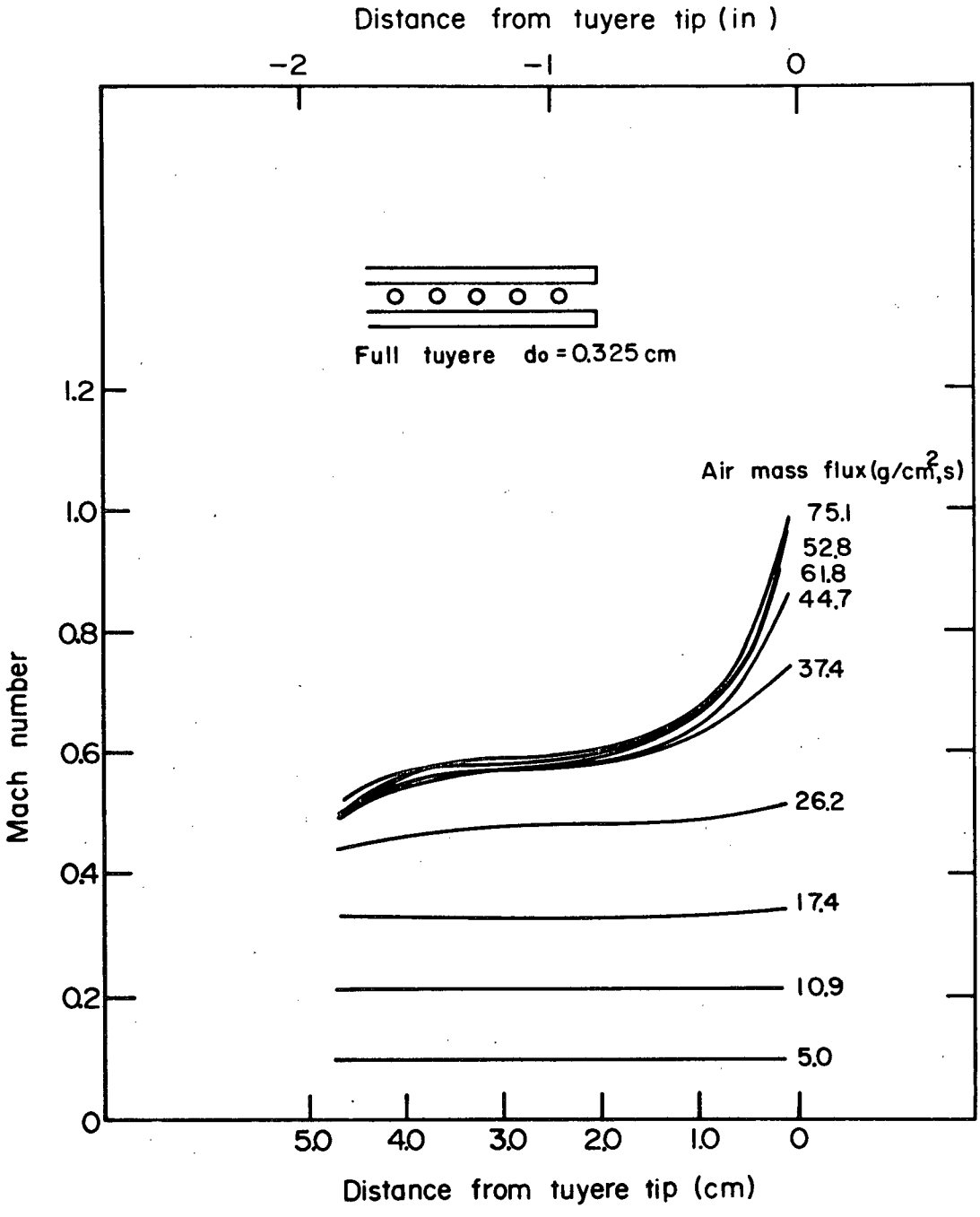

Fig. 52 Mach Number Profiles, 0.325 cm. dia., Full-Tuyere, Air-Hg.

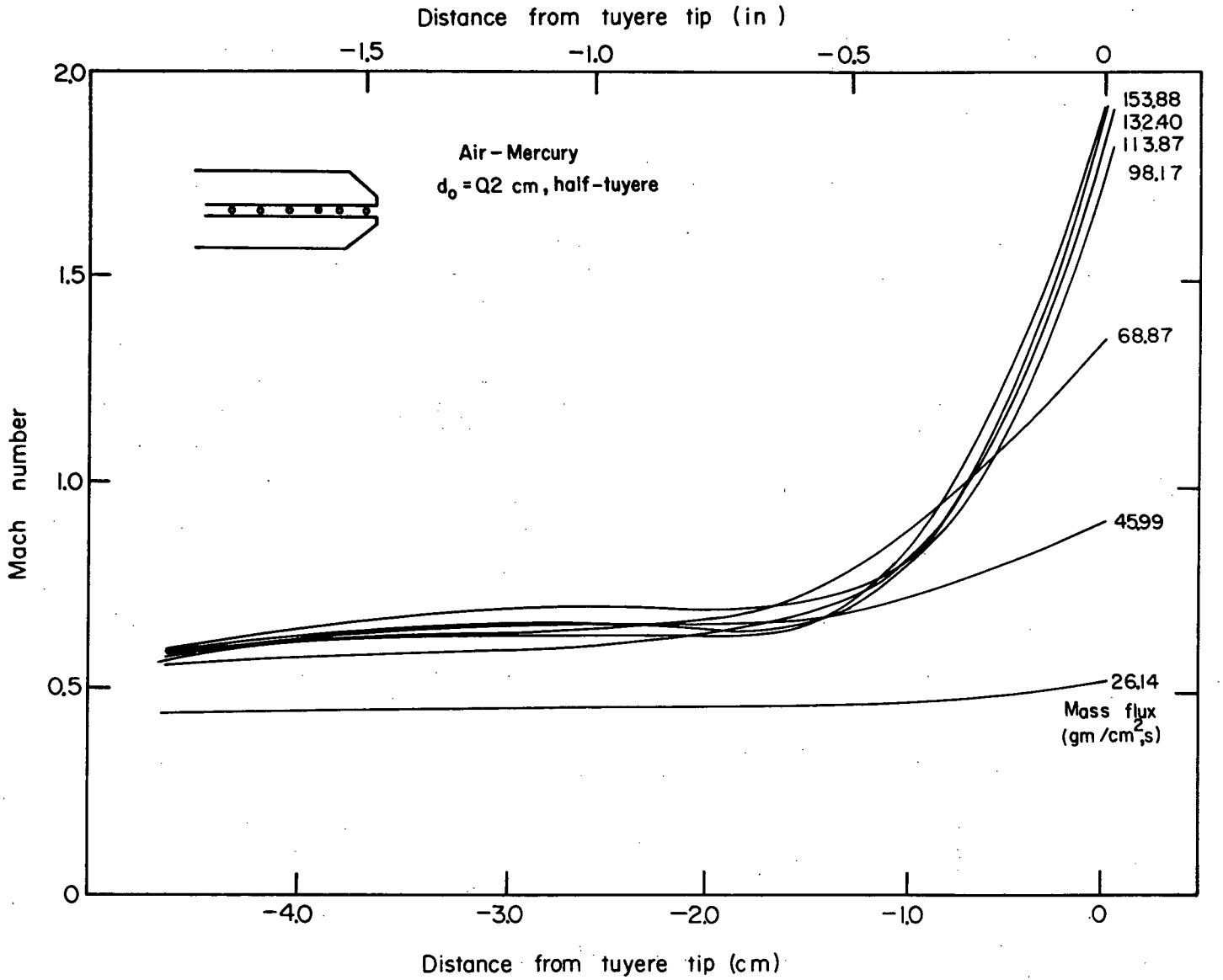

Fig. 53 Mach Number Profiles, 0.2 cm, dia., Half-Tuyere, Air-Hg.

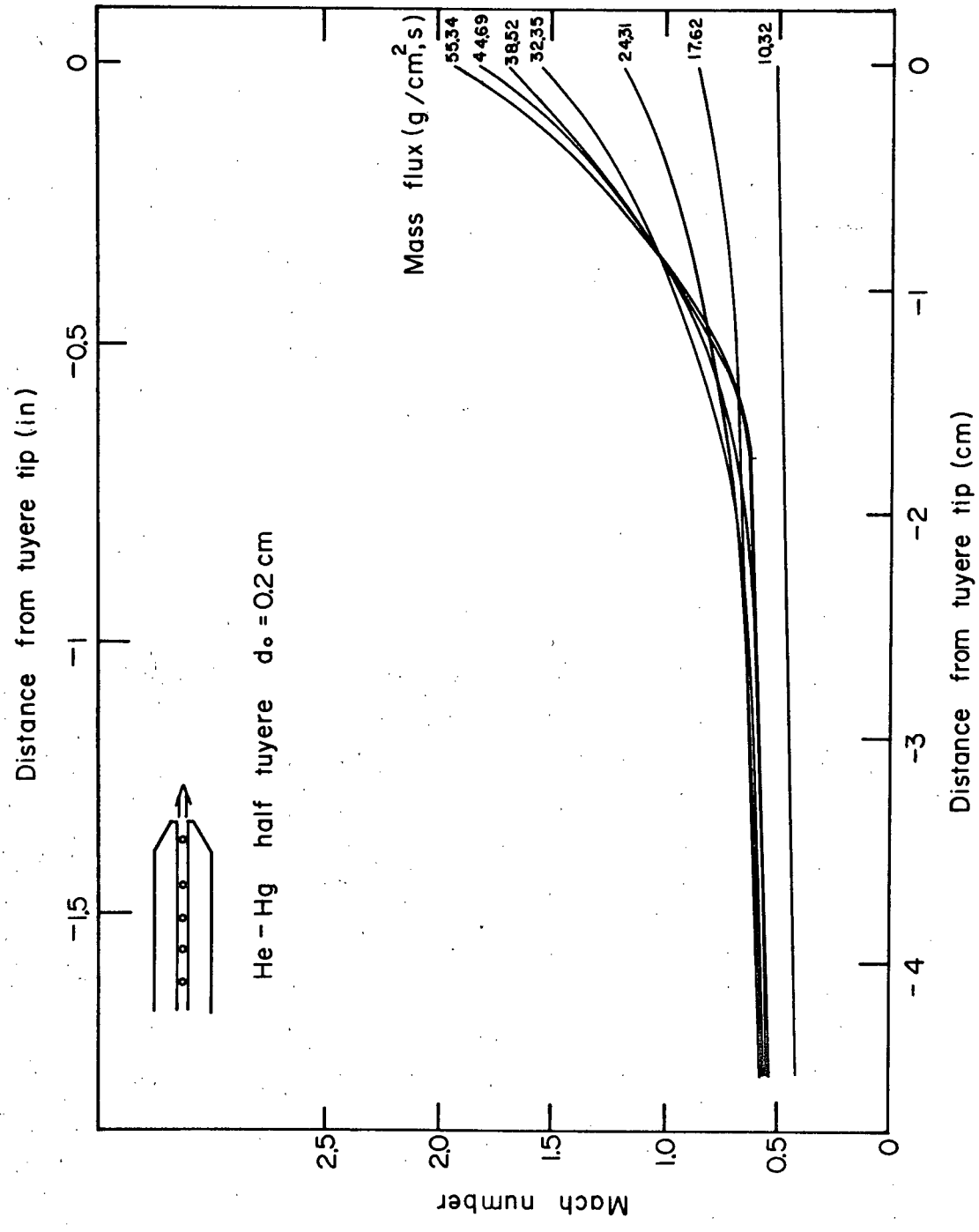

Fig. 54 Mach Number Profiles, 0.2 cm. dia., Half-Tuyere, He-Hg.

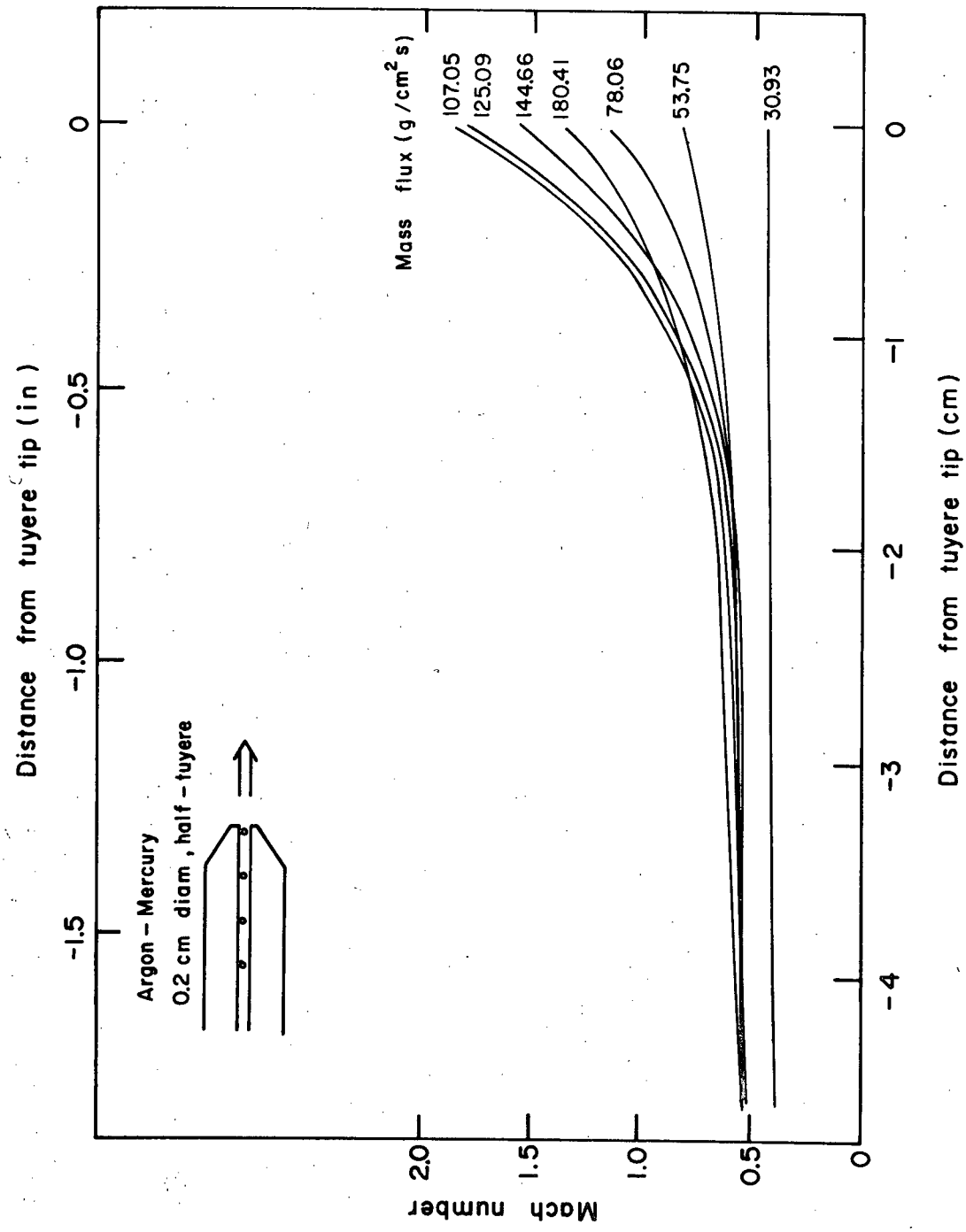

Fig. 55 Mach Number Profiles, 0.2 cm. dia., Half-Tuyere, Ar-Hg.

APPENDIX IV

Table VII

RESULTS FOR AIR-MERCURY, STRAIGHT-BORE, HALF-TUYERE

Diameter = 0.325 cm

Volumetric Flow at 1 atm. and Room Temp. [$cm^3\ s^{-1}$]	Distance from Tuyere Tip								Froude Number	Gas Speed [$cm\ s^{-1}$]	Mass Flux [$g\ cm^{-2}\ s^{-1}$]	Reynolds Number
	x_1 = 0. cm		x_2 = -1.53 cm		x_3 = -3.05 cm		x_4 = -4.57 cm					
	Press. (psi)	Mach	Press. (psi)	Mach	Press. (psi)	Mach	Press. (psi)	Mach				
337.1	0	0.205	0	0.205	0.12	0.203	0.46	0.199	28.9	7270	10.51	10369
764.8	0	0.464	0.92	0.440	1.60	0.423	2.52	0.402	147.9	16445	23.84	23469
1285.0	1.15	0.729	3.89	0.631	6.19	0.567	7.56	0.534	394.0	25853	34.02	39758
1530.2	2.29	0.815	6.87	0.655	10.31	0.571	12.37	0.530	528.6	28504	47.69	47698
1819.0	4.35	0.873	11.22	0.656	15.12	0.576	16.95	0.544	680.9	30960	56.69	57227
2068.8	7.10	0.877	15.35	0.650	17.93	0.601	19.98	0.567	787.5	31103	64.48	67792
2312.5	9.85	0.878	17.25	0.685	22.70	0.590	26.33	0.540	889.8	31138	72.07	74177
2712.9	13.29	0.911	24.97	0.654	29.96	0.584	33.60	0.542	1033.3	32309	84.56	87753
3200.3	19.07	0.900	31.33	0.669	37.23	0.596	41.77	0.549	1289.0	31919	99.75	104589
3693.1	24.06	0.901	39.95	0.647	45.85	0.586	51.76	0.535	1484.0	31954	111.38	120188

Table VIII

RESULTS FOR AIR-Hg, STRAIGHT-BORE, FULL-TUYERE

Diameter = 0.325 cm

Volumetric Flow at 1 atm. and Room Temp. [$cm^3\ s^{-1}$]	Distance from Tuyere Tip								Froude Number	Gas Speed [$cm\ s^{-1}$]	Mass Flux [$g\ cm^{-2}\ s^{-1}$]	Reynolds Number
	x_1 = -0.16 cm		x_2 = -1.68 cm		x_3 = -3.21 cm		x_4 = -4.73 cm					
	Press. (psi)	Mach	Press. (psi)	Mach	Press. (psi)	Mach	Press. (psi)	Mach				
323.7	0	0.099	0	0.099	0	0.099	0	0.099	16.5	3511	5.05	8195
700.1	0	0.213	0	0.213	0.01	0.212	0.02	0.210	76.2	7554	10.91	17633
1113.2	0	0.339	0.46	0.330	0.46	0.330	0.46	0.330	193.0	12023	17.35	28064
1666.5	0	0.511	1.15	0.478	1.15	0.478	2.75	0.44	438.6	18123	26.15	42303
2398.6	0	0.731	3.89	0.591	4.81	0.565	7.33	0.506	911.0	25925	37.38	60515
2865.5	0	0.872	7.788	0.593	8.71	0.571	12.83	0.491	1296.2	30925	44.66	72186
3387.9	0.69	0.991	11.91	0.599	12.60	0.585	17.87	0.510	1752.8	35146	52.80	85890
3965.5	4.123	0.966	16.34	0.606	17.25	0.590	24.06	0.491	2037.1	34259	61.80	102403
4468.8	6.87	0.960	21.79	0.586	22.70	0.572	29.96	0.483	2305.5	34046	69.64	116622
5051.6	8.71	0.960	23.61	0.603	24.52	0.590	32.23	0.496	2502.2	34046	75.09	126571

Table IX

RESULTS FOR AIR-MERCURY, STRAIGHT-BORE, HALF-TUYERE

Diameter = 0.2 cm

Volumetric Flow at 1 atm. and Room Temp. [$cm^3\ s^{-1}$]	Distance from Tuyere Tip								Froude Number	Gas Speed [$cm\ s^{-1}$]	Mass Flux [$g\ cm^{-2}\ s^{-1}$]	Reynolds Number
	x_1 = 0. cm		x_2 = -1.53 cm		x_3 = -3.05 cm		x_4 = -4.57 cm					
	Press. (psi)	Mach	Press. (psi)	Mach	Press. (psi)	Mach	Press. (psi)	Mach				
317.6	-0.23	0.516	1.82	0.458	2.72	0.458	2.72	0.436	290.5	18230	26.1	15749
558.8	-0.11	0.901	5.45	0.672	8.17	0.598	9.59	0.566	899.6	31954	46.0	27835
836.8	0	1.340	13.62	0.733	18.16	0.637	20.88	0.591	2005.3	47523	68.9	41709
1192.9	1.23	1.777	28.15	0.705	28.60	0.698	36.32	0.596	3821.5	63021	98.2	60112
1383.6	2.98	1.876	38.14	0.668	39.05	0.657	48.12	0.565	4726.7	66532	113.9	70234
1608.8	5.96	1.892	48.12	0.657	49.03	0.647	58.11	0.569	5617.9	67100	132.4	82775
1869.6	9.16	1.923	58.11	0.661	61.74	0.631	64.47	0.609	6704.6	68199	153.9	97164

Table X

RESULTS FOR HELIUM-MERCURY, STRAIGHT-BORE, HALF-TUYERE

Diameter = 0.2 cm

Volumetric Flow at 1 atm. and Room Temp. [$cm^3\ s^{-1}$]	Distance from Tuyere Tip								Froude Number	Gas Speed [$cm\ s^{-1}$]	Mass Flux [$g\ cm^{-2}\ s^{-1}$]	Reynolds Number
	x_1 = 0. cm		x_2 = -1.53 cm		x_3 = -3.05 cm		x_4 = -4.57 cm					
	Press. (psi)	Mach	Press. (psi)	Mach	Press. (psi)	Mach	Press. (psi)	Mach				
948.7	0	0.498	0.91	0.472	1.82	0.449	2.72	0.427	315.4	53889	10.32	6297
1619.1	0	0.850	4.09	0.681	7.26	0.590	9.08	0.548	918.9	91979	17.62	10748
2234.7	0	1.173	9.08	0.756	14.07	0.632	18.61	0.551	1749.9	126930	24.31	14832
2973.3	0.46	1.519	16.80	0.773	24.52	0.627	29.51	0.559	3026.4	164371	32.35	19808
3540.5	1.37	1.716	24.52	0.747	32.69	0.623	39.95	0.543	4054.1	185688	38.52	23721
4174.0	3.21	1.803	32.65	0.722	42.68	0.600	49.94	0.534	5037.5	195103	44.64	27778
5086.6	6.64	1.903	44.95	0.716	57.20	0.597	64.47	0.544	6686.7	205924	55.34	34935

Table XI

RESULTS FOR ARGON-MERCURY, STRAIGHT-BORE, HALF-TUYERE

Diameter = 0.2 cm

Volumetric Flow at 1 atm. and Room Temp. [$cm^3\ s^{-1}$]	Distance from Tuyere Tip								Froude Number	Gas Speed [$cm\ s^{-1}$]	Mass Flux [$g\ cm^{-2}\ s^{-1}$]	Reynolds Number
	x_1 = 0. cm		x_2 = -1.53 cm		x_3 = -3.05 cm		x_4 = -4.57 cm					
	Press. (psi)	Mach	Press. (psi)	Mach	Press. (psi)	Mach	Press. (psi)	Mach				
272.6	0	0.452	0.91	0.428	1.82	0.407	2.72	0.388	262.4	15483	30 93	36486
473.6	-0.91	0.831	4.54	0.616	6.81	0.556	8.63	0.516	832.1	28465	53.75	62925
687.8	-2.72	1.367	10.44	0.698	14.53	0.606	18.16	0.543	1956.0	46825	78.06	89922
943.2	-2.72	1.874	21.34	0.682	25.88	0.609	30.87	0.544	3676.0	64192	107.05	123273
1102.2	0	1.828	28.60	0.676	34.50	0.591	41.77	0.517	4292.2	62616	125.09	147569
1274.6	5.45	1.589	38.14	0.638	44.95	0.567	52.21	0.507	4446.1	54430	144.66	175834
1589.6	20.88	1.163	53.57	0.620	57.80	0.585	66.69	0.522	4205.6	39837	180.41	227258

Table XII

RESULTS FOR AIR-MERCURY, CONVERGENT-DIVERGENT, HALF-TUYERE

Volumetric Flow at 1 atm. and Room Temp. [$cm^3\ s^{-1}$]	Distance from Tuyere Tip								Froude Number	Gas Speed [$cm\ s^{-1}$]	Mass Flux [$g\ cm^{-2}\ s^{-1}$]	Reynolds Number
	x_1 = 0. cm		x_2 = -1.53 cm		x_3 = -3.05 cm		x_4 = -4.57 cm					
	Press. (psi)	Mach	Press. (psi)	Mach	Press. (psi)	Mach	Press. (psi)	Mach				
388.4	0	0.110	0	0.139	0	0.110	0	0.110	5.7	3901	5.64	8148
695.8	0	0.192	0	0.249	0.34	0.183	0.46	0.191	18.2	6987	10.11	14593
1097.1	0	0.309	0	0.390	0.92	0.293	1.15	0.289	44.8	10953	15.87	22889
1607.9	0	0.455	1.15	0.618	2.98	0.385	3.665	0.372	97.1	16137	23.36	33704
2380.6	-0.46	0.692	-3.89	1.115	10.54	0.411	11.80	0.392	217.7	24542	34.59	49654
2847.6	-0.69	0.840	-2.06	1.16	17.18	0.394	18.10	0.384	315.5	29791	43.08	59300
3328.3	-1.15	1.011	0.46	1.158	22.70	0.396	24.06	0.382	442.1	35855	48.36	69026
3846.7	-1.15	1.169	3.89	1.113	29.06	0.393	30.42	0.382	591.2	41459	55.89	79815
4444.9	0	1.257	7.33	1.100	35.87	0.396	37.23	0.385	741.3	44580	73.56	93109
5062.7	1.83	1.288	10.31	1.114	43.13	0.396	44.49	0.387	875.3	45679	73.56	107285
5772.0	4.12	1.305	13.74	1.125	51.76	0.394	53.57	0.384	1023.2	46282	83.86	123764

APPENDIX V

RELATION BETWEEN MOLECULAR WEIGHT AND GAS MASS FLUX AT THE TRANSITION

For an ideal gas, the speed of sound is given by

$$u_s = \sqrt{\frac{\gamma RT}{M}}$$

where γ = C_p/C_v is the ratio between specific heat capacity at constant pressure (C_p) and at constant volume (C_v)

R = gas constant

T = absolute temperature

M = molecular weight

Relate to mass flux:

$$\dot{m} = \frac{m}{A \cdot t}$$

$$\dot{m} = \frac{\dot{V} \cdot \rho}{A} = u\rho$$

where A = cross-sectional area

$\dot{V}$ = volumetric flow

ρ = gas density

u = gas velocity

For ideal gases we have

$$p = \rho RT$$

Therefore

$$\dot{m} = u \frac{P}{RT}$$

At Mach = 1, $u = u_s$, and

$$\dot{m} = \sqrt{\frac{\gamma RT}{M}} \cdot \frac{P}{RT}$$

$$\dot{m} = P\sqrt{\frac{\gamma M}{RT}}$$

Under similar conditions of pressure and temperature, and assuming that γ does not change noticeably for gases that are almost ideal, we obtain for two different gases 1 and 2:

$$\frac{\dot{m}_1}{\dot{m}_2} = \sqrt{\frac{M_1}{M_2}}$$

Thus, the ratio between the mass fluxes for two different gases at their transition value from fully-expanded to underexpanded jets is proportional to the square root of the ratio of their molecular weights.